TECHNISCHE UNIVERSITÄT MÜNCHEN

Fakultät für Medizin

Klinik für Herz- und Kreislauferkrankungen Deutsches Herzzentrum München des Freistaates Bayern

und

1.Medizinische Klinik und Poliklinik Klinikum der Universität Münchnen Ludwig-Maximilians-Universität München

Autonomous Migration of Anucleated Platelets Facilitates Thrombus Consolidation

Florian Reinfried Gärtner

Vollständiger Abdruck der von der Fakultät für Medizin der Technischen Universität München zur Erlangung des akademischen Grades eines

Doctor of Philosophy (Ph.D.)

genehmigten Dissertation.

Vorsitzende: Univ.-Prof. Dr. Agnes Görlach

Betreuer: Univ.-Prof. Dr. Steffen Massberg

Prüfer der Dissertation:

1. Univ.-Prof. Dr. Dirk Busch

2. Univ.-Prof. Dr. Dr. Stefan Engelhardt

Die Dissertation wurde am 23.03.2015 bei der Fakultät für Medizin der Technischen Universität München eingereicht und durch die Fakultät für Medizin am 27.07.2015 angenommen.

Eidesstattliche Erklärung

Ich erkläre an Eides statt, dass ich die der Fakultät für Medizin der Technischen Universität München vorgelegte Arbeit mit dem Titel:

Autonomous Migration of Anucleated Platelets
Facilitates Thrombus Consolidation

am Deutschen Herzzentrum München und der 1.Medizinischen Klinik und Poliklinik, Klinikum der Universität München, Ludwig-Maximilians-Universität München, unter der Anleitung und Betreuung durch Herrn

Prof. Dr. med. Steffen Massberg

ohne sonstige Hilfe erstellt und bei der Abfassung nur die gemäß § 6 Abs. 6 und 7 Satz 2 angegebenen Hilfsmittel benutzt habe.

Ich habe keine Organisation eingeschaltet, die gegen Entgelt Betreuerinnen und Betreuer für die Anfertigung von Dissertationen sucht, oder die mir obliegenden Pflichten hinsichtlich der Prüfungsleistungen für mich ganz oder teilweise erledigt.

Ich habe die Dissertation in dieser oder ähnlicher Form in keinem anderen Prüfungsverfahren als Prüfungsleistung vorgelegt.

Ich habe den angestrebten Doktorgrad noch nicht erworben und bin nicht in einem früheren Promotionsverfahren für den angestrebten Doktorgrad endgültig gescheitert.

Die öffentlich zugängliche Promotionsordnung der Technischen Universität München ist mir bekannt, insbesondere habe ich die Bedeutung von § 28 (Nichtigkeit der Promotion) und § 29 (Entzug des Doktorgrades) zur Kenntnis genommen. Ich bin mir der Konsequenzen einer falschen Eidesstattlichen Erklärung bewusst.

München, den

(Florian Reinfried Gärtner)

Danksagung

Ich bedanke mich herzlich bei Herrn Prof. Steffen Massberg für die stetige Unterstützung und Möglichkeit in seinem Labor zu arbeiten. Besonderer Dank gilt auch meinen Kollegen Sue Chandraratne, Michael Lorenz, Zerkah Ahmad und Gökce Yavuz.

Für *Carina - Vielen Dank für Deinen Rückhalt und Deine Geduld.

Contents

List of Figures

Abbreviations

ACD	Acid Citrate Dextrose
ADP	Adenosine Triphosphate
AFM	Atomic Force Microscopy
ANOVA	Analysis of Variance
ATP	Adenosine Diphosphate
BAPTA	1,2-bis(o-aminophenoxy)ethane-N,N,N',N'-tetraacetic acid
BSA	Bovine Serum Albumin
CCD	Charge-Coupled Device
CFP	Cyan Fluoresent Protein
DIC	Differential Interference Contrast
Fbg	Fibrinogen
$FeCl_3$	Ferric Chloride
GFP	Green Fluoresecent Protein
GP	Glycoprotein
GTP	Guanine Triphosphate
fCol	fibrillar Collagen
HSA	Human Serum Albumin
IL	Interleukin
LPS	Lipopolysaccharide
MLCK	Myosin Light Chain Kinase
MYH9	Myosin Heavy Chain 9
NA	Numerical Arperture
pMLC	phosphorylated Myosin Light Chain

PAF	Platelet Activating Factor
PAR	Protease Activated Receptor
PCA	Principle Component Analysis
PF4	Platelet Factor 4
PMT	Photo Multiplier Tube
PPP	Platelet Poor Plasma
PRP	Platelet Rich Plasma
QFSM	Quantitative Fluorescent Speckle Microscopy
RFP	Red Fluorescent Protein
RGDS	Arginine-Glycine-Aspartate-Serine
SHG	Second Harmonic Generation
TNF	Tumor Necrosis Factor
TXA2	Thromboxane A_2
vWF	von Willebrand Factor
YFP	Yellow Fluoresecent Protein
2P-IVM	Two photon intravital microscopy

1 Abstract

Platelets are anucleated cells that circulate in mammalian blood relentlessly scanning the vasculature for damage of the endothelial surface. When encountering endothelial injury, platelets are immediately recruited to form tightly packed thrombi and prevent excessive bleeding. Once recruited from the blood stream, platelets are generally considered to be immotile, attaching firmly and spreading on whatever subendothelial matrix or plasma protein they first encounter. However due to the high platelet density within a thrombus and the small platelet size, we actually know only very little about the exact behavior of individual platelets within a forming thrombus. By single cell tracking in multicolor platelet reporter mice, we demonstrate autonomous locomotion of activated platelets within their physiological environment. Platelets polarize, become motile and migrate while undergoing the typical cycles of cell migration established for other cell types. By quantitative single cell analysis we show that the major intra- and extracellular factors governing platelet migration include actin-mediated protrusion and integrin-dependent adhesion formation at the leading edge, balanced by calcium-mediated myosin IIa-dependent contraction and adhesion release at the trailing edge to maintain polarization and forward movement. We show that these processes are regulated by the balance of adhesive and anti-adhesive forces, coordinated by the plasma proteins fibrinogen and albumin, as well as calcium. Governed by the local adhesiveness of the microenvironment, platelet migration facilitates the redistribution of individual platelets towards regions of higher adhesiveness, thereby reorganizing thrombi *in vivo*. Here we identify anucleated platelets as motile cells and demonstrate autonomous platelet migration as a platelet function regulating thrombus formation.

2 Introduction

2.1 The role of platelets during arterial thrombosis

Thrombus formation following vascular injury is an highly regulated, locally restricted and multi-cellular process requiring precise spatio-temporal regulation of events in order to prevent excessive bleeding, while at the same time avoiding vascular occlusion (Furie and Furie, 2008; Engelmann and Massberg, 2013). Platelets are circulating anucleated cell fragments shed into the blood stream by polyploid megakaryocytes residing in the bone marrow (Zhang et al., 2012). Approximately 750 billion of platelets circulate in human blood relentlessly scanning the vasculature for damage of the endothelial surface. When encountering endothelial injury, platelets are immediately recruited in a well characterized cascade of events including initial platelet tethering and rolling, followed by platelet activation, adhesion and spreading, eventually leading to fibrin(ogen)-dependent platelet aggregation and subsequent thrombus retraction (Jackson, 2007) (Figure 2.1).

"'Tethering"' describes the initial contact of circulating platelets with the activated, injured endothelium resulting in deceleration and rolling of platelets. This process is mainly mediated through binding of the platelet receptors GPVI and GPIb to their ligands collagen and von Willebrand factor (vWF), respectively (Savage et al., 1998; Massberg et al., 2003; Bergmeier et al., 2006). By binding to their receptor these ligands trigger signaling cascades converging in activation of integrins ("'outside-in signaling"') (Li et al., 2010). Platelets express two major integrins, collagen-binding $\alpha_2\beta_1$ and the most abundant platelet adhesion-receptor $\alpha_{\mathrm{IIb}}\beta_3$. $\alpha_{\mathrm{IIb}}\beta_3$ predominately binds to fibrinogen but also recognizes the "'RGD"' binding motif of additional plasma proteins including Fibronectin, vWF and vitronectin (Bennett et al., 2009). Activation of integrins is a critical prerequisite of firm platelet adhesion. Besides the afore mentioned contact activation, soluble mediators can trigger platelet activation and subsequent in-

tegrin ligation. As such, Thrombin, a serine protease acts as a potent platelet activator. Thrombin accumulation at sites of vascular injury is mainly regulated by tissue factor dependent conversion from its inactive precursor prothrombin. Binding to the g protein coupled receptors PAR1 and PAR4 (PAR3 and PAR4 in mice, respectively) thrombin is a strong platelet activator triggering adhesion, secretion, aggregation and thrombus formation (Weiss et al., 2002; Coughlin, 2005; Dubois et al., 2006; Mangin et al., 2006; Cornelissen et al., 2010).

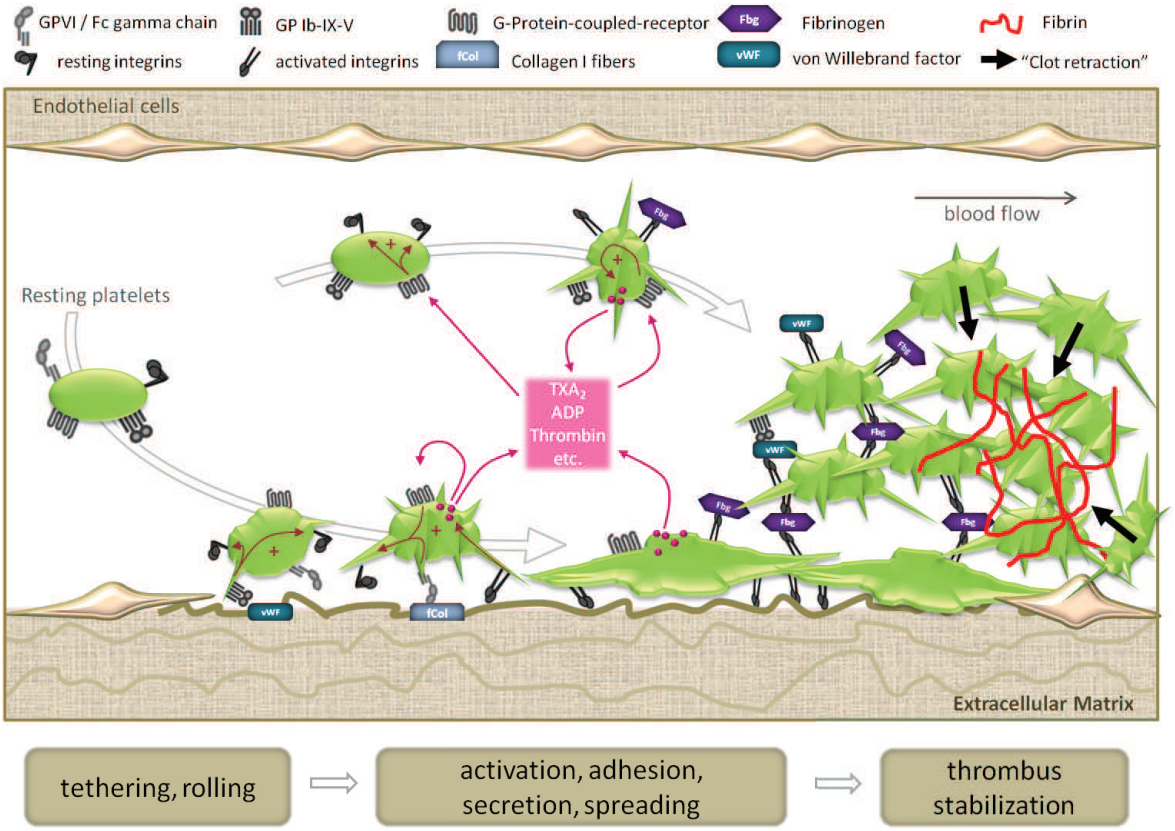

Figure 2.1 – Sequential steps of platelet activation.

During a second wave of activation the so called "'Secondary Mediators"' Thromboxane A_2 (TXA_2) and Adenosine-diphosphate (ADP) are released from platelets (Thomas et al., 1998). TXA_2 is an eicosanoid derived from arachidonic acid and probably released by the transporter MRP4 (Reid et al., 2003; Jedlitschky et al., 2012). ADP is a nucleoside-diphosphate stored in "'dense granules"' of platelets which are secreted upon activation (Gachet, 2008). Both, TXA_2 and ADP bind to "'G-Protein-Coupled-Receptors"' (GPCRs) and amplify thrombus formation by recruiting additional platelets

to the site of injury (Offermanns, 2006). Besides TXA_2 and ADP, a plethora of different molecules is secreted from intracellular stores. While dense granules mainly contain low molecular constituents like ADP, ATP, Serotonin and Calcium that directly amplify platelet activation, the so called alpha granules store high molecular components with multiple functions. Plasmaproteins like fibrinogen, fibronectin and von willebrand factor, to name some of them, directly modulate platelet function during thrombosis, while coagulation factors, their co-factors, as well as inhibitors, have a major impact on the initiation and maintenance of the secondary hemostasis (Blair and Flaumenhaft, 2009). Finally, secretion of alpha granules involves the release of chemokines and cytokines that were shown to play a major role during inflammatory processes, development and angiogenesis, thus highlighting the versatile role of platelets in mammalian (patho-)physiology (Gleissner et al., 2008). Platelet secretion also triggers the recruitment of additional platelets to the inital platelet monolayer, primarily mediated through adhesion to von Willebrand factor (Bergmeier et al., 2006). When getting in contact platelets start to form aggregates which requires the activation of the $\alpha_{IIb}\beta_3$ integrin. Activated $\alpha_{IIb}\beta_3$ binds to fibrinogen, the most important molecule bridging adjacent platelets. Correspondingly, patients with mutated $\alpha_{IIb}\beta_3$ often present with bleeding disorders known as Glanzmann thrombasthenia (Nurden, 2005). However, it is now well established that efficient thrombus formation requires the concerted action of many additional molecules modulating platelet aggregation(Denis and Wagner, 2007).

Once an aggregate is formed, interacting platelets start to collectively retract, a process dependent on acto-myosin contraction (Ono et al., 2008). Simultaneously, a network of fibrin is generated to stabilize the tightly packed aggregate and to prevent fragmentation and embolization of thrombi (Chou et al., 2004). Figure 2.1 provides a graphical overview of the most important steps of thrombus formation.

2.2 Basic principles of cell migration

Migration is the functional property of a cell to change position over time and thus a critical requirement to spatio-temorally control celluar processes from embryonic development throughout the adult life. Consequently, the failure of cells to migrate or its misguidance to inappropriate locations leads to a wide range of pathologies including developmental defects, immunodeficiency and cancer metastasis. Even though highly

regulated by a complex interplay of intra- and extracellular factors, cell migration can be mechanistically described by cycles of four major sequential steps (Lauffenburger and Horwitz, 1996): (1) extension of a protrusion (leading edge); (2) adhesion to matrix contacts; (3) contraction of the cytoplasm; (4) release from contact sites. Initiation of these cycles in stationary cells has been shown to result in a characteristic morphological polarization composed of a steering leading edge lamellipodium and a trailing cell body (Ridley et al., 2003). Quantitative microscopic analysis of shape variations of migrating cells revealed insight into the underlying intracellular molecular shape determininants as well as extracellular modifying factors (Keren et al., 2008; Barnhart et al., 2011). While leading edge morphology was demonstrated to be mainly depend on actin-polymerization coupled to cell-matrix-adhesion-assembly, the trailing edge of a migrating cell was shown to be essentially shaped by myosinIIa-mediated contraction and adhesion-disassembly. Both processes have to be tightly coordinated to efficiently generate traction force and forward movement and their balance was shown to determine overall cell shape and speed (Palecek et al., 1997; Gupton and Waterman-Storer, 2006; Yam et al., 2007; Lammermann et al., 2008). Intracellular mechanisms regulating the functional segregation of front and rear involve spatially distinct Rho-GTPase-dependent signalling, trafficking of adhesion receptors towards the leading edge, and localized calcium signals (Fukata et al., 2003; Petrie et al., 2009). The latter has previously been demonstrated to increase towards the rear of a migrating cell, thereby reinforcing myosin-dependent adhesion (Brundage et al., 1991; Lee et al., 1999). It is now well established that the coordination of these intracellular regulators itself largely depends on the biophyical and biochemical composition of the extracellular environment. Thus, various substrate compositions may have a dramatic effect on the shape and migratory response of the same cell (Palecek et al., 1997; Gupton and Waterman-Storer, 2006).

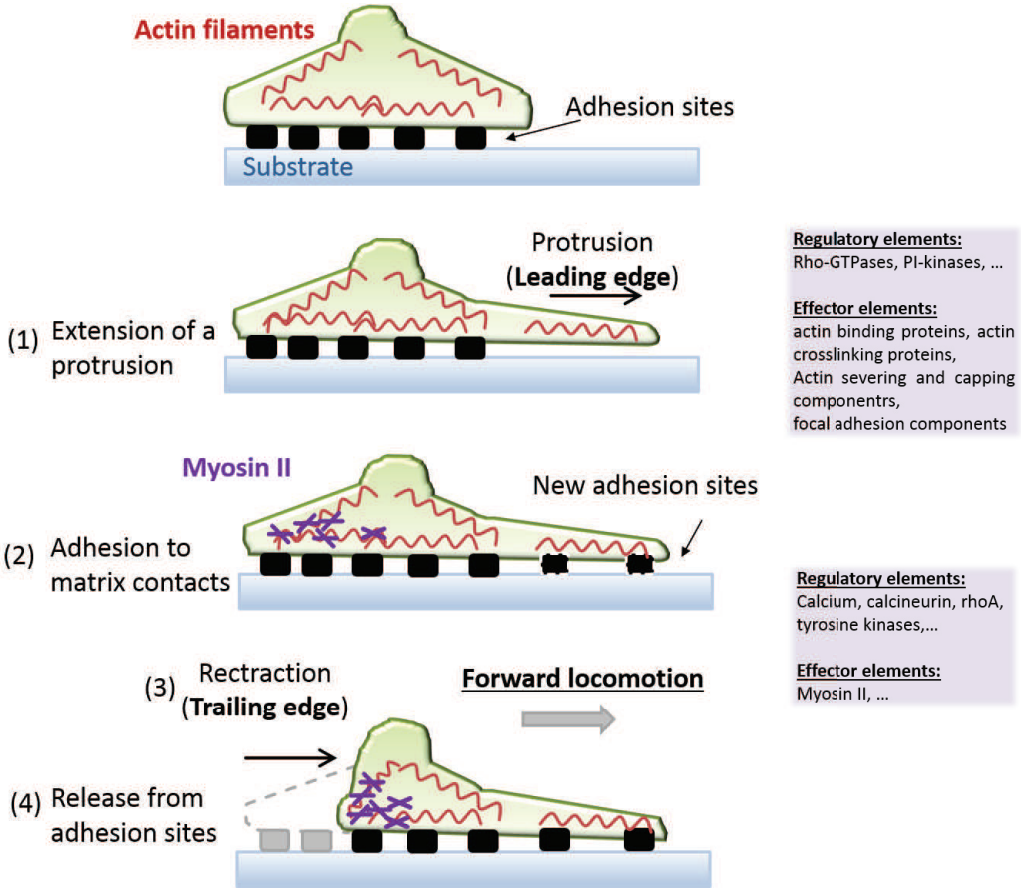

Figure 2.2 – Steps of cell migration. Adapted from (Lauffenburger and Horwitz, 1996; Ladoux and Nicolas, 2012)

2.3 Platelets and cell migration

Platelets posses the anatomic and biochemical machinery to undergo locomotion. Following activation platelets adhere to and spread on adhesive matrices, a prerequisite for entering the cycle of cell migration (see above). Different groups of adhesion proteins can mediate this process. While selectins, such as P- or E-selectin predominantly mediate platelet rolling and initial recruitment (Kansas, 1996), integrins support spreading and firm adhesion to vascular sites of injury (Bennett et al., 2009). Integrins are heterodimeric transmembrane receptors, composed of an α and a β subunit, both together forming an extracellular ligand binding site (Bennett et al., 2009). The extracellular domain of activated integrins facilitates the tight platelet binding to extracellular proteins like fibronectin, vitronectin and fibrinogen (see above). The cytoplasmic tails of

integrins provide a scaffold for regulatory adaptor proteins necessary for the linkage to the actin cytoskeleton (Legate and Fässler, 2009). Thus, integrins are physically connecting the extracellular matrix to the actin cytoskeleton allowing platelets to generate mechanical force on their environment - an essential requirement for cell migration. Generation of forces that drive locomotion depend on both actin polymerization as well as myosin contraction and the presence of a dense actomyosin network in platelets has been demonstrated (Lauffenburger and Horwitz, 1996; Bettex-Galland and Luscher, 1959). Just recently the mechanical force generated by this contractile machinery was measured in individual platelets by atomic force microscopy, revealing forces per cell volume exceeding those of myoblasts and most migrating cells (Ananthakrishnan and Ehrlicher, 2007; Lam et al., 2011). Hence, it is well accepted that platelets posses the basic mechanical machinery to generate traction forces required for forward locomotion. When spreading on matrix-protein coated substrates, platelets generate isotropic traction forces pointing towards the cell center (Schwarz Henriques et al., 2012). Similar traction force profiles have previously been reported for other stationary cells (Burton et al., 1999). Traction forces of migrating cells typically have an anisotropic distribution along the cell-substratum contact area. Asymmetry of traction forces is essential for rapid, polarized cell movement because high traction stresses at the rear promote retraction, whereas low traction at the front allows protrusion (Lombardi et al., 2007). Polarity is established by the spatio-temporal reorganization of cytoskeletal components tightly regulated by a plethora of signaling pathways (Ridley et al., 2003). Even though it has been demonstrated that intrinsic, purely stochastic variations in actomyosin contractility might be sufficient to initiate motility (Wedlich-Soldner and Li, 2003; Yam et al., 2007), many extrinsic cues are well established to trigger and maintain cellular polarity and directional migration (Petrie et al., 2009). Interestingly, platelets posses many structural properties to sense their environment implying their ability to migrate. As an example, platelets express different chemokine receptors that have previously been reported to be critical for guidance of locomoting cells. Chemokines are a group of proteins with shared structural characteristics that trigger cellular motility. When offered as soluble or immobilized gradients *in vitro* and *in vivo* these molecules are known to induce directional cell migration, referred to as chemotaxis or haptotaxis respectively (Schumann et al., 2010; Weber et al., 2013). Importantly, platelets themselves contain chemokines in their alpha granules that are ligands for their corresponding chemokine receptors (Gleissner et al., 2008). Thus, chemokine release was proposed to act as feedback mechanisms for amplification of spatially restricted platelet activation (Gleissner et al., 2008). To elicit

a cellular response, external cues like chemokines have to be recognized by and relayed into the cell. G-protein-coupled receptors are crucial components mediating this signal transduction. Upon ligation, these seven transmembrane receptors change their conformation thereby allowing the interaction with the appropriate heterotrimeric G-protein within the cell (Kamps and Coffman, 2005). Each G-protein activates several downstream effectors initiating a cascade of signaling events ultimately mediating diverse cellular functions including directional cell migration (Kamps and Coffman, 2005). It is well known that platelets express G-protein-coupled receptors and their importance for regulation of cytoskeleton dynamics has been studied extensively (Offermanns, 2006). Hence, platelets posses the structural basis for interpreting extracellular guidance cues as previously described for migrating cells.

These, as well as many other structural characteristics of platelets that imply their ability to migrate, motivated researchers to investigate platelet locomotion. Lowenhaupt et al. were the first to study the motility of platelets *in vitro* (Lowenhaupt et al., 1973). They loaded capillary tubes with platelet rich plasma and observed outward movement after incubation in a buffer-filled petri-dish, a method previously used to study macrophage migration (George and Vaughan, 1962). Stereomicroscopic examination after 18 h of incubation revealed a movement of discoid platelets out of the tube, a process reinforced by placing a collagen thread in close proximity to the capillary. Directed patelet movement towards collagen was blocked in the presence of metabolic inhibitors and inhibitors of actin-polymerization, indicating the active nature of this process (Lowenhaupt et al., 1977). Based on their results the authors hypothesized that platelet migration might be involved in the recruitment of platelets to sites of injury. Later, Lowenhaupt et al. developed a novel 7-compartment chamber, allowing a more quantitative analysis of platelet chemotaxis towards collagen in the presence of plasma (Lowenhaupt et al., 1982). Gel-filtered platelets were ^{111}In-oxine labeled and placed into the central compartment separated from the other compartments by a filter membrane. When collagen was added to an end-compartment, platelets left the central compartment and localized towards this end as measured by an increase of radioactivity (Lowenhaupt et al., 1982). Based on these experiments the authors concluded that platelet chemotaxis does not require physical contact with collagen since it was separated from platelets by the filter membrane. They postulated the existence of soluble "'chemotaxins"' induced by the interaction of collagen with plasma that were able to pass the membrane and guide platelet movement (Lowenhaupt et al., 1982). Others were using a modified Boyden chamber

approach, to analyze the translocation of platelets through filter pores of 8 μm of size (Boyden, 1962; Valone et al., 1974). The Boyden chamber consists of two compartments separated by a filter membrane with a thickness of 100 μm. Platelets are loaded into the upper compartment and translocation of platelets into the membrane was quantified at a depth of 40-70 μm. Platelet movement in this assay was shown to be directional towards prostaglandins and dependent on temperature, pH, protein-level of the buffer as well as the absence of calcium and magnesium (Valone et al., 1974). Dependency on temperature was also reported by others, with maximal migration being observed at 30°C (Nathan, 1973), 25°C (Duquesnoy et al., 1975), 22-37°C (Lowenhaupt et al., 1977) and 30-37°C (Valone et al., 1974). It was further demonstrated that anticoagulants used for platelet and plasma preparation were critically modulating the observed platelet responses. Lowenhaupt et al. systematically tested various anticoagulants in their assay, including sodium citrate, ACD, EGTA, Na-EDTA, Mg-Na-EDTA and sodium oxalate (Lowenhaupt et al., 1977). They obtained the best migratory response when sodium citrate or ACD was used, while heparin inhibited migration. Most of the initial *in vitro* work was performed on isolated platelets of healthy donors in the presence of unperturbed plasma highlighting migration as a platelet function taking place under physiologic conditions. Indeed, analysis of platelet migration was proposed as a novel, sensitive method for assessment of platelet function. As such the microcapillary assays of Lowenhaupt et al. were capable of detecting anti-platelet activity in serum of patients with idiopathic thrombocytopenic purpura and dogs infected with Erlichia canis (Duquesnoy et al., 1975; Kakoma et al., 1978). The fact that platelets move towards collagen resulted in speculations that this process might be important during thrombosis and wound healing (Lowenhaupt et al., 1973). However, first indirect evidence implying that platelets might be able to migrate *in vivo* was observed under inflammatory conditions where platelets have been found outside the vasculature within inflamed tissue. By performing electron microscopy on lungs in guinea-pigs challenged with intravenous injection of platelet activating factor (PAF) Lellouch-Tubiana et al. detected extravascular platelets in proximity to bronchial smooth muscle cells (Lellouch-Tubiana et al., 1985). Further studies investigated the role of platelet migration in non-thrombotic conditions such as allergic inflammation and asthma (Pitchford et al., 2008). Ovalbumin-sensitized mice were challenged with aerosolized antigen and platelet translocation was observed by immunohistochemistry. 30 hours after allergen exposure the authors detected platelets localized underneath the airway epithelium, a process dependent on antigen-specific IgE as well as binding to FcRγ. Using the Boyden chamber approach, an antigen-mediated

directional platelet movement was also demonstrated in platelets isolated from allergic human donors. Others, performed serial electron microscopic sections to visualize how platelets exit the vasculature (Feng et al., 1998). In their study acute inflammation was induced by injecting F-Met-Peptide into the skin of guinea pigs. The authors observed single platelets outside the blood vessels and inside of large, membrane-lined vacuoles within endothelial cell cytoplasm, thus proposing a trans-cellular pathway of platelet diapedesis. More recently, another study was showing the potential role of F-Met-Peptides and their corresponding formyl peptide receptor FPR in mediating platelet chemotaxis *in vitro* (Czapiga et al., 2004). Extravasation of platelets was also observed in the liver in response to LPS (Nakamura et al., 1998), where platelets were found in the Disse space as well as inside of hepatocytes; a process dependent on Kupffer cell-derived IL-1 and TNF. Finally, CXCL12 a chemokine linked to cardiovascular disease (Doering et al., 2014), was proposed to be an essential guidance cue of platelet migration *in vitro* (Kraemer et al., 2010, 2011; Schmidt et al., 2011, 2012).

2.4 Aims of the thesis

Taken together the above studies suggest that platelets recruited to vascular injuries or sites of inflammation can change their position. However, direct visual evidence of whether platelet migration occurs in a physiological context *in vivo* has not been demonstrated and fundamental questions regarding the underlying cell biological mechanisms still remain unaddressed. This has resulted in a general skepticism as to whether true autonomous migration of platelets exists in the mammalian organism.

Here, we aim to develop a novel imaging approach allowing the dynamic visualization of individual platelets during thrombus formation *in vitro* and *in vivo*. Based on the established imaging platform we aim to study the basic cell biological mechanisms underlying platelet migration. We aim to critically challenge our observations by verifying the well accepted concepts of cell migration. Finally, we aim to define the relevance of platelet migration *in vivo* in the context of thrombosis.

3 Materials and Methods

3.1 Mice

PF4-Cre (Tiedt et al., 2006), *R26R-Confetti* (Snippert et al., 2010) and C57Bl/6 -mice were purchased from The Jackson Laboratory and maintained and cross bred at our animal facility. *PF4-Cre/MYH9*$^{fl/fl}$ -mice were a gift of Dr. Gachet. *GPIIB-/-*mice were a gift of Dr. Frampton (Emambokus and Frampton, 2003). *GPIB-IL4R*-mice were a gift of Dr. Ware (Kanaji et al., 2002). Experiments were performed at the age of 10-20 weeks. All procedures performed on mice were approved by the local legislation on protection of animals (Regierung von Oberbayern, Munich).

3.2 Inhibitors and blocking antibodies

For inhibition $\alpha_{\mathrm{IIb}}\beta_3$, migration assays were performed in the presence of non-specific linear RGDS peptides (200μM, Biomol). RGES (200μM, Biomol) was used as negative control (Basani et al., 2001). To analyze the dynamic platelet response following $\alpha_{\mathrm{IIb}}\beta_3$ inhibition, human platelets were allowed to spread and to migrate for 15 min before adding 10μg/ml C7E3-Fab (Reopro, Lilly), a blocking β3-specific Fab-fragment (Coller, 1985). To exclude the involvement of $\alpha_{\mathrm{v}}\beta_3$ experiments were performed in the presence of the specific blocking antibody LM609 (30μg/ml, Merck Millipore). To inhibit actin polymerization in migrating platelets, platelets were allowed to spread and migrate for 5 min and subsequently treated with 2μM Cytochalasin D (Sigma) (Casella et al., 1981). MyosinIIa was inhibited pharmacologically by adding Blebbistatin(-) (Cayman Chemical) (5μM or 50μM) to the buffer. Blebbistatin(+) (Cayman Chemical) was used as negative control (Lammermann et al., 2008). Extracellular calcium was removed by

adding 100mM of citrate to the experiment. Intracellular calcium was depleted by incubating platelets with BAPTA-AM (10μM or 30μM, Molecular Probes) for 30 min at 37°C, as previously reported (Inoue et al., 2003).

3.3 2P-IVM of thrombus formation and bone marrow megakaryocytes

Animals were anesthetized by intraperitoneal injection of a solution of midazolame (5 mg/kg body weight; Ratiopharm), medetomidine (0.5 mg/kg body weight; Pfizer), and fentanyl (0.05 mg/kg body weight; CuraMed Pharma GmbH) as described previously (Massberg et al., 2002) and supplied with oxygen. Mice were placed in a lateral position to allow careful immobilization of the ear-pinnae (ventral side up) to a custom-built imaging platform using 30G-needles, as previously reported (Stark et al., 2013). A 3mmx3mm piece of dermis was carefully removed to expose small subcutaneous veins. Two injury models were used to subsequently induce thrombus formation. We either mechanically injured the vessel wall with a 30G needle or disrupted the vascular integrity by focusing a high power laser-beam of our two-photon microscope onto the vessel wall. Both injury models, triggered the exposure of subendothelial collagen as well as the accumulation of Fibrin(ogen) at the site of injury (Fig. 4.4) and are established models to study hemostasis (Stalker et al., 2013). To exclude passive platelet movement imitated by migrating leukocytes, we depleted leukocytes by i.p. injection of anti-Ly-6G (150μg/mouse 24h and 4h prior to injury; clone RB6-8CG5, eBioscience) and anti-CD45 (100μg/mouse 24h prior to injury; clone 30-F11, eBioscience) (Wulf et al., 2002; Daley et al., 2008). Depletion efficiency was locally controlled by injection of fluorescently labeled (PE) anti-CD45 (eBioscience) and anti-Ly-6G (eBioscience) following the experiment and white blood cells were counted using an automated cell counter (ABX Micros ES60, Horiba Medical) (Fig. 3.1). Images were acquired using a TrimscopeII multi-photon imaging platform (LaVision Biotech) on an upright Olympus stand, enclosed in a custom-built incubator maintaining 37°C. Images were acquired using a Plan-Apochromat 20x/1.0 numerical aperature (NA) objective (Carl Zeiss Imaging) with saline as immersion medium. Fluorescent signals were collected using 4 external/non-descanned photomultipliers (PMTs). For imaging of Confetti fluorescence the following filter combination was used: mCFP was collected with a 480/40 nm bandwidth and

520nm longpass filer, cYFP with a 535/30 nm bandwith and the same 520nm longpass filter and cRFP with a 605/70 nm bandwidth and 560nm longpass filter. Fluorescence excitation was provided by a Chameleon Ti:Sapphire laser (Coherent) tuned to 910nm for simultaneous excitation of cYFP, cRFP and mCFP and generation of collagen second harmonic signal. 800 nm excitation wavelength was used for imaging of CFDA-SE, DDAO-SE, Alexa 488 and Alexa 546 using the same laser. Z-stacks were recorded with 2μm step-size and time series were captured with 1 frame every 5 s, unless otherwise specified. To visualize megakaryocytes in *PF4-Cre/R26R-Confetti*-mice we performed 2P-IVM of the mouse calvarian bone marrow, as previously described (Zhang et al., 2012). To get access to the frontoparietal skull, the scalp of an anesthetized mouse is incised in the midline. A plastic ring is inserted in the incision to spread the skin and to allow application of sterile physiologic saline solution to prevent drying of the tissue. During these procedures the animal's head is immobilized in a customized plexiglas stage equipped with a stereotactic holder. Imaging is performed using the multiphoton imaging platform as described above.

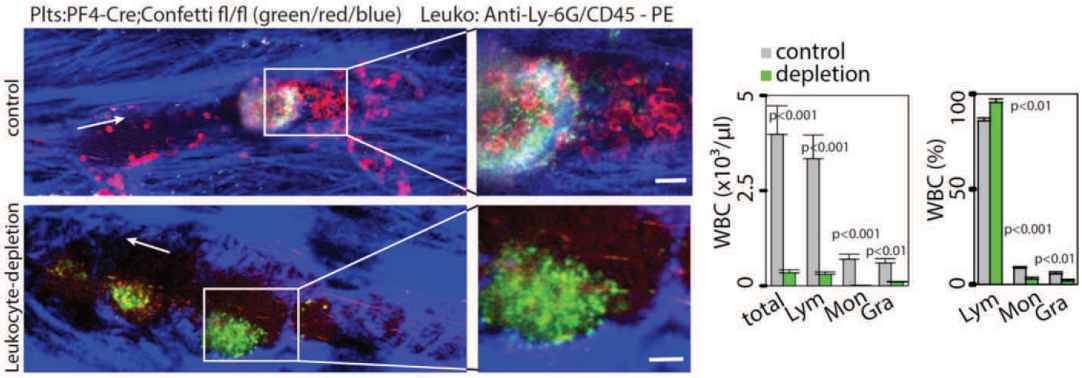

Figure 3.1 – Depletion of circulating white blood cells by i.p. injection of anti-CD45 (clone 30F11) and anti-Ly6G (clone RB6-8C5). control: n=10; depletion: n=13; p-values<0.05 indicate significance; wilcox-test; scale bar= 10μm.

3.4 Assessment of thrombus architecture after ferric chloride exposure

$FeCl_3$ injuries of carotid arteries were performed as previously described (Massberg et al., 2003). In brief, C57BL/6J recipient mice were anesthetized and fluorescence-tagged platelets (DDAO-SE, CFDA-SE, Molecular Probes) from *PF4-Cre*- and *PF4-*

Cre/MYH9$^{fl/fl}$- mice were infused intravenously into the tail vein of recipient mice. To visualize fibrinogen deposition, Alexa 546 labeled Fibrinogen (150μg/mouse) (Molecular Probes) was co-infused. Thereafter, the common carotid artery was dissected free and a filter paper (0.5x1.0 mm) saturated with 10% $FeCl_3$ was applied to the adventitial surface of the vessel for 3min. Occlusion of the vessel was monitored by epi-fluorescent microscopy using a Zeiss Axiotech microscope (water immersion objective, W 20//0.5; Carl Zeiss Imaging). Two hours after injury, vessels were excised, immediately rinsed with PBS, embedded in OCT, and frozen at -80°C. The carotid artery was cut with a cryotome into sections of 5 μm thickness. Specimens were fixed with 4% formalin for 4 min, washed in PBS and a coverslip was placed by mounting medium (DAKO). Images were acquired using a Zeiss Axio Imager M2 epifluorescent microscope with a Plan Apochromat 20x/0.8 air objective and an AxioCam MRm camera (Carl Zeiss Microscopy). Image processing and analysis was performed using FIJI (Schindelin et al., 2012). A low-pass Gaussian filter of the radius 0.5 μm was first applied to all images to suppress the noises while retaining the platelet and fibrinogen signal. The thrombus region was then determined by manually masking the image in the brightfield channel. A Background subtraction was then performed using the "'rolling ball"' algorithm (size=20px). Thrombi were manually segmented into zones of equal area based on the fibrinogen (Alexa 546) intensity (Fig. 3.2). Binary images of the centroids of DDAO-SE and CFDA-SE positive platelets were co-localized with each thrombus zone and counted using the Analyze Particles option of FIJI. Fibrinogen-dependent platelet redistribution was calculated by subtracting the mean global platelet density (non-segmented thrombus) from the mean platelet density at high fibrinogen areas (segmented thrombus). The fraction of migration-dependent platelet redistribution towards higher fibrinogen concentrations was calculated by: [(density of redistributed migrating platelets (PF4-Cre)) - (density of redistributed non-migrating platelets (PF4-Cre;MYH9$^{fl/fl}$)]/[density of redistributed migrating platelets (PF4-Cre)]*100.

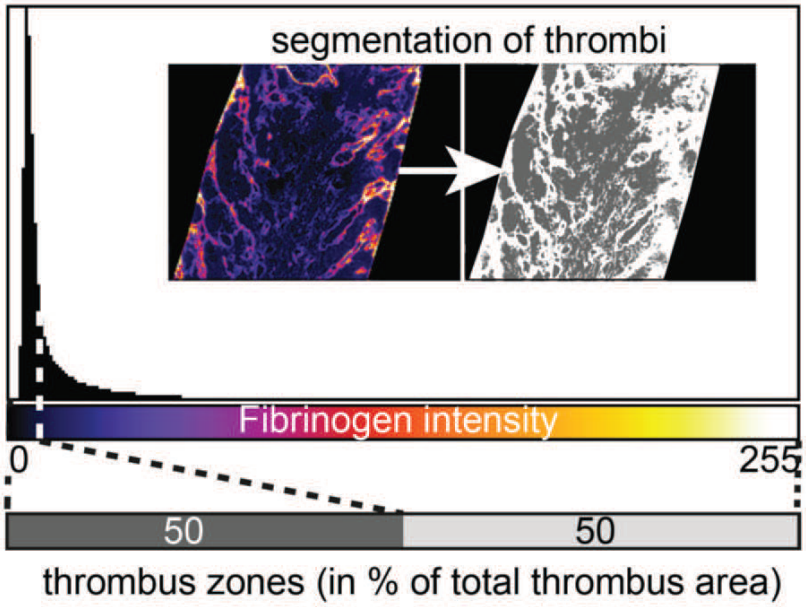

Figure 3.2 – Segmentation of Thrombi. The intensity based segmentation of thrombus zones of different fibrinogen concentration is shown. Area fractions are assigned to the corresponding values of the histogram (Alexa 546 labeled Fibrinogen).

3.5 Confocal imaging of platelets and megakaryocytes isolated from PF4-Cre/R26R-Confetti-mice

Isolated washed platelets were incubated on fibrinogen coated coverslips (100μg/ml) in the presence of 0.1U/ml bovine Thrombin for 20min at 37°C and subsequently imaged without prior fixation. Megakaryoctes were isolated as previously described (Mazharian et al., 2011). Bone marrow cells were isolated from femurs and tibias of mice by flushing, and cells were linage depleted using immunomagnetic beads (Linage depletion kit, Miltenyl Biotec). The purified population was cultured in 2.6% serum-supplemented StemPro medium with 2mM l-glutamine, penicillin/streptomycin, and 20 ng/mL of murine stem cell factor at 37°C under 5% CO2 for 2 days. Cells were then cultured for a further 4 days in the presence of 20 ng/mL of stem cell factor and 50 ng/mL of TPO. After 4 days of culture in the presence of TPO, the cell population was enriched in mature MKs using a 1.5%/3% BSA gradient under gravity (1g) for 45 minutes at room temperature. Megkaryocytes from *PF4-Cre/R26R-Confetti*-mice were allowed to

spread on fibrinogen coated coverslips (100μg/ml) for 6h at 37°C and imaged without prior fixation. Images were captured on an inverted Zeiss LSM 780 confocal microscope using a Plan-Apochromat 100x/1.46 oil-immersion objective (Carl Zeiss Imaging).

3.6 Isolation and live staining of human and murine platelets

Human blood was drawn from the cubital vein of healthy voluntary donors into a syringe containing 1/7 volume of Acid-Citrate-Dextrose (39 mM citric acid, 75 mM sodium citrate, 135 mM dextrose; ACD). Whole blood was diluted 1:1 with modified Tyrode's buffer (137 mM NaCl, 2.8 mM KCl, 12 mM $NaHCO_3$, 5.5 mM glucose, 10 mM Hepes, pH=6.5) and centrifuged with 70 g for 30 min at room temperature with the break switched off. The supernatant contains the platelet rich plasma (PRP), either used for experiments or transferred into a second tube to prepare washed platelets. Platelets were washed by further diluting PRP (1:3) with PGI_2 (0.1 μg/ml, Abcam) - containing, modified Tyrode buffer (pH=6.5) followed by centrifugation with 1250 g for 10 min at room temperature. The pellet was then carefully re-suspended in modified Tyrode's buffer (pH=7,4) and platelets were counted with an automated cell counter (ABX Micros ES60, Horiba Medical). Mouse blood was drawn intra-cardially from anesthetized (isoflurane (Delt Select GmbH), fentanyl i.p. (0.05 mg/kg body weight; CuraMed Pharma GmbH)) mice and processed as described for human platelets. In some cases washed platelets were stained with either 4.5 μM CFDA-SE (Carboxyfluorescein diacetate succinimidyl ester, Molecular Probes) or 4.5 μM DDAO-SE (CellTrace Far Red, Molecular Probes) for 30 min at room temperature, followed by additional washing with modified Tyrode's buffer (pH=6.5).

3.7 Plasma and serum preparation

Platelet poor plasma (PPP) was isolated from human or mouse anti-coagulated whole blood (ACD 1:7) and diluted in modified Tyrode's buffer (pH=7.4) (1:1); followed by centrifuation with 1750 g for 10 min at room temperature. PPP from the supernatant

was either used for experiments or further processed to generate serum. PPP was incubated with bovine thrombin (1U/ml, Sigma) for 30 min at room temperature to initiate coagulation. Fibrin was removed from the solution by centrifugation (2000 g, 15 min, room temperature) and thrombin activity was blocked by adding 2U/ml Lepirudin (Refludan, Schering) and 40 μM PPACK (D-Phenylalanyl-prolyl-arginyl Chloromethyl Ketone, Enzo Life Science). To determine the protein concentration of serum, Bradford assays were performed (Quick Start Bradford Protein Assay, Bio-Rad) using bovine serum albumin (BSA) as protein standard. Absorbance at 595nm was measured using a monochromator-based microplate reader (Synergy Mx, BioTek). In some experiments, serum was further processed. To heat-denature serum proteins, samples were incubated at 37°C, 50°C, 70°C and 90°C (Thermomixer, Eppendorf) for 30 min and cooled down to room temperature prior to the experiment. To fractionate serum by size and to remove low molecular components, dialysis was performed against PBS using dialysis cassettes of 2 kDa molecular weight cut-off (Slide-A-Lyzer Dialysis Cassettes, Thermo Scientific).

3.8 Preparation of platelet supernatants

Supernatants of collagen-activated platelets were generated from PRP preincubated with 10 μg/ml fibrillar collagen (Chrono-Log) for 20 min at 37°C. Some preparations were performed in the presence of 2 U/ml apyrase (New England Biolabs) and 10 μM Indomethacin (Sigma) or vehicle (Succinate buffer, Ethanol). Activated platelets were removed by centrifugation at 9000 g for 10 min and PPP containing the platelet releasate was used for experiments.

3.9 Preparation of cover-slip and migration buffer

To generate adhesive substratess for the *in vitro* analysis of platelet adhesion, spreading and migration, glass cover-slips (No. 1.5, D263T, Nexterion) were prepared according to the following protocol. Cover-slips were acid washed (20% HNO_3) for 1 hour at room temperature and thoroughly rinsed in ddH_2O for another hour (Giannone et al., 2004). Freshly cleaned coverslips were air-dried by spin-coating (KLM SCI, Schaefer) at 90

rps for 10 s, silaned with hexamethyldisilazane (HMDS, Sigma Aldrich, Germany) and subsequently spin-coated at 80 rps for another 30 s to ensure homogeneous silanization (Palecek et al., 1997).

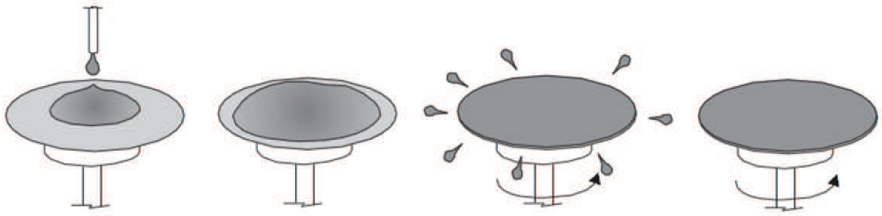

Figure 3.3 – The spin-coating process (adapted from Jones et al. (1999)).

Migration buffer containing modified Tyrode's buffer (pH=7.4) was supplemented with adhesive proteins (PPP or serum/fibrinogen (Sigma) or rHSA (Sigma)/fibrinogen), platelet activators (collagen (Chromo-Log) or platelet-releasate or purified ADP (Sigma)/U46619 (Tocris Bioscience)) and divalent cations (calcium or magnesium or manganese) at the concentrations indicated in Results. If not otherwise stated the following concentrations were used: serum (1500 μg/ml), rHSA (1500μg/ml), fibrinogen (150 μg/ml), collagen (10 μg/ml), calcium (200 μM), ADP (4 μM), U46619 (2 μM). A plastic ring was glued to the pretreated cover-slips to build a custom made migration chamber (Lammermann et al., 2008). The chamber was filled with migration buffer and incubated for 5 min at room temperature (for the immobilization of collagen fibers (200 μg/ml) slides were incubated for 2h at room temperature and washed with Tyrode's buffer pH=7.4). Within these 5 min proteins from the supernatant adsorbed to the cover slip to build an homogeneous protein layer (Fig. 4.22) (Turbill et al., 1996) and either washed platelets or PRP were added to the migration buffer to reach a final concentration of 10x10^3 platelets/μl. Platelet spreading and migration were subsequently observed using time-lapse video microscopy.

3.10 Characterization of plasma coated surfaces

AFM measurements were carried out on a Dimension 3100 AFM with a Nanoscope IV controller (Bruker, Santa-Barbara, California) in ambient conditions. The measurements were performed in tapping mode, to minimize abrasion of the molecule layer by the AFM tip. Silicon cantilevers (NSC 35 AIBS C, Mikromasch, Estonia) with a nominal

resonance frequency of 150 kHz, spring constant of 4.5 Nm^{-1}, and tip diameter of less than 10 nm were used (Davydovskaya et al., 2012). Immunostainigs of fixed plasma coated coverslips were performed using the following primary antibodies (anti-fibrinogen (ab34269, Abcam) , anti-vWF (ab6994, Abcam) , anti-fibronectin (ab2413, Abcam)). Slides were incubated with antibodies for 1h at room temperature, washed with PBS and stained with Alexa 488 labeled secondary antibodies (Molecular Probes) for another hour.

3.11 Flow chamber assay

To observe platelet migration under flow conditions circular glass cover-slips (30 mm, Bioptechs) were pretreated as described above and placed into a parallel plate flow chamber (FCS2, Bioptechs). Coverlips were incubated with migration buffer (tyrode's buffer pH=7.4, serum (1500 μg/ml), fibrinogen (150 μg/ml), ADP (4 μM) / U46619 (2 μM)) and washed platelets (10x10^3 platelets/μl) were added after 5min. Once fully spread the flow-chamber was perfused with migration buffer (shear rate: 1300/s) using a recirculating air pressure pump (Ibidi) and migration was observed using time-lapse microscopy.

3.12 Time-lapse video microscopy

Differential interference contrast (DIC) movies (1frame every 12s) were recorded on an automated inverted IX83 Olympus microscope with an UPlan 40x/1.0 oil-immersion objective (Olympus) and a cooled CCD camera (XM10, Olympus). The microscope was equipped with a stage incubator (37°C, humidified) (Tokai Hit).

3.13 Tracking protocol

Spreading and migrating platelets were manually counted and tracked using the "'Manual Tracking"' or the "'MTrackJ"' plugin in FIJI (Schindelin et al., 2012; Meijering et al.,

2012) and the fraction of migrating platelets was calculated by dividing the total number of spreading platelets by the number of migrating platelets. The pseudonucleus of a migrating platelet served as a morphological landmark for tracking. Platelets covering a distance ≥1 platelet diameter were classified as migrating. Single cell velocities were only measured for freely migrating platelets, not in contact with neighboring platelets. In some experiments, the straightness of migration was calculated by dividing the Euclidean distance of migration by the accumulated distance of migration. The directionality towards a vessel injury was quantified by the forward migration index (FMI), defined by the ratio of the fractional displacement along the line connecting starting point of migration and injury and the total accumulated distance of migration; maximal directionality = 1; minimal directionality = -1. The duration of platelet migration is plotted in respect to the initial starting-point within the observation time and duration $_{\text{effective}}$ / duration $_{\text{max}}$ defines the ratio of the effective duration of migration or spreading and the maximum duration possible in respect to the initial starting-point. For representation of *in vivo* migration tracks the starting points were normalized to zero and plotted in respect to the direction of blood flow or the localization of the vessel injury. To illustrate the localization of platelet migration in the context of micro-thrombus formation, migration tracks of individual platelets from independent experiments were manually aligned, scaled and depicted in respect to the site of injury and the thrombus core region. Migration dependent micro-aggregate formation was measured by counting aggregates (≥ 2 platelets) during the course of the migration assay (30 min, Image size=900x690 pixel (114x86 μm) (8-bit)). Platelets were manually tracked in MTrackJ and the positions of single platelet centroids were represented as closed white circles with opacity adjusted to 50% (diameter=20px, gray-value=184) (Meijering et al., 2012). During aggregation, circles were overlapping and thus the opacity further decreased (gray-value≥185). Platelet-aggregates were classified based on the increased grey value (≥2 platelets, gray-value≥185) and counted automatically. Heat maps illustrating retraction speed were generated using QFSM software (Mendoza et al., 2012).

3.14 Shape analysis

We performed an unbiased, systematic analysis of platelet shapes to analyze the morphological variations of migrating and non-migrating platelets without pre-selecting partic-

ular shape measurements (e.g. area, cell-diameter...). Platelet shapes were represented as polygonal outlines and principal component analysis (PCA) was performed to extract principal modes of shape variation along which to measure each platelet (Fig. 3.4). Platelet shapes from DIC movies were manually masked and converted into binary images using FIJI (Schindelin et al., 2012). Polygonal outlines were extracted from masks and sampled at evenly spaced 200 points. To ensure, that all polygons were orientated equally, an algorithm based on Procrustes analysis was used to rotate and translate the polygons until corresponding points were optimally aligned. Next, we used the pseudonucleus as a characteristic landmark defining the rear of a migrating platelet. The pseudonuclei were manually marked in FIJI and extracted to another set of binary images. This additional landmark was also used in the Procrustes procedure and improved the alignment. Finally the alignment was manually verified. Aligned contours were further analyzed by principle component analysis (PCA). The principle components, scaled by the standard deviation of the analyzed population for each mode of shape were depicted. To explore whether the classified shape modes allow the discrimination of functionally distinct platelet subpopulations (e.g. migrating vs. non-migrating), platelet polygons were arrayed in a scatterplot. Finally, the following cellular characteristics were measured based on shape modes detected by PCA: (1) Area in μm^2 (mode 1) and (2) Aspect Ratio = long axis/short axis (mode 2). In some experiments polygon curvature was measured as an approximation of membrane roughness. The average of the absolute values of the pointwise curvature of the contour is computed over a specified range, and multiplied by the contour length over the same range. Absolute values must be used because otherwise positive and negative curvatures would cancel out; the sum is multiplied by the arc length to make the measurement scale-invariant. All algorithms are implemented in the "'Celltool"' software package (Pincus and Theriot, 2007). To analyze the spatio-temporal coordination of leading-edge protrusion and trailing edge retraction kymographs were extracted along the central axis of migrating platelets.

3.15 Fura-2 imaging

Platelets were loaded with 5 μM Fura-2/AM (Invitrogen) at 37°C 25 minutes before imaging. Fura-2 images were taken on an inverted iMIC2 (Fei) stand equipped with

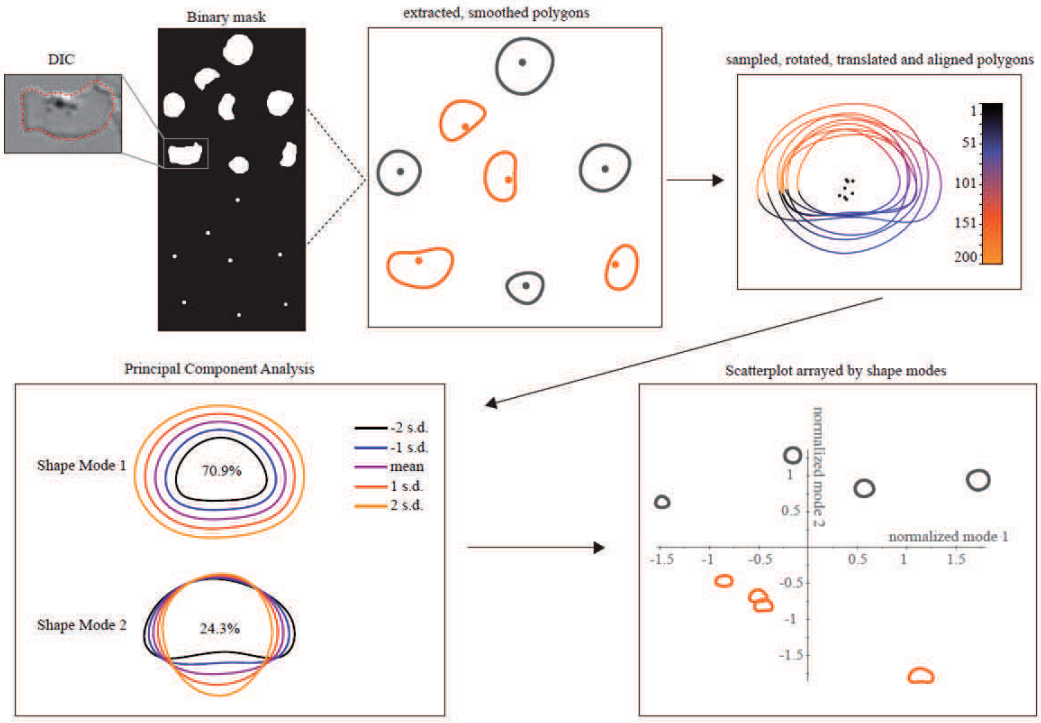

Figure 3.4 – Platelet shape analysis. Sequential steps of shape analysis as measured by Principle Component Analysis are depicted. More detailed information can be found in the text and Pincus and Theriot (2007).

a climate chamber (37°C, humidified) (Ibidi) and using an UplanSApo 60x/1.35 oil-immersion objective (Olympus). 340nm and 380nm filters were used for the excitation of Ca^{2+}-bound Fura-2 and Ca^{2+}-free Fura-2, respectively and emission at 510 nm was captured with an EMCCD camera (iXon 897, Andor), gain=120. Time-lapse movies were recorded with a frame rate of 1/30 s. Image processing was performed as previously published by using ImageJ (Kardash et al., 2011; Tsai and Meyer, 2012). A mask image to separate platelets and the background was created by manually drawing the platelet contour in the brightfield image. Background subtraction was performed using the "'rolling ball"' algorithm. To determine intracellular Ca^{2+} ocillations, the ratio images (Ca^{2+}-bound/Ca^{2+}-free) were created by dividing the images generated using 340 nm over 380 nm excitation of Fura-2.

3.16 Immunofluorescence of pMLC and $\alpha_{IIb}\beta_3$

Polarized, migrating or spread, non-migrating platelets were fixed at 37°C in 1% paraformaldehyde for 10 minutes. Platelets were washed three times with PBS and incubated with 2% Glycin (Roth) for 5min, followed by incubation with 0.2% Triton X-100 (Fluka) and 3% bovine serum albumin (Roth), to permeabilize the cells and to block unspecific binding, respectively. For pMLC (Ser19) staining, cells were incubated for 1h at RT with primary antibodies (1:50, # 3671, Cell Signaling) followed by 1h at RT with secondary antibodies (goat anti-rabbit IgG Alexa 488, 1:200, A11008, Molecular Probes). For $\alpha_{IIb}\beta_3$ staining, platelets were incubated for 1h at RT with primary antibodies (1:50, HIP8, Abcam) followed by 1h at RT with secondary antibodies (goat anti-mouse IgG Alexa 488, 1:200, A11001, Molecular Probes). Activated $\alpha_{IIb}\beta_3$ was stained in live cells during migration for 20min (PAC1-FITC, 1μg/ml, BD) followed by incubation for 1h at RT with secondary antibodies (rabbit anti-FITC Alexa 488, 1:200, A11090, Molecular Probes). Filamentous actin was stained by Rhodamin-Phalloidin (1:40, Molecular Probes). Images were captured on a Zeiss LSM 780 confocal microscope using a Plan-Apochromat 100x/1,46 Oil DIC objective (Carl Zeiss Imaging).

3.17 pMLC Westernblot

Washed human platelets, resuspended in migration buffers were activated in the presence or absence of 100 mM citrate. In some experiments platelets were pretreated with BAPTA-AM (10 μM). After the indicated time points platelet suspensions were centrifugated at 1900g for 8 min at RT in a microcentrifuge. Obtained platelet pellets were lysed in ice cold RIPA buffer (20 mMTris-HCl-pH 7.5, 150 mMNaCl, 1 mM EDTA, 1 mM EGTA, 1% IGEPAL, 2.5 mM sodium pyrophosphate, 1mM β-glycerophosphate, Pierce) containing protease and phosphatase inhibitor cocktails (cOmplete Mini, EDTA-free, Roche and Halt Phosphatase Inhibitor Cocktail, Pierce). After incubation on ice for 15 min insoluble cell debris were removed by centrifugation at 16,000g for 15 min at 4°C in a tabletop microcentrifuge, protein concentrations were quantified using Bio-Rad DC protein assay reagents and an appropriate amount of supernatants containing 40 μg total protein was mixed with 1/5 volume of 5x Laemmli sample buffer containing 5% 2-mercaptoethanol, heated at 95°C for 5 min and subjected to SDS-polyacrylamide elec-

trophoresis under reducing conditions using precast Novex 4-20% Tris-Glycine gradient gels (Life Technologies). Resolved proteins and prestained standards were transferred to nitrocellulose membranes (Life Technologies) by using a Semi-Dry Transfer Unit (Sigma Aldrich), probed with an antibody directed against phosphorylated Myosin Light Chain (1:1000, Abcam) and the signal was normalized for that of total Myosin Light chain using an antibody against Myosin Light Chain (1:1000, Cell Signaling Technology). Immunreactive protein bands were detected using horseradish peroxidase-labeled secondary antibodies (1:2000, Cell Signaling Technology) and enhanced chemiluminescence Western blotting detection reagents (Perkin Elmer).

3.18 Statistical analysis

T-tests and analysis of variance (ANOVA) were performed after data were confirmed to fulfill the criteria of normal distribution (Kolmogorov-Smirnov-test), otherwise Kruskal-Wallis tests or Wilcox-rank-sum test were applied. If overall ANOVA or Kruskal-Wallis tests were significant, we performed a post hoc test (Tukey-HSD for ANOVA and Wilcox rank sum post hoc test for Kruskal-Wallis, respectively. Analyses were performed with R (http://www.r-project.org/).

4 Results

4.1 In vivo tracing of single platelets during thrombus formation reveals yet unidentified motility pattern

Platelet-rich thrombi are rapidly formed following vascular injury and spatially coordinated platelet-platelet interactions are required for preventing extensive blood loss. Two-photon intra-vital microscopy provides a powerful tool to study the dynamics of cell-cell-interactions with high spatial resolution deep within tissue and was recently demonstrated to permit visualization of thrombus formation in several vascular injury models (Koike et al., 2011; von Brühl et al., 2012). However, due to the small size and the high number and density of individual platelets within a hemostatic thrombus, dynamical analysis on a single platelet level is technically challenging. In order to overcome this problem and to trace individual platelets and their interactions within thrombi *in vivo*, we generated a multicolor platelet reporter mouse. *R26R-Confetti* were cross-bred with megakaryocyte/platelet-specific *PF4-Cre*-mice to generate *PF4-Cre/R26R-Confetti* or *PF4-Cre/R26R-Confetti*-mice (Tiedt et al., 2006; Snippert et al., 2010). After Cre-mediated recombination the *R26R-Confetti*-Reporter stochastically drives expression of one of the four fluorescent proteins mCFP, nGFP, cYFP or cRFP (Snippert et al., 2010). Megakaryocytes are polyploid cells with mean ploidy levels of 16N (Corash et al., 1987). Thus, megakaryocytes express more than one R26R-Confetti-transgene and Cre-recombination results in combinatorial expression of multiple fluorescent proteins (Livet et al., 2007) (Fig. 4.1). Indeed, when we examined *PF4-Cre/R26R-Confetti* -mice, we detected co-expression of multiple colors in individual megakaryocytes resulting in distinct combinatorial XFPs (Fig. 4.2). Most importantly, color diversity was retained on a platelet level, permitting unique single cell contrast within tightly packed platelet rich thrombi *in vitro* and *in vivo* (Fig. 4.3).

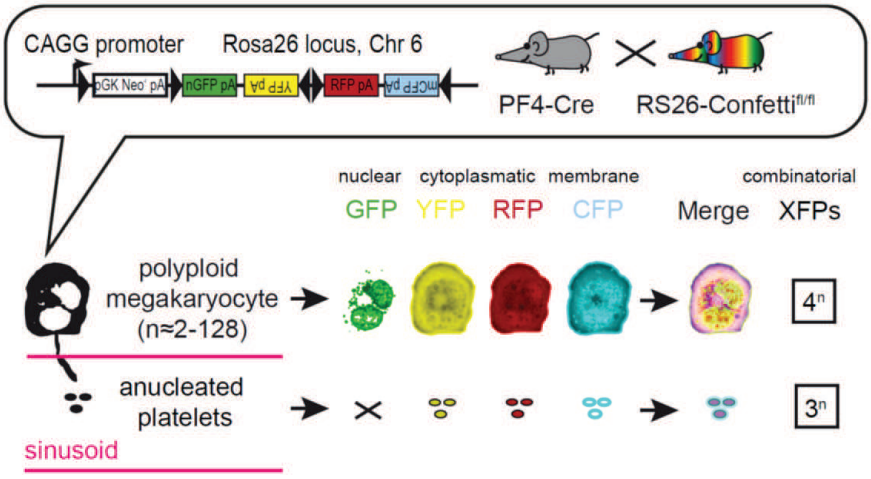

Figure 4.1 – Principle of multicolor labeling of megakaryocytes and platelets using the *PF4-Cre/R26R-Confetti*-mouse model.

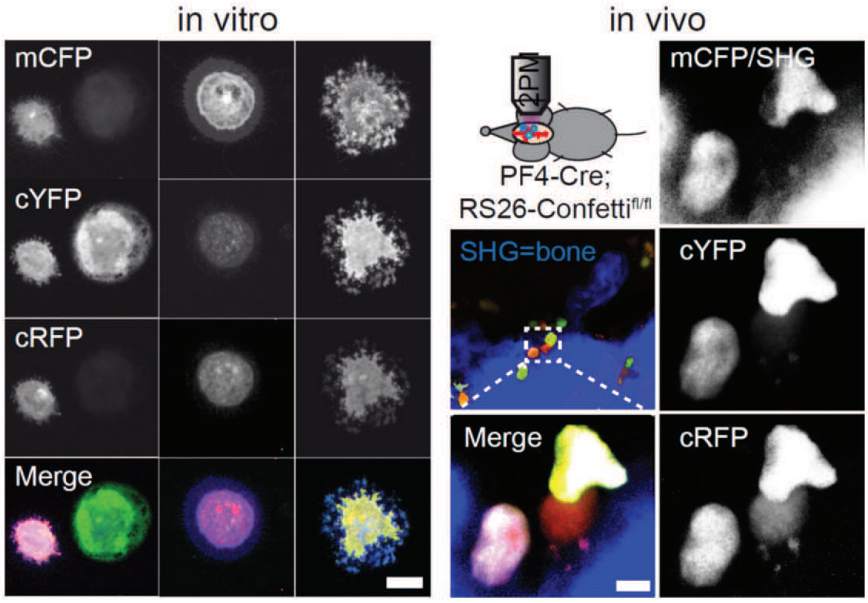

Figure 4.2 – Confocal sections of megakaryocytes isolated from *PF4-Cre/R26R-Confetti*-mice (left penal). Intravital 2-photon microscopy of the calvarian bone of *PF4-Cre/R26R-Confetti*-mice. Note that our imaging setup could not detect GFP-positive nuclei. SHG=Second Harmonic Generation. Scale bar=20μm.

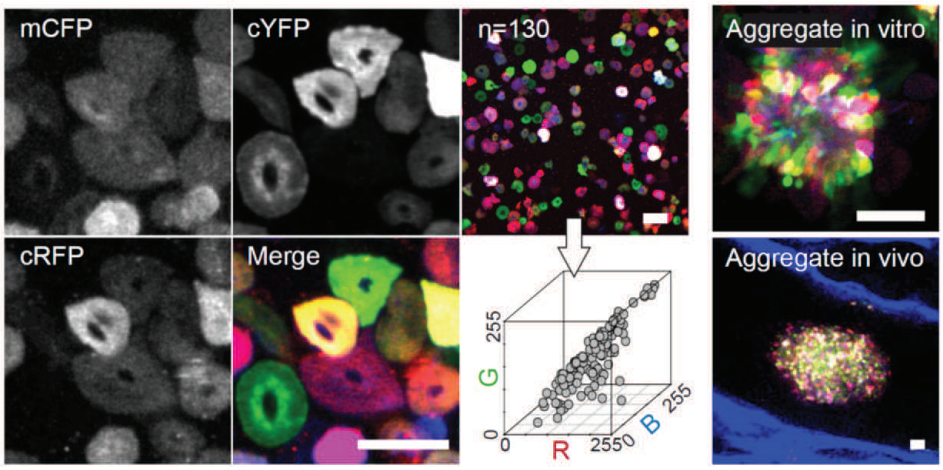

Figure 4.3 – Left panel: Confocal sections of spreading platelets isolated from *PF4-Cre/R26R-Confetti*-mice. CFP, YFP and RFP are co-expressed and result in combinatorial XFP expressions. Note that single platelets have distinct coordinates in RGB-colorspace. Right panel: Distinct colorization permits single platelet tracing within aggregates formed *in vitro* (confocal microscopy) and *in vivo* (2-photon-microscopy). Scale bars=10 μm

Using *PF4-Cre/R26R-Confetti*-mice, we analyzed the spatio-temporal dynamics of thrombosis on a single platelet level in two different models (needle and laser-induced injury) by intravital two-photon microscopy (2P-IVM; Fig. 4.4). At early stages of thrombus formation, platelets roll in the direction of blood flow, followed by adhesion and the formation of loosely packed aggregates of discoid platelets (Fig. 4.5, Movie 1) (Maxwell et al., 2006). Platelets subsequently adopt a spherical shape and jointly retract, leading to the collective centripetal translocation of adjacent platelets towards the centroid of injury (Fig. 4.6, Movie 1). Recurring cycles of these steps eventually generated a multilayered thrombus with a stable core region and less densely packed platelets at the periphery (Fig. 4.6) (Stalker et al., 2013). Interestingly, when individual platelets were monitored over a time course of $\approx$ 2-10 min we observed additional as yet undescribed motility patterns: Single adherent platelets in the periphery of a thrombus remained motile and rearranged their position independent of the collective contractile movement, suggesting autonomous motility (Fig. 4.7 and Movie 1). The mean velocity of these platelets was significantly lower and migration paths were less straight compared to platelet rolling and clot retraction (Fig. 4.8). The directionality was independent of blood flow and platelets were able to migrate against the shear stress, suggesting that this is an active process rather than a passive translocation (Fig. 4.7). Migration tracks were

not directed at the localization of the injury, suggesting that the local micro-environment surrounding individual platelets provides the primary signal controlling their migration (Fig. 4.7, Fig. 4.9). Together, the above findings provide the first *in vivo* evidence of platelet migration within the thrombus, facilitating spatio-temporal re-localization of individual platelets.

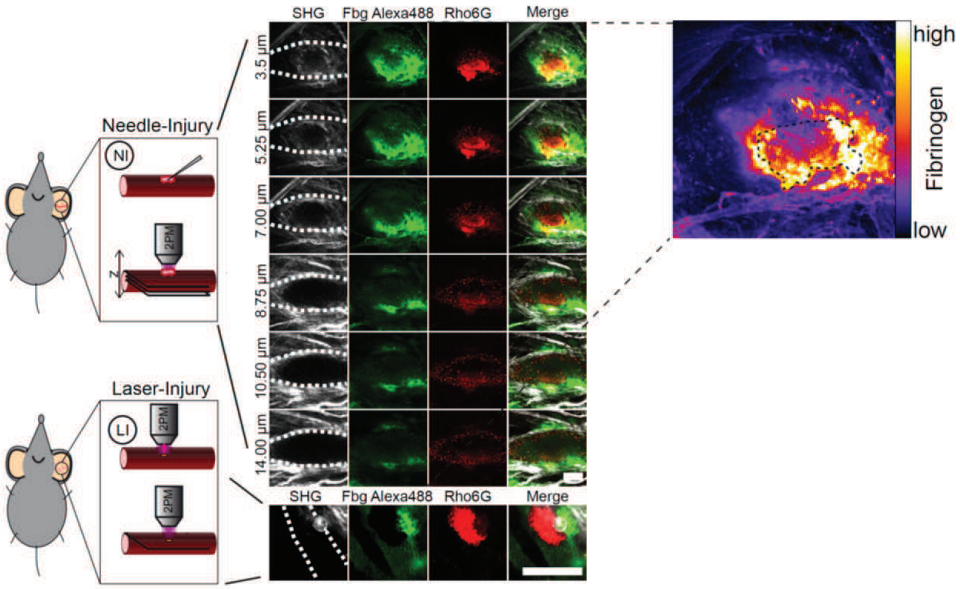

Figure 4.4 – Injury models of thrombus formation in the microcirculation of the ear. Needle-Injury was induced using a 30G needle and a z-scan of the vessel surface shows the localized injury. Laser-Injury was induced by focusing the laserbeam of the 2-photon microscope on the vessel wall. Note the destroyed collagen architecture (SHG) and the accumulation of fibrinogen/fibrin at the site of injury (Fbg-Alexa488) in both injury models. Fibrin(ogen) is inhomogeneously distributed around the injury with a maximum at the center of the lesion, as highlighted by the color-coded intensity of Alexa-488-labeled fibrinogen. Dashed lines indicate the vessel wall. Scale bar=50μm.

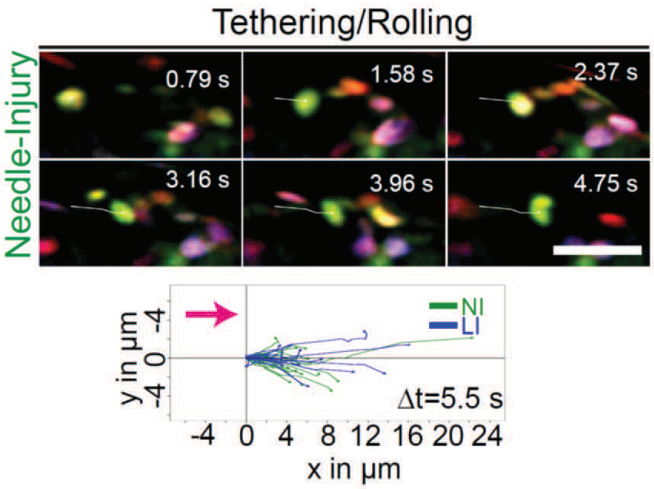

Figure 4.5 – Upper panel: Visualization of platelet tethering/rolling using intravital 2-photon-microscopy of *PF4-Cre/R26R-Confetti*-mice. Platelet tracing is highlighted by the white line. Lower panel: Directionality plots of rolling platelets. Platelet tracks are orientated with respect to the direction of the blood flow (pink arrow). Scale bar=10μm.

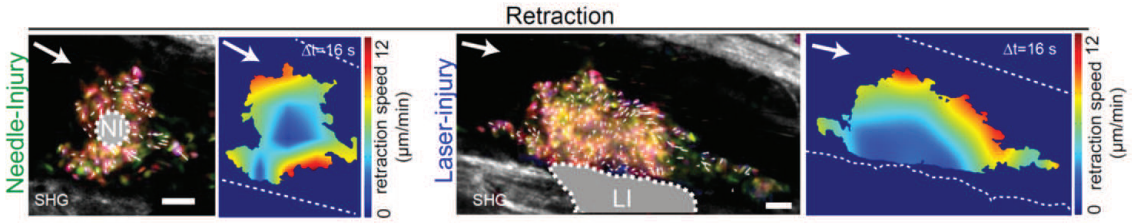

Figure 4.6 – Visualization of clot retraction using intravital 2-photon-microscopy of *PF4-Cre/R26R-Confetti*-mice. Vector maps are overlaid (white arrows); heat maps show retraction speed. Dashed white line highlights the injury. Scale bar=10μm.

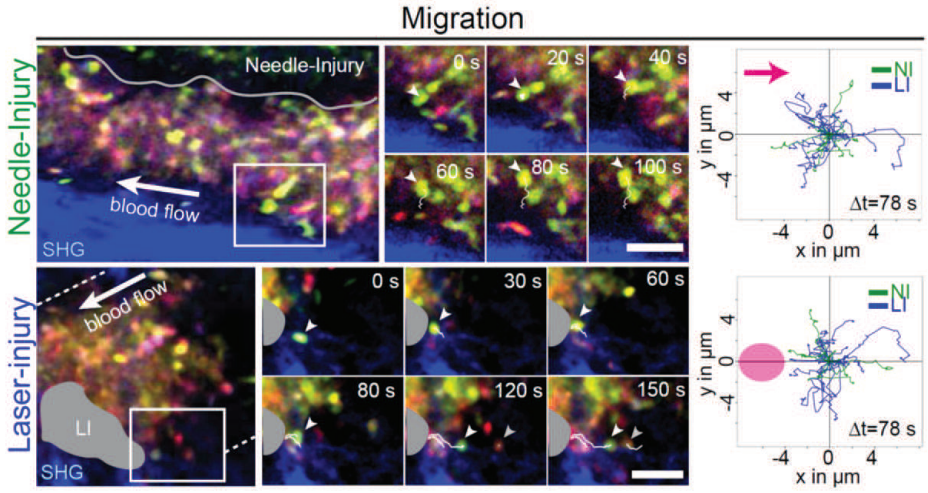

Figure 4.7 – Visualization of platelet migration using intravital 2-photon-microscopy of *PF4-Cre/R26R-Confetti*-mice. Migrating platelets are highlighted by arrow-heads and migration paths are indicated as white lines. Directionality plots of migrating platelets are shown and platelet tracks are orientated with respect to the injury (pink circle) (lower) or direction of the blood flow (pink arrow) (upper). Scale bar=10μm.

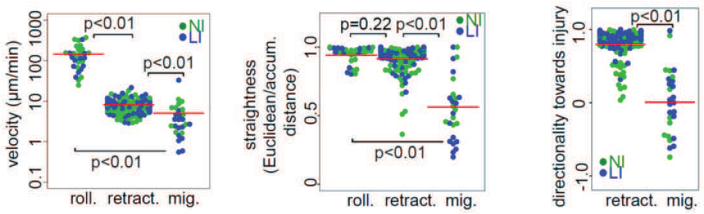

Figure 4.8 – Quantification of velocity and straightness (euclidean distance / accumulated distance) of rolling, retracting and migrating platelets. Directionality was measured by the forward migration index (FMI). Each dot represents a single platelet. rolling: n=30 pooled from 4 experiments; retraction: n=115 pooled from 2 experiments; migrating: n=27 pooled from 11 experiments). Red bars = mean. Kruskal-Wallis/Pairwise Wilcox. SHG=Second Harmonic Generation; NI=Needle-Injury; LI=Laser-Injury. Δt indicates mean observation time.

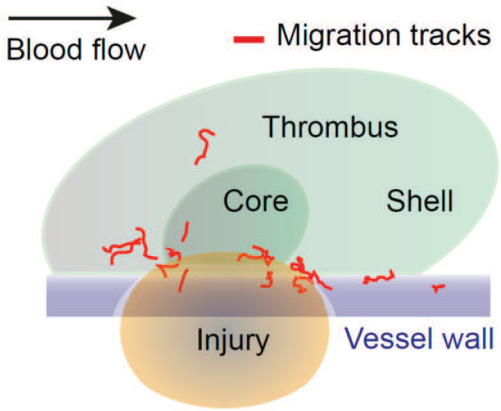

Figure 4.9 – Migration tracks of individual platelets were manually aligned, scaled and depicted in respect to the site of injury and the thrombus core region. Please note the preferential localization at the outer border of the injury and the thrombus core region.

4.2 Spreading platelets are motile and have a distinct shape

To address the patterns and mechanisms of platelet migration in greater detail *in vitro*, we added platelet-rich plasma (PRP) to coverslips precoated with fibrillar collagen plus plasma (see Material and Methods). By differential interference contrast (DIC) microscopy we visualized individual platelets and collagen fibers *in vitro* (Fig. 4.10). Platelets that encountered collagen fibers immediately started to spread and recruited additional platelets from the supernatant, forming immotile micro-aggregates. In contrast, spreading platelets that did not contact collagen fibers rearranged their morphology and became motile, migrating until reaching a collagen fiber and/or a collagen-bound immotile micro-aggregate (Fig. 4.10).

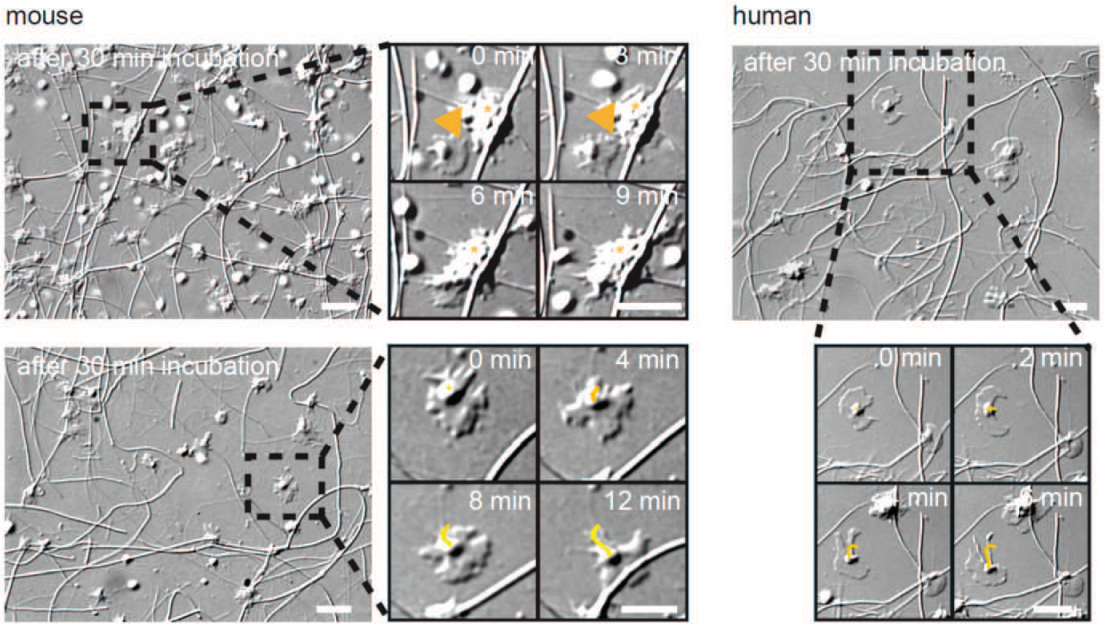

Figure 4.10 – Platelets polarize and migrate on immobilized plasmaproteins in the presence of collagen fibers. Platelets spreading on plasmaproteins and fibrillar collagen after 30min of incubation were visualized by DIC microscopy. Time lapse movies of motile platelets were subsequently recorded. Motile platelets (arrowhead) were either incorporated into a micro-aggregate (*) (upper left) or stuck to collagen fibers (lower left). Motility was observed in mouse (left) as well as human (right) platelets. Scale bar=10μm.

During initiation of migration, platelets undergo a stereotypic cascade of morphological changes occurring irrespective of the initial platelet size (Fig. 4.11 and Movie 2). Platelets first spread, developing a fried-egg-like shape with high circularity (aspect-ratio $\approx$1) (Fig. 4.11). Subsequently, platelets polarize by protruding one side of the lamellipodium and simultaneously retracting the opposite side. (Fig. 4.11). During this process the pseudonucleus moves from the center to the rear of the platelet. At the same time, the aspect ratio increases to approximately 2, as the now migrating platelet adopts a half moon shape (Fig. 4.11).

To quantify the above morphological changes, we used an approach previously described for migrating fish keratocytes, which closely resemble the morphodynamic changes of migrating platelets (Keren et al., 2008). Briefly, we defined the cell shape by principal components analysis of aligned cell outlines from a large platelet population containing both spread, non-migrating platelets and polarized, migrating platelets. Approximately 82% of the total shape variation within the studied population was captured in two

orthogonal shape modes, approximately representing cell area (mode 1; 63% of total shape variability) and the cell's aspect ratio (mode 2; 19% of total shape variability) (Fig. 4.12). The largest shape variability represented by mode 1 (63% of total shape variability) is unable to separate spread, non-migrating from polarized, migrating platelets (Fig. 4.12), indicating that the variability of cell area is similar in both populations. In contrast, mode 2 (19% of total shape variability) clearly separates both groups, whereas the higher shape modes were also mainly overlapping (Fig. 4.12). Consequently, circularity (mode 2) is the key morphological feature separating spread, non-migrating from polarized, migrating platelets. This is consistent with our initial morphological observation, that once getting motile platelets change their shape predominately by loosing circularity developing a characteristic fan shaped lamellipodium (Fig. 4.11). In most eukaryotic cells shape change and maintenance are active cellular processes requiring assembly and disassembly of actin filaments (Rafelski and Theriot, 2004; Pollard and Cooper, 2009). Cytochalasin D is a potent, cell-permeable inhibitor of actin polymerization by binding to the barbed ends of actin filaments (F-actin) and thereby inhibiting actin subunit (G-actin) addition (Casella et al., 1981; Fox and Phillips, 1981). When we added cytochalasin D, a potent, cell-permeable inhibitor of actin polymerization, platelets immediately stopped migrating, followed by shrinkage of the leading-edge (Fig. 4.13 and Fig. 4.14 and Movie 2). This indicated that actin polymerization is not just an indispensable requirement for initial platelet spreading (Olorundare et al., 1992), but also essential for maintaining platelet migration. In line with this observation, single platelet analysis revealed an immediate stop of the leading-egde protrusion followed by a decrease in the centroid velocity, after incubation with cytochalasin D (Fig. 4.13). Due to lamellipodial shrinkage the projected platelet area decreased and membrane roughness increased, leading to a more irregular platelet shape (Fig. 4.13). Shape analysis of a large platelet population revealed a significant shift towards smaller areas (Fig. 4.14). Importantly, these morphological changes resulted in an immediate, complete inhibition of platelet migration (fraction of migrating platelets=0%; Fig. 4.15), while platelet spreading was initially maintained (Fig. 4.15). Hence, platelet locomotion is an active process initiated by a cascade of morphological changes that depend on actin polymerization.

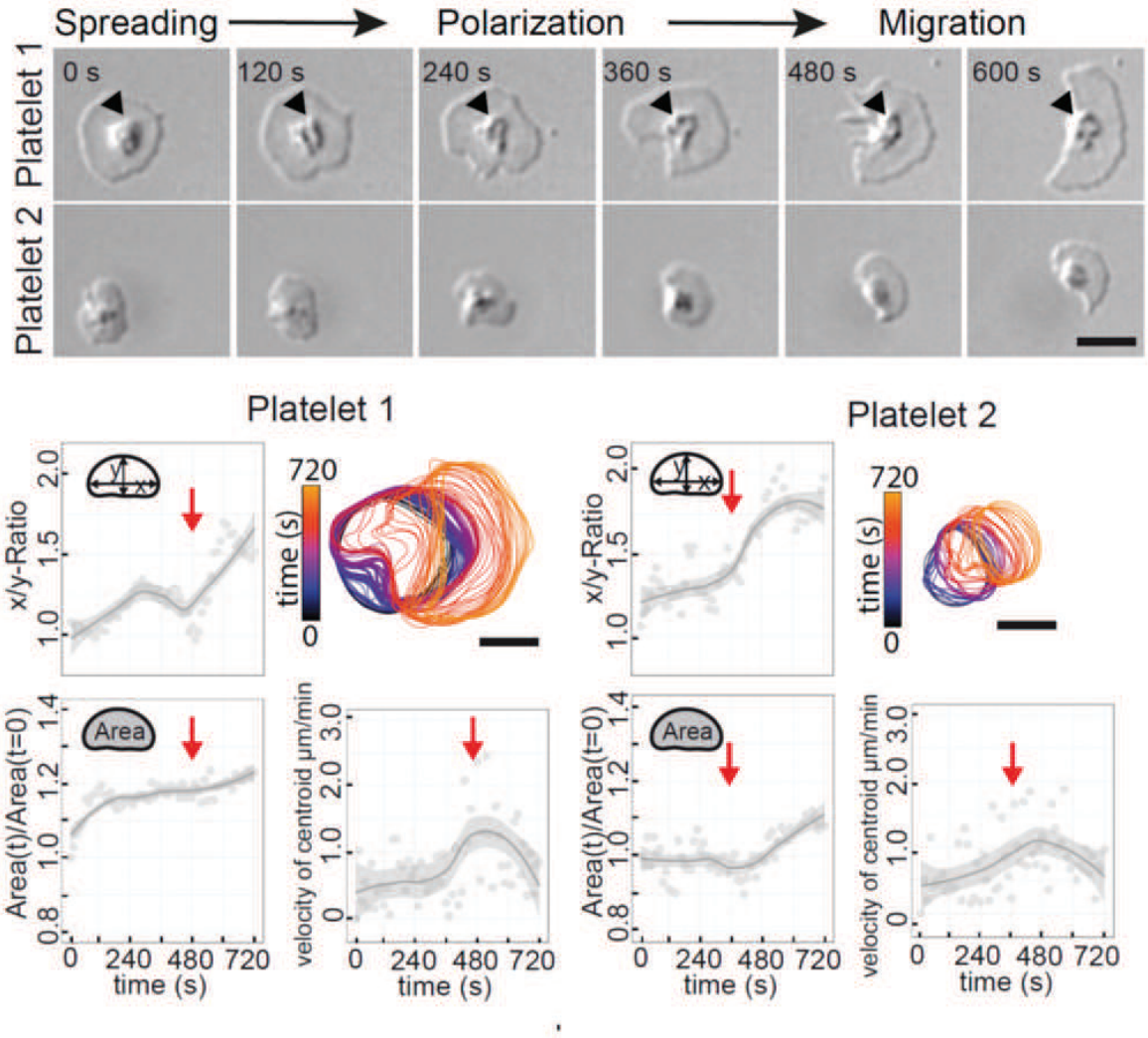

Figure 4.11 – Spreading platelets polarize *in vitro*. Upper panel: DIC microscopy reveals the sequential steps of polarization from a circular-spreading platelet (0s) to a fan-shaped-migrating (600s) platelet. Arrowheads indicate the pseudonucleus being relocated to the trailing edge after platelet polarization. These processes occur independent from platelet size (Platelet 1 > Platelet 2) Scale bar= 5μm. Lower panel: Color-coded time sequence of the platelet outline. Note, that rear retraction is slightly faster than front protrusion, resulting in an increase of the aspect ratio. Aspect ratio, proportional increase in area and centroid velocity were continuously recorded over a time span of 720 seconds. Scale bar=5μm.

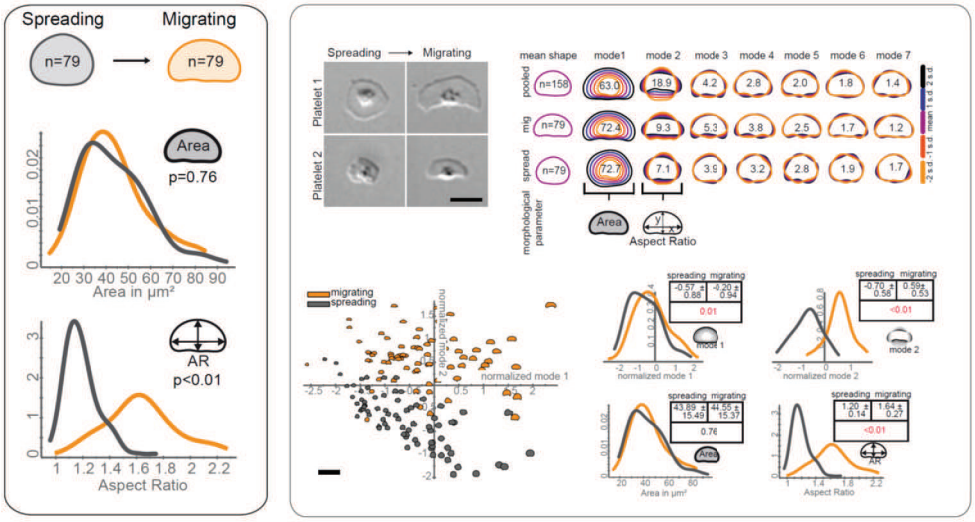

Figure 4.12 – Platelets actively migrate in vitro by adapting a characteristical shape. Left: Polarized, migrating platelets were quantitatively discriminated from spreading, non-migrating platelets by shape. Smooth density histograms displaying area and aspect ratio (x-axis) as a density function (y-axis). p-values<0.05 indicate significance; paired t-test (Area, Aspect Ratio). Right: DIC images of representative platelets before and after polarization (upper left). Upper right: The mean shape and the principal modes of shape variability are shown for the spreading-non-migrating, the polarized-migrating and the pooled platelet population; measured platelet numbers are indicated. For each shape mode of each platelet population the mean shape and the first and second standard deviation is shown. The contribution of each shape mode to the total shape variation within the population is indicated in %. Each shape mode is assigned to a characteristic morphological parameter: area and aspect-ratio. Scale bar=5μm. Lower left: Scatter plots arraying spreading-non-migrating and polarized-migrating platelets by SD-normalized shape mode 1 and 2. Scale bar=25μm. Lower right: Smooth density histograms displaying shape modes, area, aspect ratio (x-axis) as a density function (y-axis). Notice the similarity in the population-shift when measuring mode 2 and aspect ratio. The table shows mean±SD; p-values<0.05 (red) indicate significance; paired t-test (mode1, mode2, mode3, Area, Aspect Ratio).

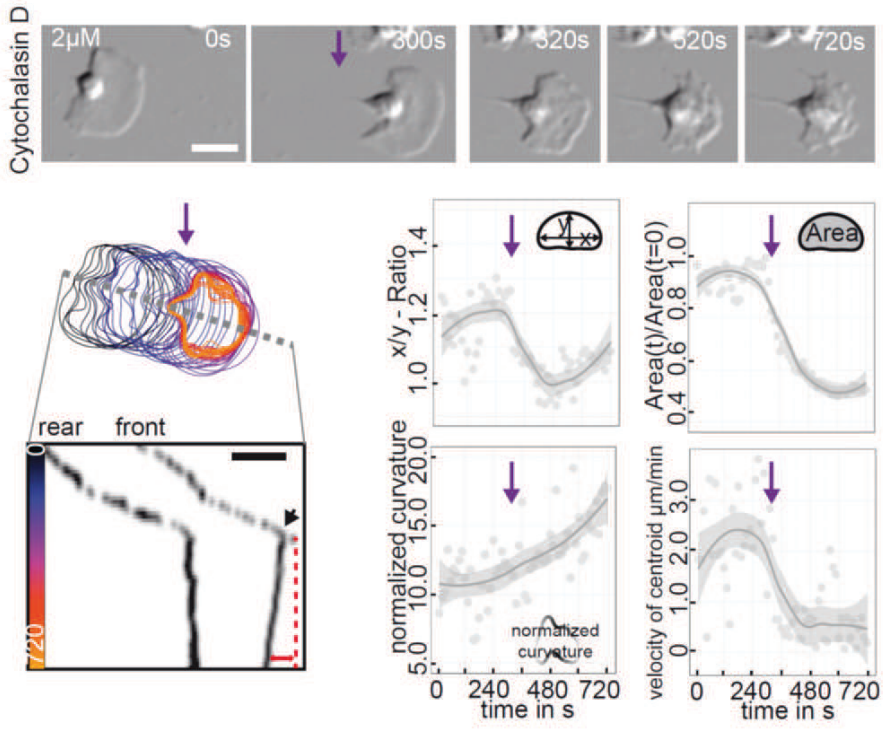

Figure 4.13 – Platelet migration critically depends on actin-polymerization. DIC time series of a representative Cytochalasin D (Cyto D) (2μM) treated platelet, spreading on immobilized plasma-proteins (upper panel); Scale bars=5μm. The color-coded platelet outlines (time) and the corresponding kymograph reveal the immediate stop of platelet migration (arrow) and the subsequent shrinkage of the lamellipodium (lower left). Tracing of x/y-Ratio, Area, Centroid-velocity, normalized curvature over time (lower right). Platelets were pooled from n=5 experiments.

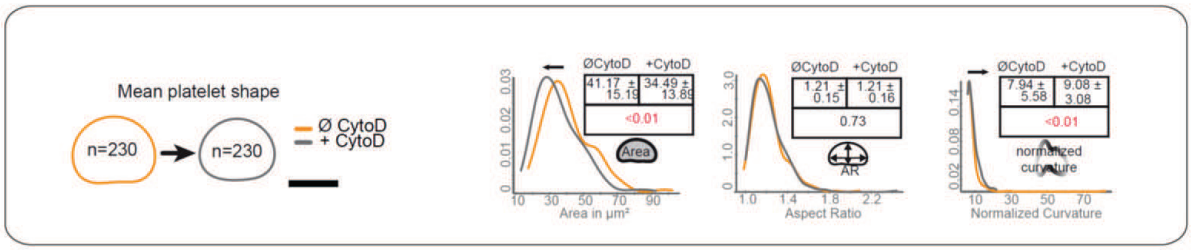

Figure 4.14 – The mean shape for vehicle and Cytochalasin D treated platelets is shown; Scale bar=5μm (left panel). Smooth density histograms displaying shape modes, area and aspect ratio before and after Cytochalasin D treatment; the table shows mean±SD; p-values<0.05 (red) indicate significance; platelets were pooled from n=5 experiments; paired wilcox test (left panel).

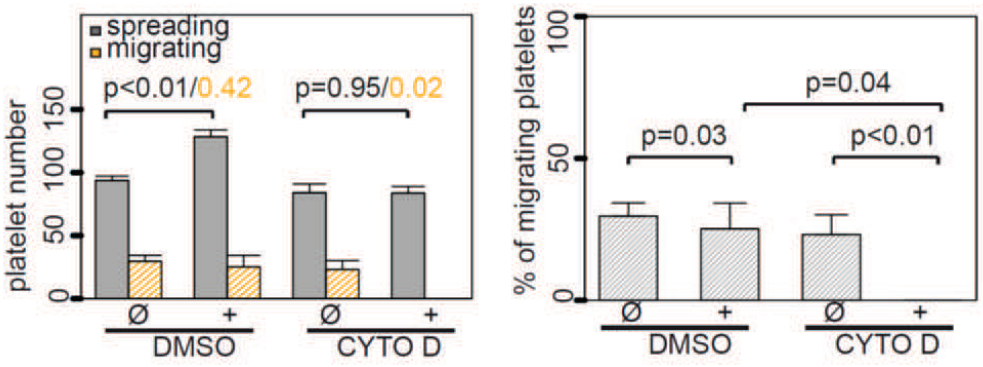

Figure 4.15 – Total number of spreading and migrating platelets per experiment, fraction of migrating platelets before and after Cytochalasin D (2μM) treatment. Platelets were pooled from n=5 experiments; error bars=SEM; paired t-test.

4.3 The soluble platelet activators TXA2 and ADP cooperate to trigger platelet chemokinesis

Platelet migration was only observed when platelets were not in direct contact with collagen fibers (Fig. 4.10). Nevertheless, migration was virtually absent when collagen was completely removed (Fig. 4.11). Collagen is known to trigger the release of secondary platelet mediators (Atkinson et al., 2001; Nieswandt et al., 2001). Hence, we hypothesized that migration of platelets without physical contact to collagen might require priming through paracrine soluble mediators released by platelets interacting with collagen. To test this, we examined platelet migration on plasma-coated but collagen-free coverslips in the presence of supernatant from either collagen-activated or resting platelets (for details see Materials and Methods). The supernatants of collagen-activated, but not of resting platelets facilitated platelet spreading and significantly enhanced platelet migration (Fig. 4.16A).

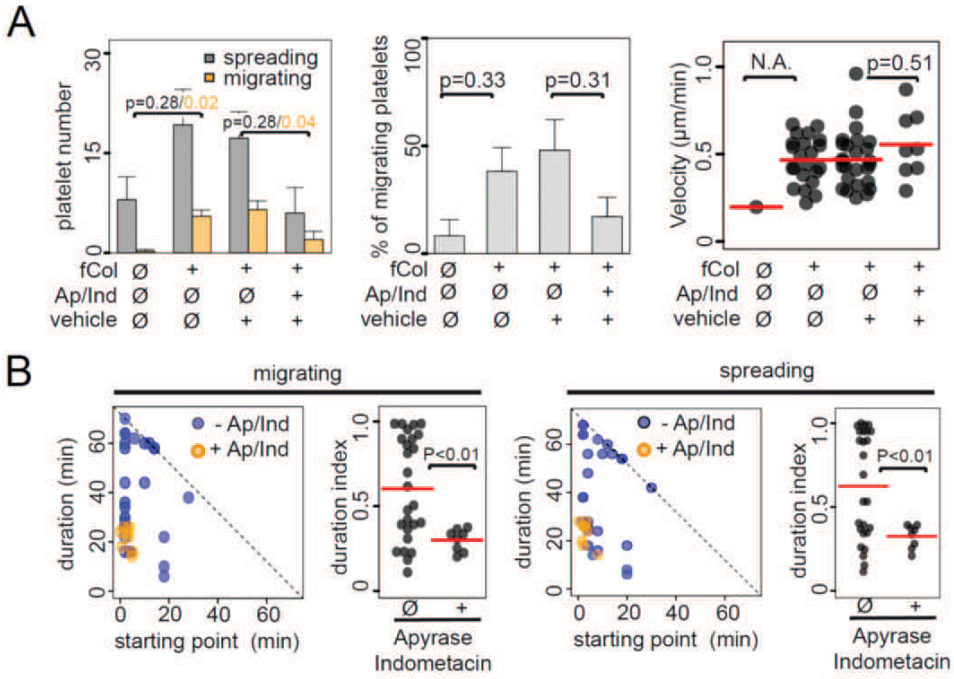

Figure 4.16 – Collagen induced ADP and TXA_2 secretion triggers platelet chemokinesis. A, Time-lapse movies of migrating platelets were recorded in the presence of conditioned platelet supernatants generated with or without activation by fibrillar collagen (+/- fCol) and in the presence or absence (+/- Ap/Ind) of Apyrase (2U/ml) and Indomethacin (10μM) . The total number of spreading and migrating platelets per experiment, fraction of migrating platelets and migration velocity are depicted. Platelets were pooled from n=4 experiments: -fCol: n=54, +fCol: n=57, -Ap/Ind: n=83, +Ap/Ind: n=27; red bars indicate mean velocity; error bars=SEM; student's t-test. B, Duration of single platelet migration (left panel) and single platelet spreading (right panel) was plotted in respect to the initial starting-point within the observation time of 65 min. The duration index is defined as the ratio of the effective duration of migration or spreading and the maximum duration possible in respect to the initial starting-point. Red bars indicate mean; platelets were pooled from n=4 experiments: -Ap/Ind: n=83, +Ap/Ind: n=27; student's t-test.

Previous studies have shown that activation by collagen induces ADP secretion from platelet dense granules, as well as formation and subsequent release of Thromboxane A_2 (TXA_2) (Packham et al., 1991; Ryningen et al., 1999). Pretreatment with indomethacin and apyrase (to inhibit TXA_2 formation and to degrade ADP, respectively) prior to collagen exposure significantly attenuated the effect of platelet supernatants on both platelet spreading as well as migration (Fig. 4.16A and Movie 3), with a significant reduction in the durability of both processes (Figure 4.16B). Correspondingly, a stop of migration indeed often preceded a termination in spreading on the single platelet level (Fig. 4.17). Platelet shape did not significantly differ between the groups (Fig.

4.18). These findings have two major implications: one, migration depends on spreading and two, collagen-induced ADP and TXA_2 release is sufficient to prime and enhance both processes. We next tested whether purified ADP and/or U46619 (a stable TXA_2 analogue) could compensate for the absence of collagen. Indeed, the combination of ADP (4μM) and U46619 (2μM) induced platelet migration at an extent resembling that observed in the presence of supernatants from collagen-activated platelets, while ADP or U46619 alone had only moderate effects (Fig. 4.19 and Movie 3). TXA_2-activated platelets release ADP (Paul et al., 1999) and ADP in turn induces platelet TXA_2 release (Packham et al., 1989; Jin et al., 2002). To better understand the nature of the synergistic action of ADP and TXA_2 we next examined platelet migration induced by U46619 (2μM) in the presence or absence of apyrase (2U/ml). The total number of spreading and migrating platelets in response to U46619 was significantly reduced in the presence of apyrase compared to control, while the fraction of migrating platelets remained constant (Fig. 4.20). In contrast, in response to ADP the number of spreading platelets remained unchanged, independent of whether or not TXA_2 generation was blocked by indomethacin (10 μM), suggesting ADP as primary trigger of spreading in our setting (Fig. 4.21A). However, the fraction of migrating platelets was significantly reduced when TXA_2-signaling was abolished (Fig. 4.21A), implying TXA_2 as a critical signal inducing migration. Correspondingly, the TXA_2 analogue U46619 (2μM) rescued defective ADP-induced platelet migration in the presence of indomethacin (Fig. 4.21A). U46619 also increased the number of spreading platelets compared to ADP activation alone (Fig. 4.21A,B), indicating that TXA_2 amplifies ADP-induced spreading, even though it is not sufficient to induce this process by itself.

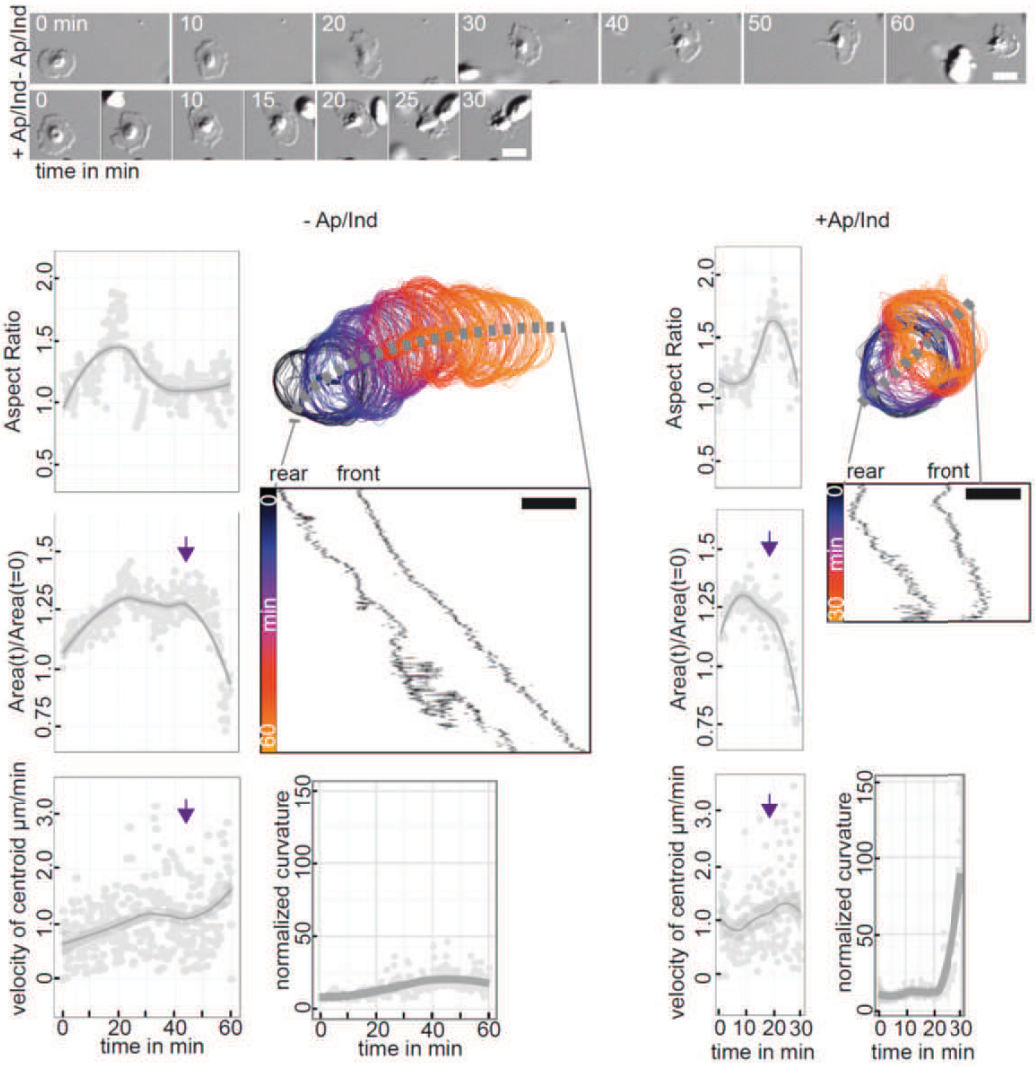

Figure 4.17 – Quantification of single platelet dynamics in the presence or absence of apyrase/indomethacin treated supernatants. Representative DIC time series of migrating platelets incubated with conditioned supernatants generated from activated platelets in the presence and absence of Apyrase (2U/ml) and Indomethacin (10μM) (upper panel). Lower panel: Color-coded time sequence of the platelet outline from above. The corresponding kymograph indicates the leading- and trailing edge movement during platelet polarization and migration. Aspect ratio, proportional increase or decrease in area, centroid velocity and normalized curvature were continuously recorded over the time span of migration. Note, that duration of migration was reduced by ≈50% in the presence of Apyrase/Indomethacin treated supernatants. Purple arrows indicate the initial drop of the platelet area. Importantly, the centroid velocity initially remained constant and only dropped with a timely delay. Scale bar=5μm.

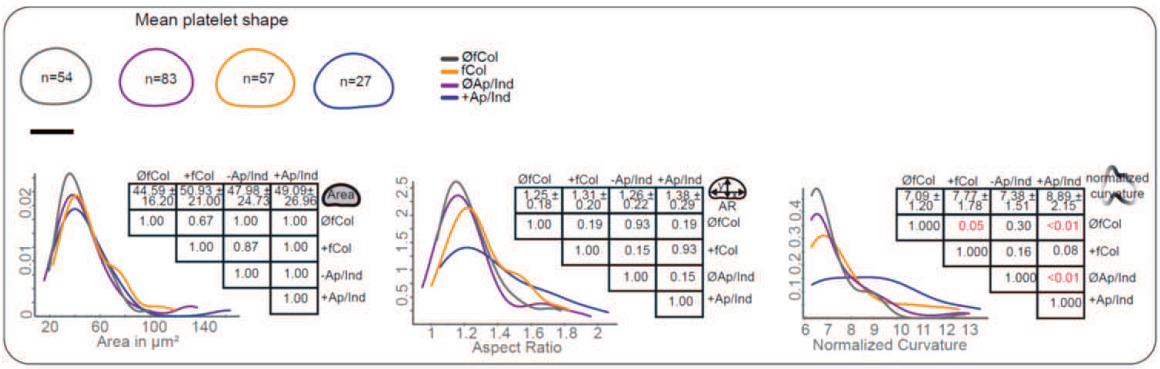

Figure 4.18 – Shape analysis of platelets migrating in the presence or absence of apyrase/indomethacin treated supernatants. Shape analysis of Apyrase/Indomethacin-treatment: Upper panel: The mean shapes are shown for the indicated groups and the measured platelet numbers are depicted. Lower panel: Smooth density histograms displaying area, aspect ratio and normalized curvature (x-axis) as a density function (y-axis). The table shows mean±SD; p-values<0.05 (red) indicate significance; Kruskal-Wallis/Wilcox.

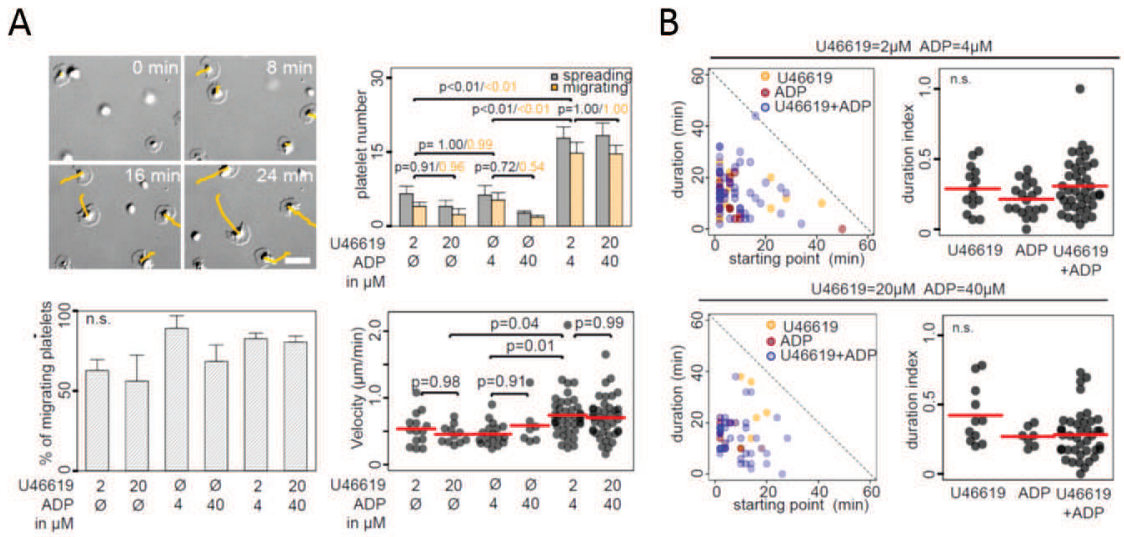

Figure 4.19 – A, Representative DIC time series of migrating platelets in the presence of ADP (4μM) and TXA_2 (2μM) (upper left). Total number of spreading and migrating platelets per experiment, fraction of migrating platelets and the migration velocity were quantified for platelet activation by ADP and TXA_2 at the indicated concentrations (in μM). Platelets were pooled from n=4 experiments; red bars indicate the mean velocity; error bars=SEM; ANOVA/TukeyHSD; scale bar = 5μm. B, Duration of single platelet migration was plotted in respect to the initial starting-point within the observation time of 65 min. The duration index is defined as the ratio of the effective duration of migration and the maximum duration possible in respect to the initial starting-point. Red bars indicate mean; platelets were pooled from n=4 experiments; n.s. indicates no significance; Kruskal-Wallis.

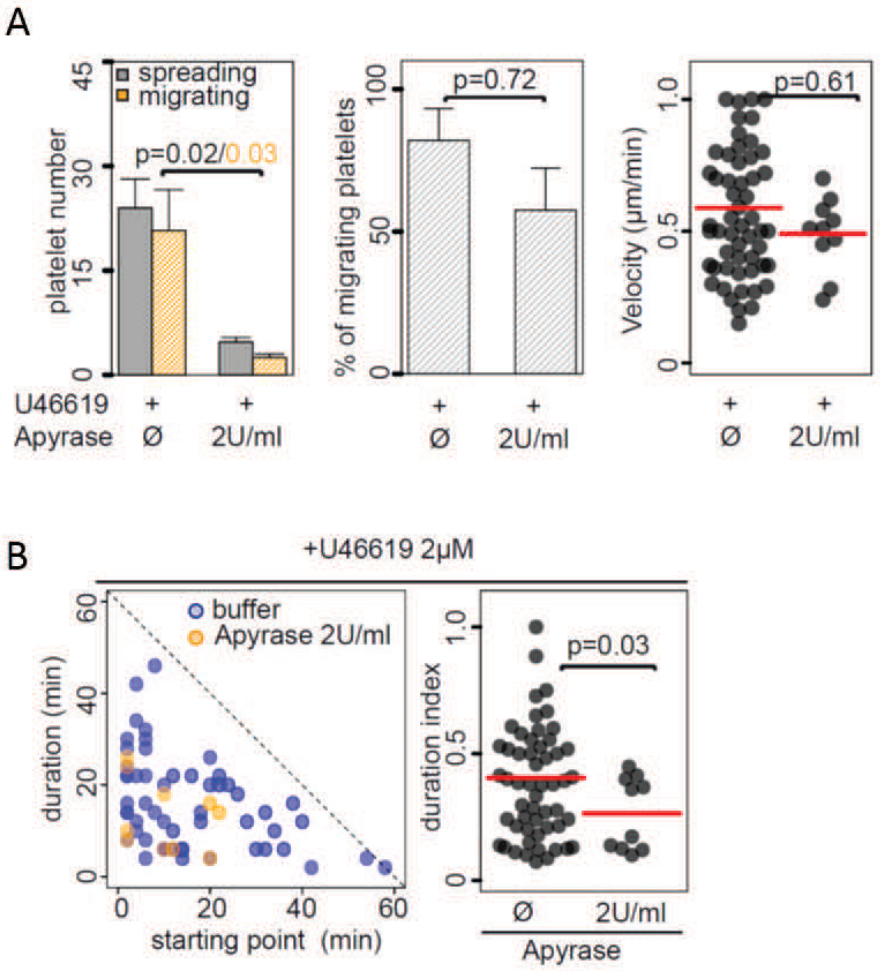

Figure 4.20 – A, Total number of spreading and migrating platelets per experiment, fraction of migrating platelets and the migration velocity were quantified for platelet migration after activation by U46619 (2μM) in the presence or absence of Apyrase (2U/ml). Platelets were pooled from n=4 experiments; red bars indicate the mean velocity; error bars=SEM; ANOVA/TukeyHSD. B, Platelets from A, were further analyzed for duration of migration as described for Fig. 4.19B; platelets were pooled from n=4 experiments; red bars indicate mean; ANOVA/TukeyHSD.

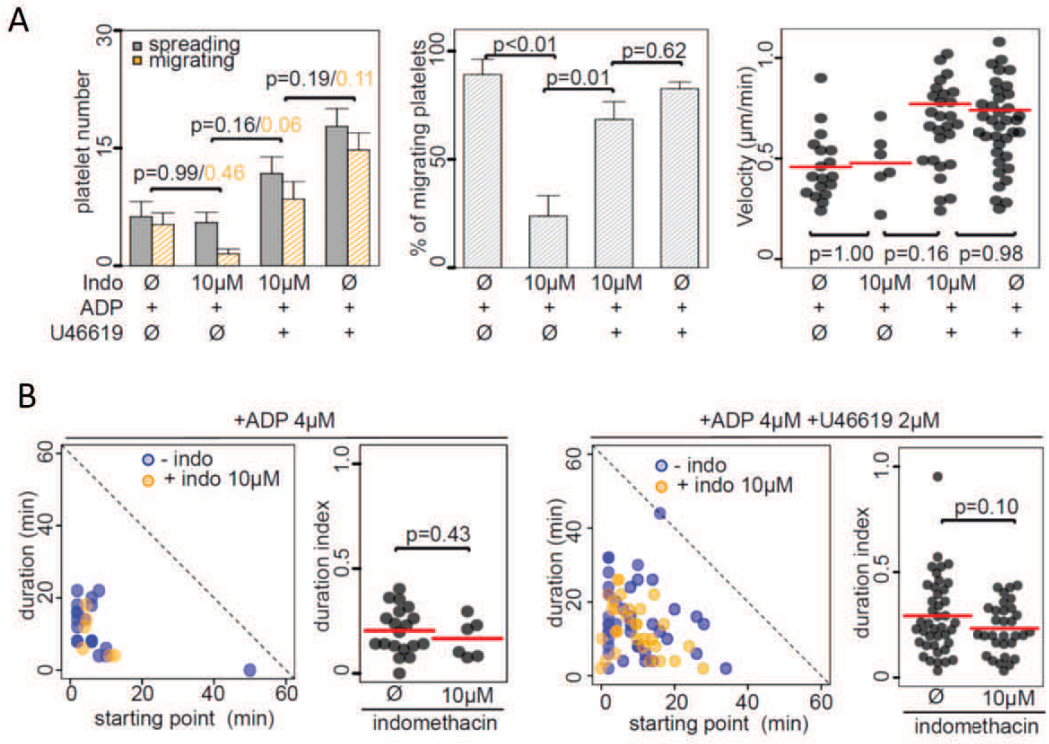

Figure 4.21 – A, Total number of spreading and migrating platelets per experiment, fraction of migrating platelets and the migration velocity were quantified for platelet migration after activation by U46619 (2μM) in the presence or absence of Apyrase (2U/ml). Platelets were pooled from n=4 experiments; red bars indicate the mean velocity; error bars=SEM; ANOVA/TukeyHSD. B, Platelets from A, were further analyzed for duration of migration as described for Fig. 4.19B; platelets were pooled from n=4 experiments; red bars indicate mean; ANOVA/TukeyHSD.

4.4 Platelet migration is $\alpha_{IIb}\beta_3$ integrin dependent

But what substrate are platelets migrating on? Since interaction with collagen fibers does not promote but rather terminates platelet migration, we hypothesized that immobilized plasma proteins form the surface promoting platelet migration *in vitro* (Fig. 4.10). Atomic Force Microscopy (AFM) confirmed that plasma-coating of cover slips provided a ≈15nm thick homogeneous substrate layer with surface variations of ≈6nm, compared to the native untreated coverslips with major surface peaks of ≈50nm (most likely representing dust) (Fig. 4.22). Immunosstaining also confirmed the presence of immobilized plasma proteins (Fig. 4.22).

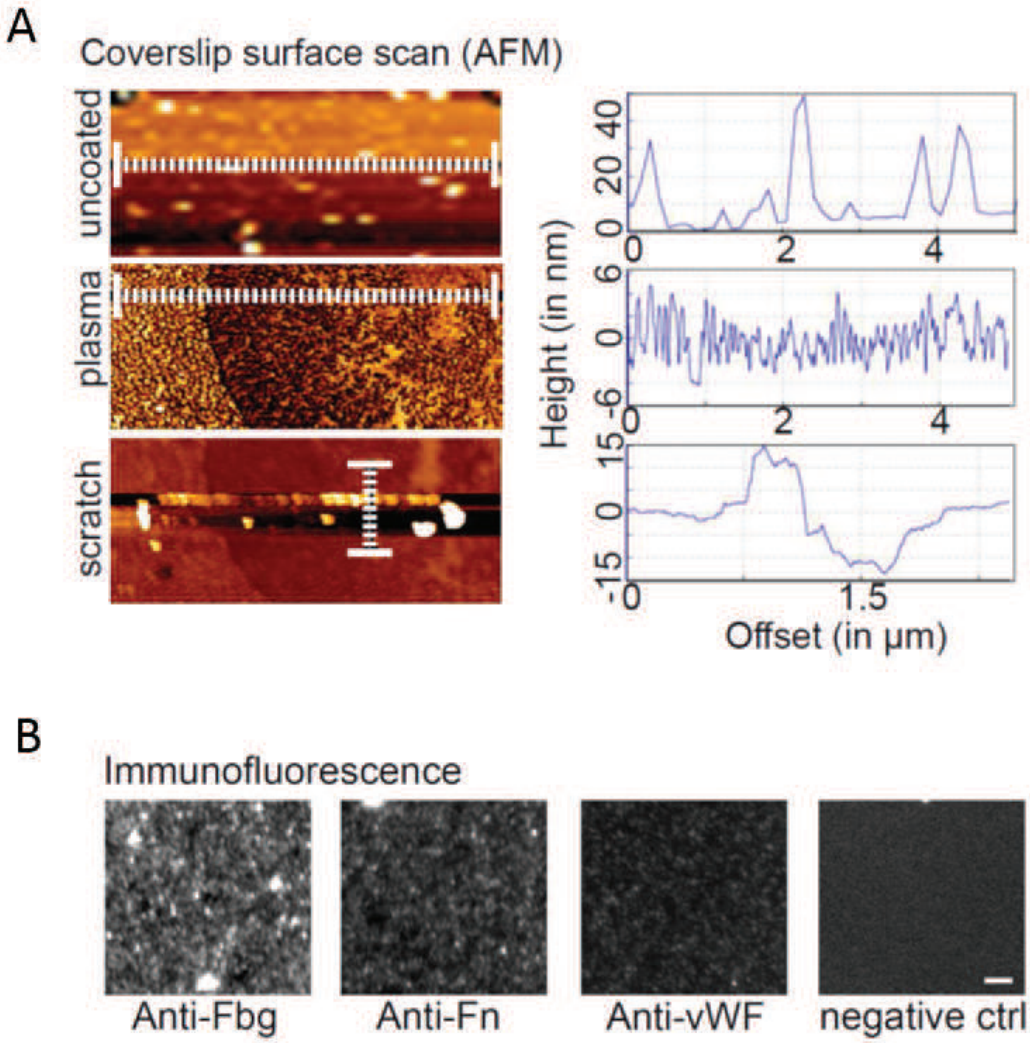

Figure 4.22 – Surface characterization of plasma coated cover slips. A, Surface topography of an uncleaned and a plasma-coated coverslip was measured by atomic force microscopy. Note, that after cleaning and coating slides are covered by a homogeneous, ≈15nm thick surface layer with only small height variations of ≈6nm, while larger irregularities (≈50nm) (most likely representing dust) were removed. B, The presence of immobilized plasmaproteins relevant for platelet adhesion and spreading was confirmed by immunostainings for Fibrinogen (Fbg), Fibronectin (Fn) and von Willebrandt Factor (vWF). Scale bar=5μm.

Adhesive interactions with plasma proteins are predominately mediated by platelet integrins (-β_1, -β_3) and the vWF-binding complex (GPIb-IX-V) (reviewed in Denis and Wagner, 2007). While platelets from β_1 integrin-deficient and GPIb-ILR4 mutant mice spread and migrated normally, α_{IIb} integrin-deficient platelets did not develop lamel-

lipodia but only short filopodia (Mccarty et al., 2004), and did not show spreading or migration (Fig. 4.23). This indicates that $\alpha_{\mathrm{IIb}}\beta_3$ integrin is indispensable for spreading and migration of mouse platelets. It is also critical for spreading and migration of human platelets. Correspondingly, we found activated $\alpha_{\mathrm{IIb}}\beta_3$ integrin homogeneously distributed over the leading edge of migrating human platelets (Fig. 4.24). Compared to unactivated $\alpha_{\mathrm{IIb}}\beta_3$ integrin, the activated form was localized in clusters (Isenberg et al., 1987) (Fig. 4.24). In the presence of non-specific linear RGDS peptides blocking β-integrins, the number of spreading human platelets is significantly reduced with a decrease in both mean platelet area and aspect ratio (Fig. 4.25A,C). This defect in spreading is associated with a significant reduction also of platelet migration (Fig. 4.25A,B). The few platelets that still manage to migrate despite the presence of RGDS do so only for a short duration (4.25B). Platelets from a patient with Glanzmann thrombasthenia further demonstrated a critical role of $\alpha_{\mathrm{IIb}}\beta_3$ integrin for platelet spreading and subsequent migration (Fig. 4.26). While these findings supported a role of $\alpha_{\mathrm{IIb}}\beta_3$ integrin for platelet-matrix interactions required for migration, they did not allow us to discriminate whether $\alpha_{\mathrm{IIb}}\beta_3$ primarily induces spreading thereby setting the stage for migration, or rather directly mediates migration. To address this, we allowed human platelets to spread and migrate before adding C7E3-Fab (10μg/ml), a blocking β_3 integrin-specific Fab-fragment . After C7E3-Fab exposure, platelets immediately stopped migrating while still maintaining their spread morphology for several minutes (Fig. 4.27), suggesting that migration is instantly blocked despite the persistence of platelet spreading. In contrast, inhibition of $\alpha_{\mathrm{v}}\beta_3$ integrin had no effect (Fig. 4.28). Together, this identifies a critical and active role of $\alpha_{\mathrm{IIb}}\beta_3$ integrin in the process of platelet migration.

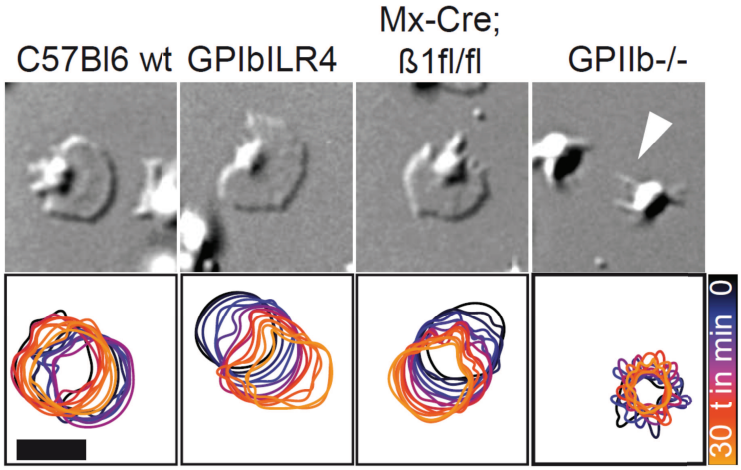

Figure 4.23 – Migration of murine platelets is $\alpha_{IIb}\beta_3$ -integrin-dependent. A, Upper row: Representative DIC images and corresponding color-coded time series of migrating platelets isolated from mice with altered adhesion receptors are shown as indicated. GPIIb-deficient platelets did not spread and only formed short filopodia (white arrow head). Scale bar=5μm.

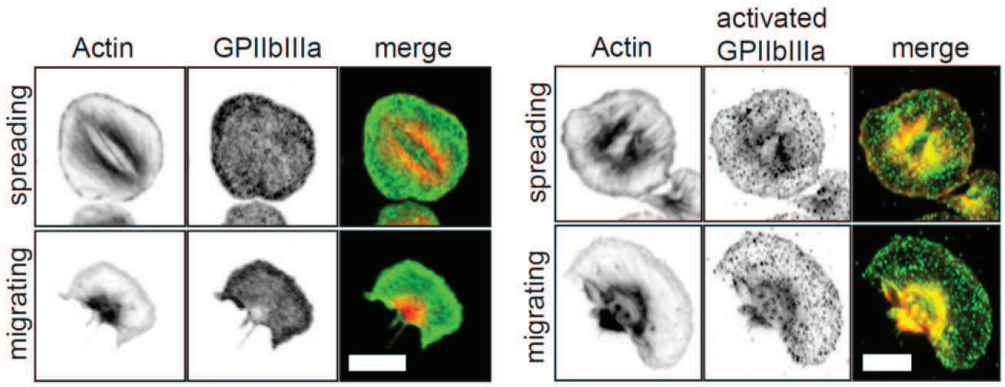

Figure 4.24 – Immunofluorescence of $\alpha_{IIb}\beta_3$ integrin. Left panel: Confocal sections of human isolated spreading (upper) and migrating (lower) platelets stained for actin (phalloidin, red) and GPIIb (HIP8, green).Right panel: Confocal sections of human isolated spreading (upper) and migrating (lower) platelets stained for actin (phalloidin, red) and activated GPIIb (PAC1, green). Scale bar=5μm.

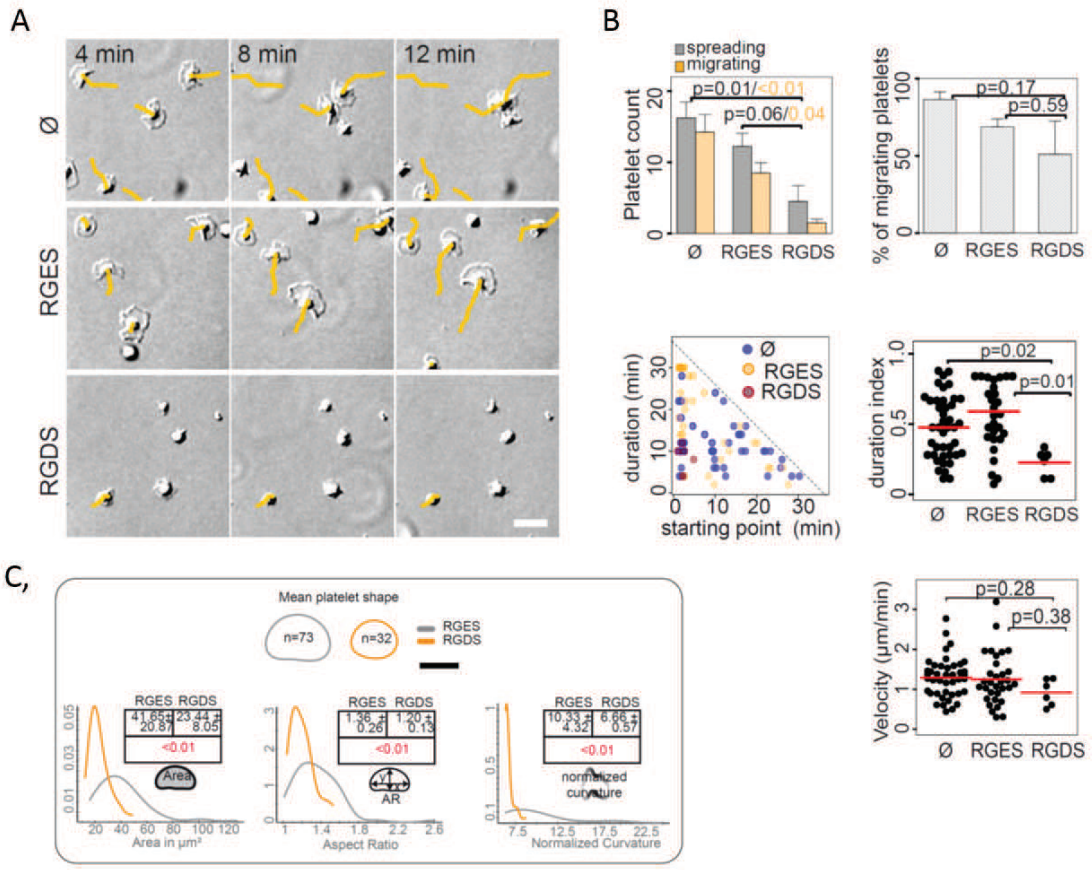

Figure 4.25 – Platelet migration in the presence of linear RGDS peptides. A, Representative time series of human migrating platelets treated with RGDS (inhibitory peptide) and RGES (negative control). B, The total number of spreading and migrating platelets per experiment and the fraction of migrating platelets was quantified. n=4 experiments; error bars=SEM; ANOVA/TukeyHSD; scale bar=10μm. Duration of single platelet migration was plotted in respect to the initial starting-point within the observation time of 65 min. The duration index is defined as the ratio of the effective duration of migration and the maximum duration possible in respect to the initial starting-point. Platelets were pooled from n=4 experiments; red bars indicate mean; Kruskal-Wallis/Wilcox. C, Shape analysis of RGDS treatment: Upper panels: The mean shapes are shown for the indicated groups and the measured platelet numbers are depicted. Scale bar=5μm. Lower panels: Smooth density histograms displaying area, aspect ratio and normalized curvature (x-axis) as a density function (y-axis). The table shows mean±SD; p-values<0.05 (red) indicate significance; area, aspect-ratio: student's t-test; curvature: wilcox test.

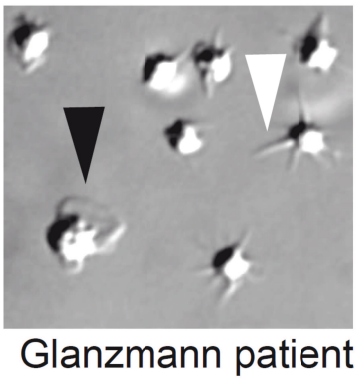

Figure 4.26 – Morphology of platelets isolated from a patient with Glanzmann thrombasthenia. Platelets isolated from a Glanzmann patient were seeded on plasmaprotein coated coverslips. Note, that only a small fraction of platelets formed unstable lamellipodia (black arrow head) and only extended short filopodia (white arrow head).

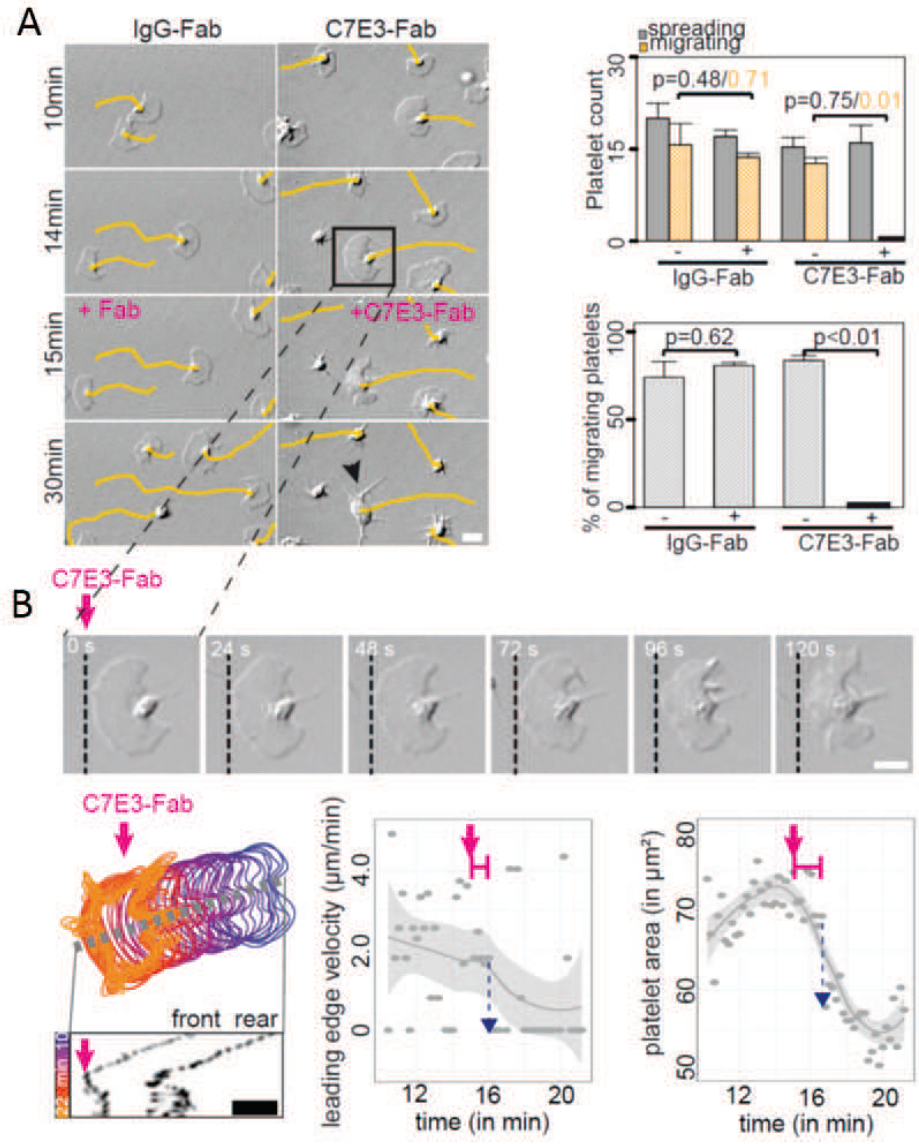

Figure 4.27 – Platelet migration in the presence of β_3 integrin-blocking C7E3-Fab. A, Left panel: Representative DIC time series of migrating platelets before and after treatment with C7E3-Fab (10 μg/ml) and control-Fab (10 μg/ml). Fab-fragments were added after 15 min of platelet migration (highlighted in pink). The black arrow head indicates the complete shrinkage of lamellipodia after ≈15min of C7E3-Fab treatment. Scale bar=5μm. Right panel: The total number of spreading and migrating platelets per experiment and the fraction of migrating platelets was quantified before and after treatment. n=3 experiments; error bars=SEM; paired t-test. B, Analysis of single platelet dynamics after C7E3-Fab-treatment at higher spatial and temporal resolution. Upper: DIC time series. Note, that after treatment platelets immediately stopped migrating (black dashed line) and only started to shrink with a lag time of ≈1min. Lower: Corresponding color-coded time series of the platelet outline. The kymograph highlights the immediate stop of migration after treatment (pink arrow), while leading edge shrinkage followed with a timely delay. Measurements of the leading edge velocity and platelet area further revealed the time delay of lamellipodium shrinkage as indicated by the width of the pink bar. Scale bar=5μm.

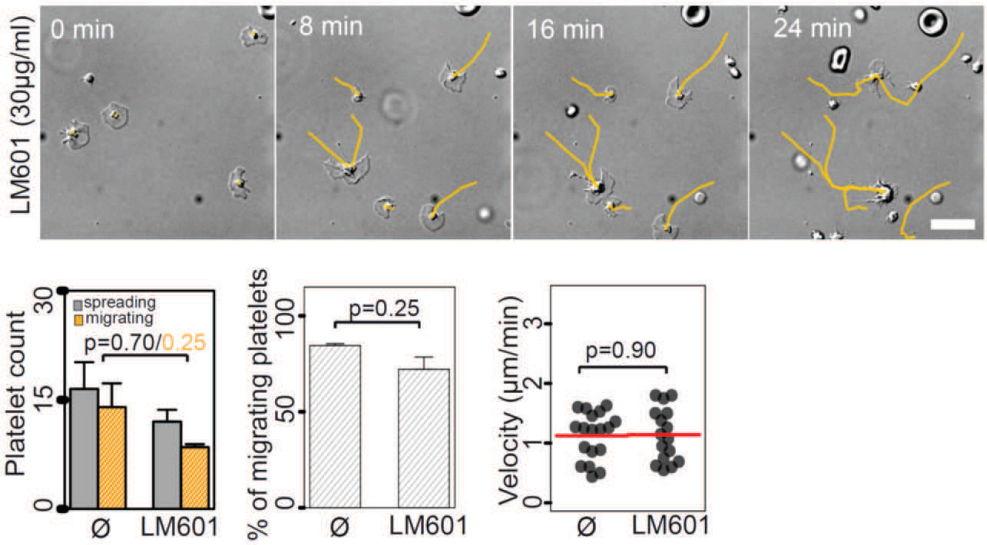

Figure 4.28 – Platelet migration in the presence of $\alpha_v\beta_3$ integrin-blocking antibody. Time series of platelets migrating in the presence of 30μg/ml anti-αvβ3 integrin antibody (LM601). Quantification of the total number of spreading and migrating platelets per experiment, fraction of migrating platelets and migration velocity did not reveal a significant difference compared to the control group. Platelets were pooled from n=2 experiments; red bars indicate mean velocity; error bars=SEM; student's t-test.

4.5 Platelet migration depends on adhesive and anti-adhesive plasma components plus extracellular calcium

Since the fibrinogen receptor $\alpha_{IIb}\beta_3$ integrin acts as the platelet adhesion receptor mediating migration, we replaced plasma by different concentrations of fibrinogen (Materials and Methods). Under these conditions, we observed robust spreading but no migration of platelets (Fig. 4.29), indicating the requirement for additional serum factors. When we reconstituted purified fibrinogen (150μg/ml) with various concentrations of serum the number of spreading platelets decreased with increasing serum concentration and no spreading was observed at 12,5mg/ml (Fig. 4.30A,B). At the same time the absolute number and fraction of migrating platelets was increasing with a peak at 3000 μg/ml (Fig. 4.30A,B). However, at higher serum concentrations (6250μg/ml) the duration of platelet migration was significantly lowered. Consequently, the mean accumulated dis-

tance of platelets migrating at this serum concentration remains unexpectedly short, despite their higher velocity (Fig. 4.30C,D). Morphologically, the increase in migration in response to serum was paralleled by an increase in platelet polarity as defined by an increase in the aspect ratio (Fig. 4.31). By time lapse microscopy we observed that platelets that start to migrate in response to serum develop membrane fluctuations at the leading edge, previously described as ruffles (Fig. 4.30A, Movie 1), translating into an increase in the normalized platelet curvature (Fig. 4.31). Membrane ruffling typically identifies membrane protrusions that are less efficiently anchored to the substrate and therefore continuously retracted (Borm et al., 2005; Gupton and Waterman-Storer, 2006), suggesting that increasing serum concentrations lower the substrate adhesiveness. To address whether the serum-to-fibrinogen ratio rather than absolute concentrations of serum components modulate platelet migration, we next modified the absolute fibrinogen concentration while maintaining a constant absolute serum concentration (1500μg/ml). Increasing the fibrinogen concentration and hence lowering the serum-to-fibrinogen ratio reduced migration while increasing spreading (Fig. 4.32). While migration velocities were decreasing at higher fibrinogen concentrations, the mean duration of migration was increasing, resulting in a constant mean accumulated migration distance (Fig. 4.32). Titration of fibrinogen concentrations mainly modified the normalized curvature, while the aspect ratio remained unaffected (Fig. 4.31). Together with the above findings this indicates that membrane ruffling is mainly determined by the serum-to-fibrinogen ratio, while the polarization depends on the absolute serum concentration. To better compare both dilution series we plotted our measurements in respect to the serum-fibrinogen-ratio rather than the absolute protein concentrations (Fig. 4.34). The ratio-curves had the same tendency in all measurements (Fig. 4.34): low ratios supported platelet spreading and blocked migration, while higher ratios supported platelet migration and reduced the number of spreading platelets. However, at low-intermediate serum-fibrinogen-ratios, migration was significantly more efficient when higher absolute serum concentrations were present (Fig. 4.34; ratio=5:1; Serum 1500 μg/ml : Fbg 300 μg/ml > Serum 750 μg/ml : Fbg 150 μg/ml). Importantly, this correlated with an even more pronounced increase in platelet polarization (aspect ratio and normalized curvature). Based on these observations we propose two distinct serum-dependent premises for platelet migration: One, serum has to be present at a minimum absolute concentration to facilitate platelet cytoskeletal rearrangement and polarization. Two, the serum-to-fibrinogen ratio has to be sufficiently high to establish the required low substratum adhesiveness required for promoting subsequent migration.

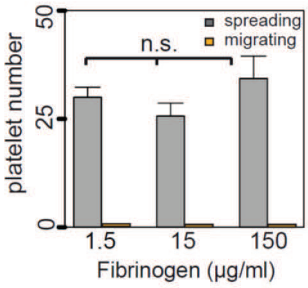

Figure 4.29 – Platelets do not migrate on purified fibrinogen. Total number of spreading and migrating platelets per experiment were quantified for the indicated fibrinogen concentrations. Pooled from n=3 experiments; error bars=SEM; n.s.=not significant ($p \geq 0.05$); ANOVA/TukeyHSD.

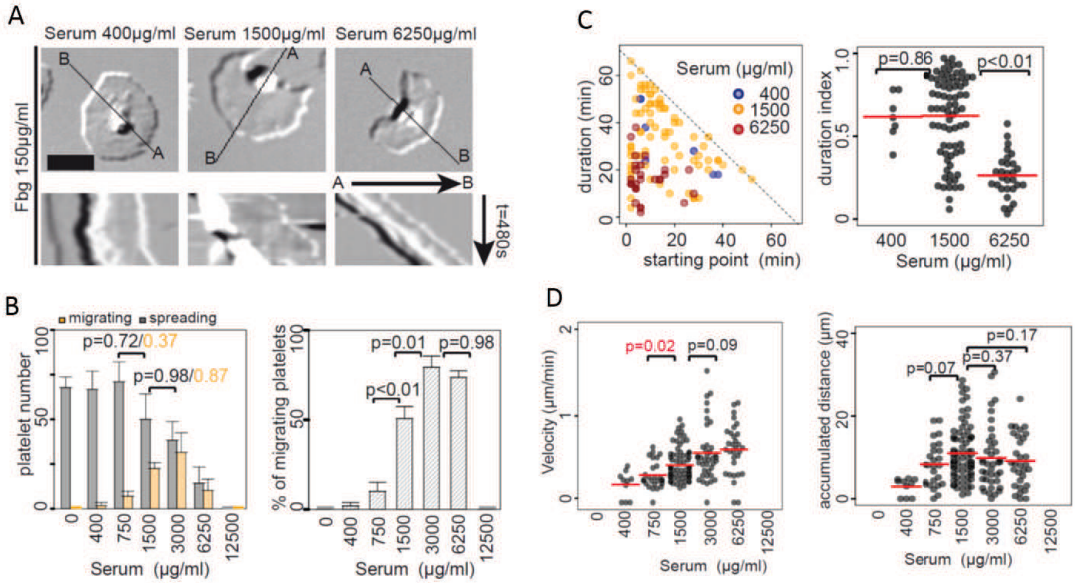

Figure 4.30 – Serum regulates platelet migration. A, Representative DIC micrographs of serum concentrations as indicated and related kymographs. Note the smooth platelet membrane at low serum concentrations. B, Total number of spreading and migrating platelets per experiment and fraction of migrating platelets were quantified for the indicated treatments. The fibrinogen concentration in the assay was adjusted to 150 μg/ml for all groups. Pooled from n=4 experiments; error bars=SEM; ANOVA/TukeyHSD. C, Duration of single platelet migration was plotted in respect to the initial starting-point within the observation time of 65 min. The duration index is defined as the ratio of the effective duration of migration and the maximum duration possible in respect to the initial starting-point. Platelets were pooled from n=4 experiments; red bars indicate mean; ANOVA/TukeyHSD. D, Quantification of single platelet migration velocity and of the accumulated distance at indicated serum concentrations; platelets were pooled from n=4 experiments; Kruskal-Wallis/Wilcox.

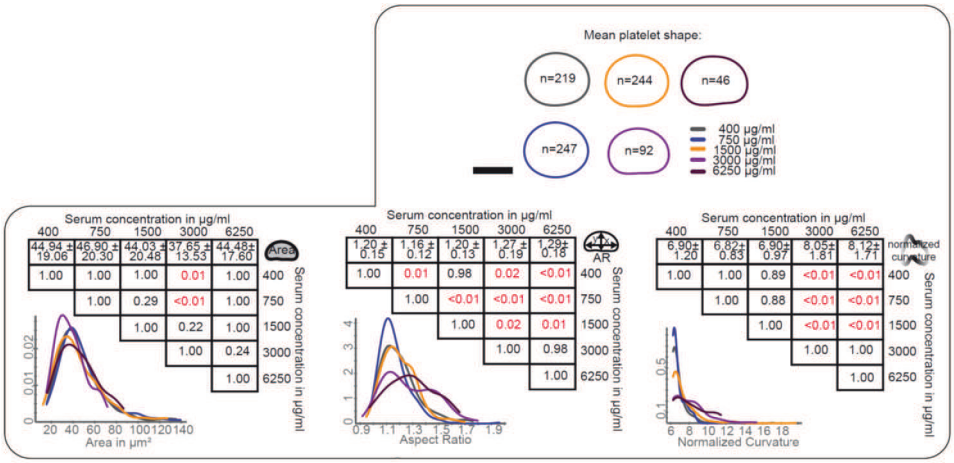

Figure 4.31 – Shape analysis of migrating platelets at various serum concentrations. The mean shape for the indicated serum concentrations is shown ; Scale bar=5μm (upper panel). Smooth density histograms display area and aspect ratio and normalized curvature at indicated serum concentrations; the table shows mean±SD; p-values<0.05 (red) indicate significance; platelets were pooled from n=4 experiments; Kruskal-Wallis/Wilcox (lower panel).

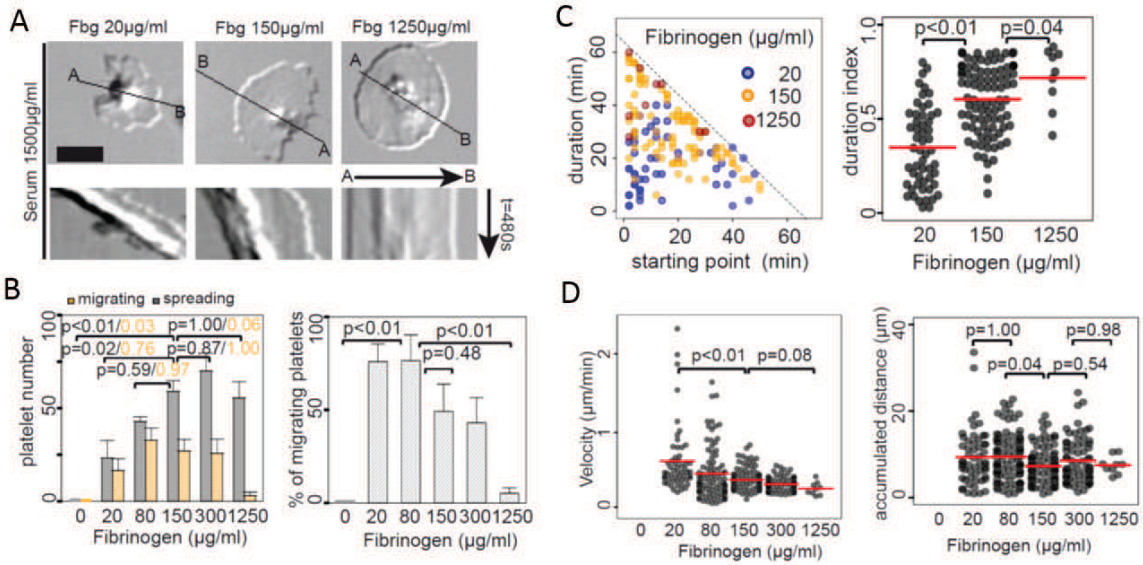

Figure 4.32 – Fibrinogen regulates platelet migration. A, Representative DIC micrographs of fibrinogen concentrations as indicated and related kymographs. Note the smooth platelet membrane at high fibrinogen concentrations. B, Total number of spreading and migrating platelets per experiment and fraction of migrating platelets were quantified for the indicated treatments. The serum concentration in the assay was adjusted to 1500 μg/ml for all groups. Pooled from n=4 experiments; error bars=SEM; ANOVA/TukeyHSD. C, Duration of single platelet migration was plotted in respect to the initial starting-point within the observation time of 65 min. The duration index is defined as the ratio of the effective duration of migration and the maximum duration possible in respect to the initial starting-point. Platelets were pooled from n=4 experiments; red bars indicate mean; ANOVA/TukeyHSD. D, Quantification of single platelet migration velocity and the accumulated distance at indicated fibrinogen concentrations; platelets were pooled from n=4 experiments; Kruskal-Wallis/Wilcox.

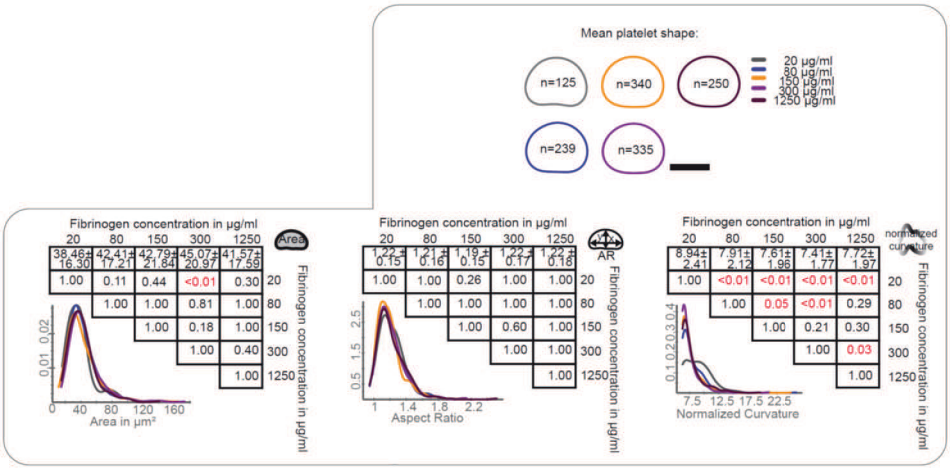

Figure 4.33 – Shape analysis of migrating platelets at various fibrinogen concentrations. The mean shape for the indicated fibrinogen concentrations is shown ; Scale bar=5μm (upper panel). Smooth density histograms display area, aspect ratio and normalized curvature at indicated fibrinogen concentrations; the table shows mean±SD; p-values<0.05 (red) indicate significance; platelets were pooled from n=4 experiments; Kruskal-Wallis/Wilcox (lower panel).

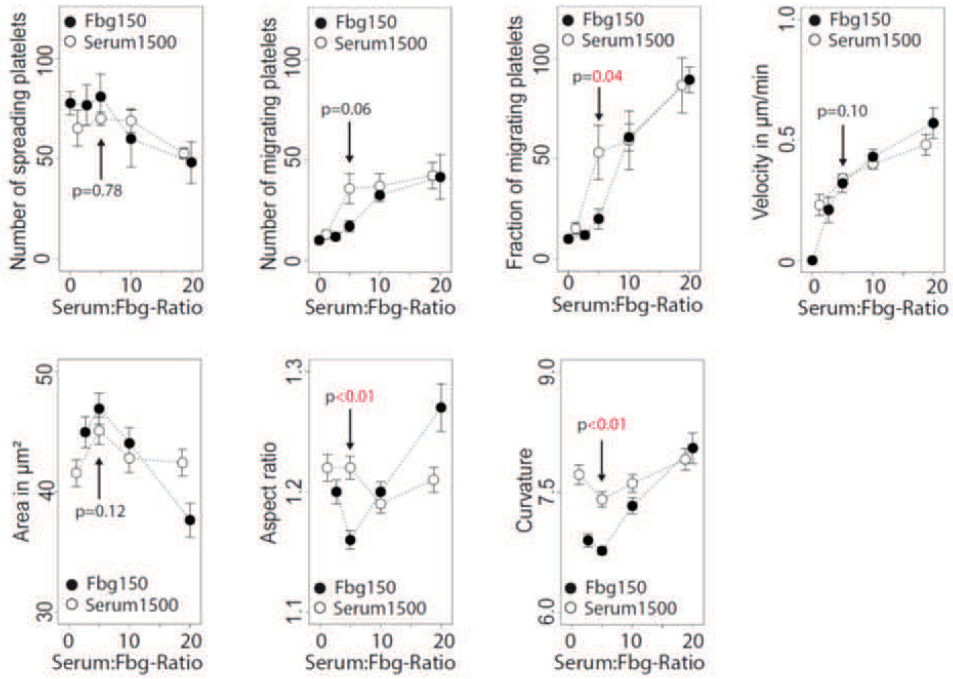

Figure 4.34 – The serum-fibrinogen-ratio modulates platelet migration. p-values<0.05 (red) indicate significance; wilcox

But what is the nature of the serum factor(s) required for platelet migration? Serum proteins are known to gradually denature at temperatures ranging from 50 °C to 100 °C (Takeda et al., 1989). Incubating serum for 30 min at 50 °C resulted in reduced platelet migration and higher temperatures further decreased the fraction and velocity of migrating platelets (Fig. 4.35). With respect to platelet morphology, heat inactivation predominantly reduced the normalized curvature of platelets, whereas the aspect ratio remained unaffected (Fig. 4.36). Based on this observation at least two serum components predetermined platelet shape and migration: one component, most likely a protein, which is heat-sensitive and primarily affects the normalized curvature, and a second component that is heat-insensitive and modulates the aspect-ratio. Albumin, the most abundant protein in serum, denatures at temperatures $\geq$50 °C (Takeda et al., 1989) and has previously been shown to compete with fibrinogen in absorption to surfaces thereby modulating platelet adhesion (Nonckreman et al., 2010). To test the role of albumin on platelet migration, we replaced serum by recombinant human serum albumin and monitored platelet motility. Albumin alone was not sufficient to induce platelet migration (Fig. 4.37); however, it increased the normalized curvature of platelets, suggesting that it lowered their substrate adhesiveness (Fig. 4.38). In search of the additional serum component(s) required for migration, we next fractionated the serum by size (see Materials and Methods). Dialysis of $\leq$2kD molecular weight components substantially diminished platelet migration without affecting platelet spreading (Fig. 4.39). In contrast to denaturation, dialysis of serum resulted in a robust decrease of the aspect ratio, while the normalized curvature remained more or less unaffected (Fig. 4.40). Since dialysis removes divalent cations, which are known to play a critical role in platelet biology, we reconstituted dialyzed serum with calcium. The presence of 100μM calcium was sufficient to recover platelet migration (Fig. 4.39) and also reestablished the aspect ratio (Fig. 4.40). However, calcium alone in the absence of dialyzed serum was unable to promote platelet migration, providing further evidence that at least two serum components are required (Fig. 4.39). Since albumin (affecting normalized curvature) and calcium (modulating aspect ratio) control different morphological aspects of platelet migration, we tested whether they synergize and are sufficient to promote and maintain migration. When we combined albumin (1500 μg/ml; normalized curvature $\approx$ 12) with calcium, the aspect ratio increased reaching a peak at 200μM (Fig. 4.42). This increase in polarization translated into an increase in platelet migration despite the absence of serum (Fig. 4.41). Hence, by quantitative morphological single cell analysis, we identified two prototypical platelet shape parameters, normalized curvature and aspect ratio,

that can be assigned to two distinct serum components, albumin and calcium, acting together to promote platelet migration (Fig. 4.43).

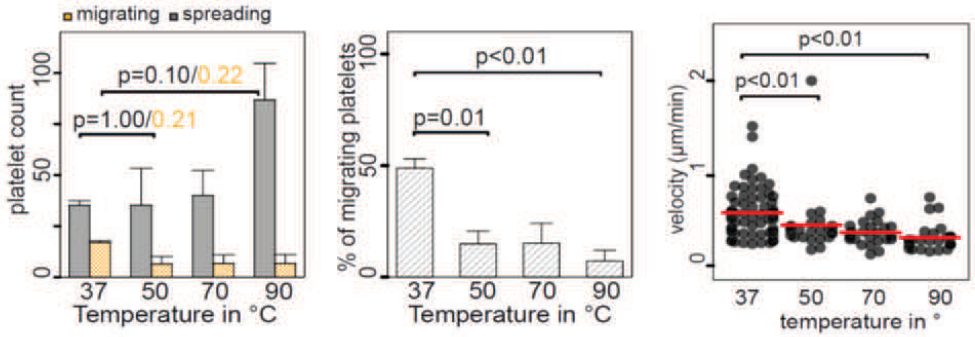

Figure 4.35 – Platelet migration in the presence of heat-inactivated serum. Total number of spreading and migrating platelets per experiment were quantified. Before starting the migration assay, serum was heated for 30 min at the indicated temperatures; pooled from n=4 experiments; error bars=SEM; ANOVA/TukeyHSD. Quantification of single platelet migration velocity at indicated temperatures of heat-inactivation of serum; platelets were pooled from n=4 experiments; Kruskal-Wallis/Wilcox.

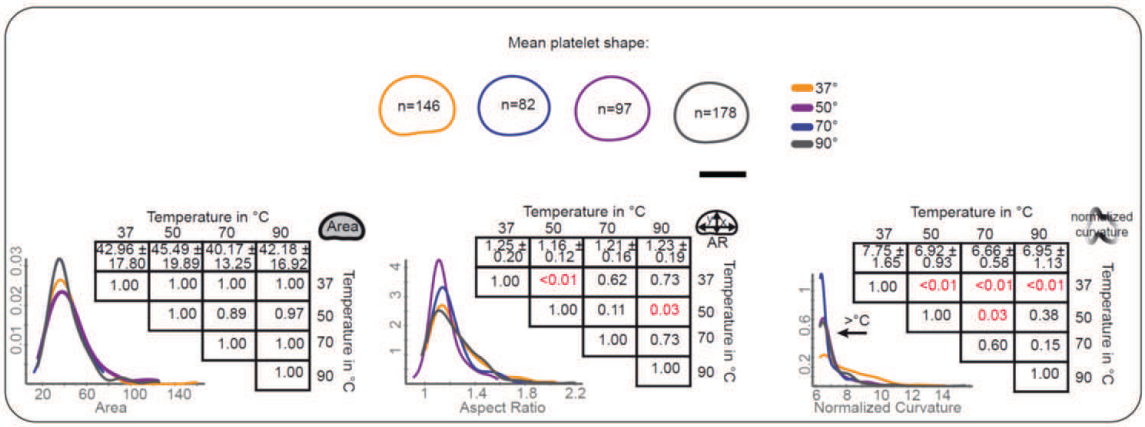

Figure 4.36 – Shape analysis of migrating platelets in the presence of pre-treated serum (30min heat-inactivation with temperatures as indicated). The mean shape for the indicated temperatures is shown; Scale bar=5μm (upper panel). Smooth density histograms display area, aspect ratio and normalized curvature at indicated temperatures; the table shows mean±SD; p-values<0.05 (red) indicate significance; platelets were pooled from n=4 experiments; Kruskal-Wallis/Wilcox (lower panel).

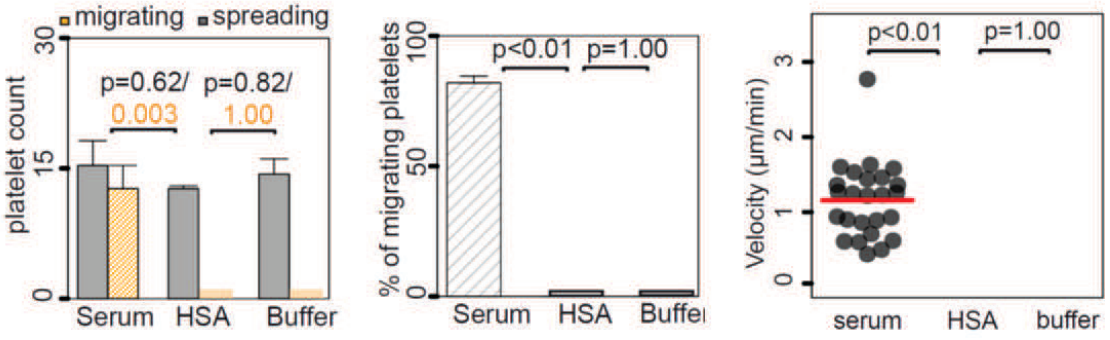

Figure 4.37 – Albumin on its own is insufficient to restore platelet migration in the absence of serum. Total number of spreading and migrating platelets per experiment and fraction of migrating platelets were quantified for the indicated treatments.pooled from n=3 experiments; error bars=SEM; ANOVA/TukeyHSD. Quantification of single platelet migration velocity in the presence of serum, albumin-rich (1500μg/ml) and albumin-poor buffer (0μg/ml); platelets were pooled from n=3 experiments; ANOVA/TukeyHSD.

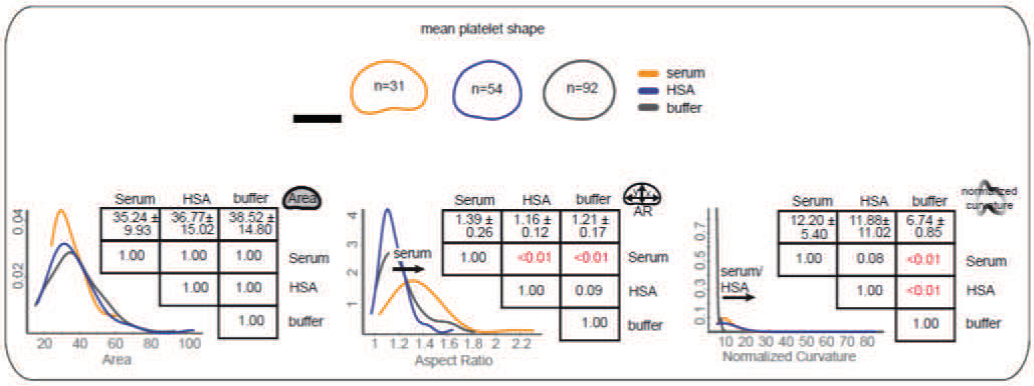

Figure 4.38 – Shape analysis of migrating platelets in the presence of serum, albumin-rich (1500μg/ml) and albumin-poor buffer (0μg/ml). The mean shape is shown for each group; Scale bar=5μm (upper panel). Smooth density histograms display area, aspect ratio and normalized curvature for each group; the table shows mean±SD; p-values<0.05 (red) indicate significance; platelets were pooled from n=4 experiments; Kruskal-Wallis/Wilcox (lower panel).

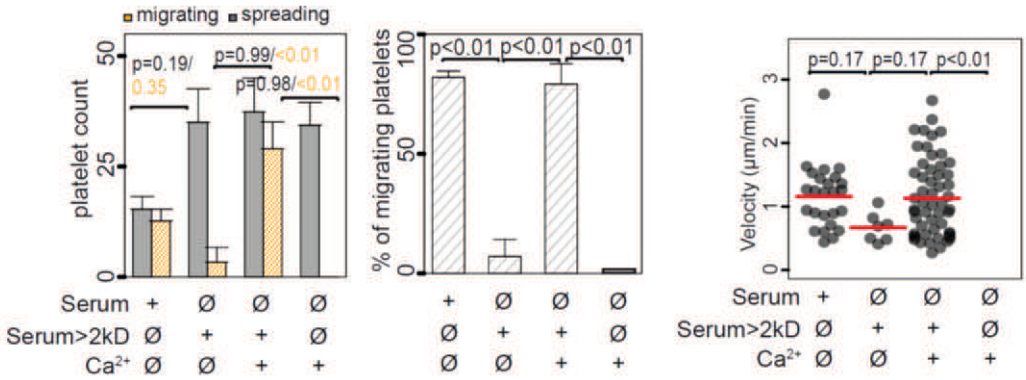

Figure 4.39 – Platelet migration requires the presence of extracellular calcium. Total number of spreading and migrating platelets per experiment and fraction of migrating platelets were quantified for the indicated treatments.pooled from n=3 experiments; error bars=SEM; ANOVA/TukeyHSD. Quantification of the single platelet migration velocities for the indicated groups ; platelets were pooled from n=3 experiments; ANOVA/-TukeyHSD.

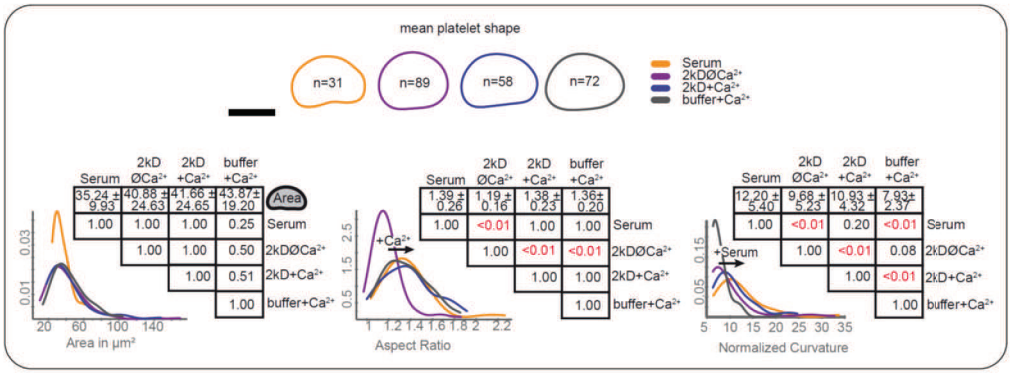

Figure 4.40 – Shape analysis of migrating platelets in the presence of serum, dialyzed serum (2kD), calcium-rich (100μg/ml) dialyzed serum (2kD) and serum-free calcium-rich (100μg/ml) buffer. The mean shape is shown for each group; Scale bar=5μm (upper panel). Smooth density histograms display area, aspect ratio and normalized curvature for each group; the table shows mean±SD; p-values<0.05 (red) indicate significance; platelets were pooled from n=3 experiments; Kruskal-Wallis/Wilcox (lower panel).

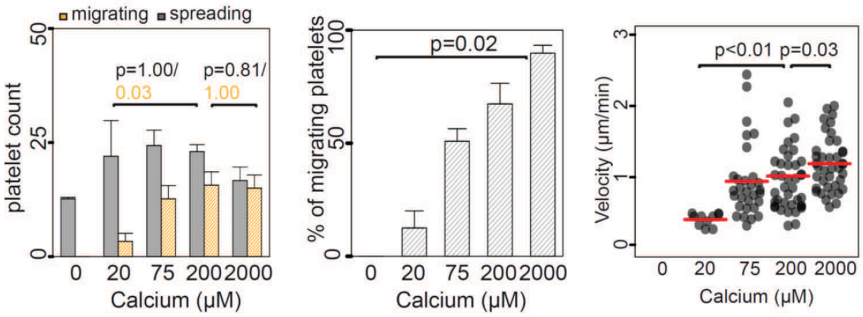

Figure 4.41 – Platelet migration requires the presence of extracellular calcium. Total number of spreading and migrating platelets per experiment and fraction of migrating platelets were quantified for the indicated calcium concentrations in the presence of 1500μg/ml albumin. pooled from n=3 experiments; error bars=SEM; ANOVA/-TukeyHSD. Quantification of the single platelet migration velocities for the indicated calcium concentrations; platelets were pooled from n=3 experiments; ANOVA/TukeyHSD.

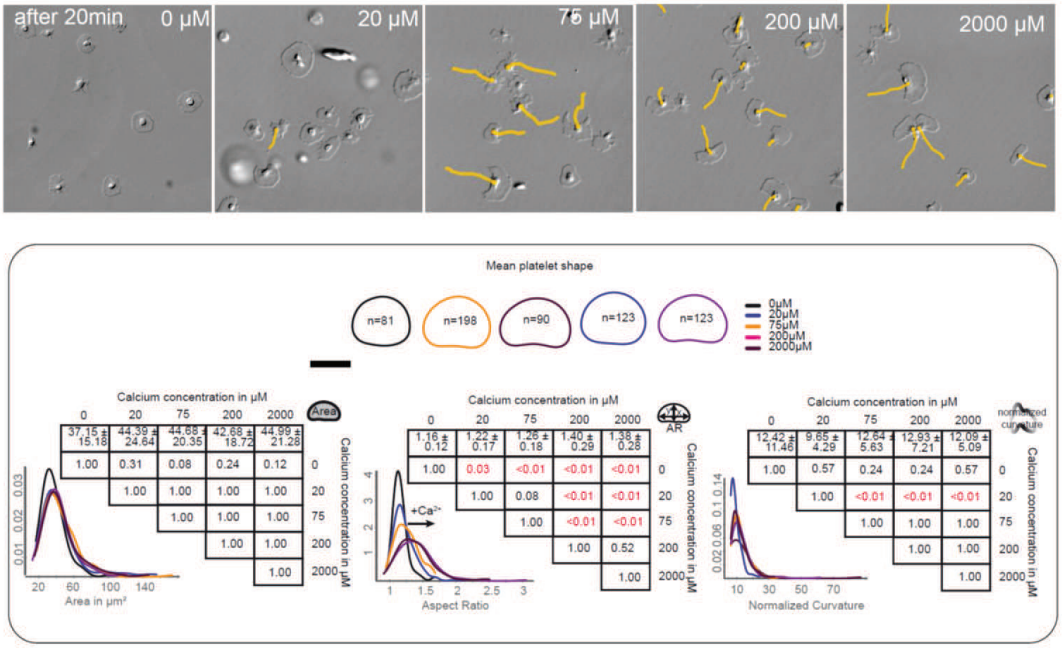

Figure 4.42 – Shape analysis of migrating platelets in the presence of extracellular calcium. Upper: Representative DIC micrographs of migrating platelets in the presence of the indicated extracellular calcium concentrations. Experiments were performed in the presence of 1500μg/ml human serum albumin. Lower: Shape analysis of migrating platelets in the presence of the indicated calcium concentrations. Human serum albumin = 1500μg/ml. The mean shape for each concentration is shown ; Scale bar=5μm. Smooth density histograms display area, aspect ratio and normalized curvature for each concentration; the table shows mean±SD; p-values<0.05 (red) indicate significance; platelets were pooled from n=3 experiments; Kruskal-Wallis/Wilcox.

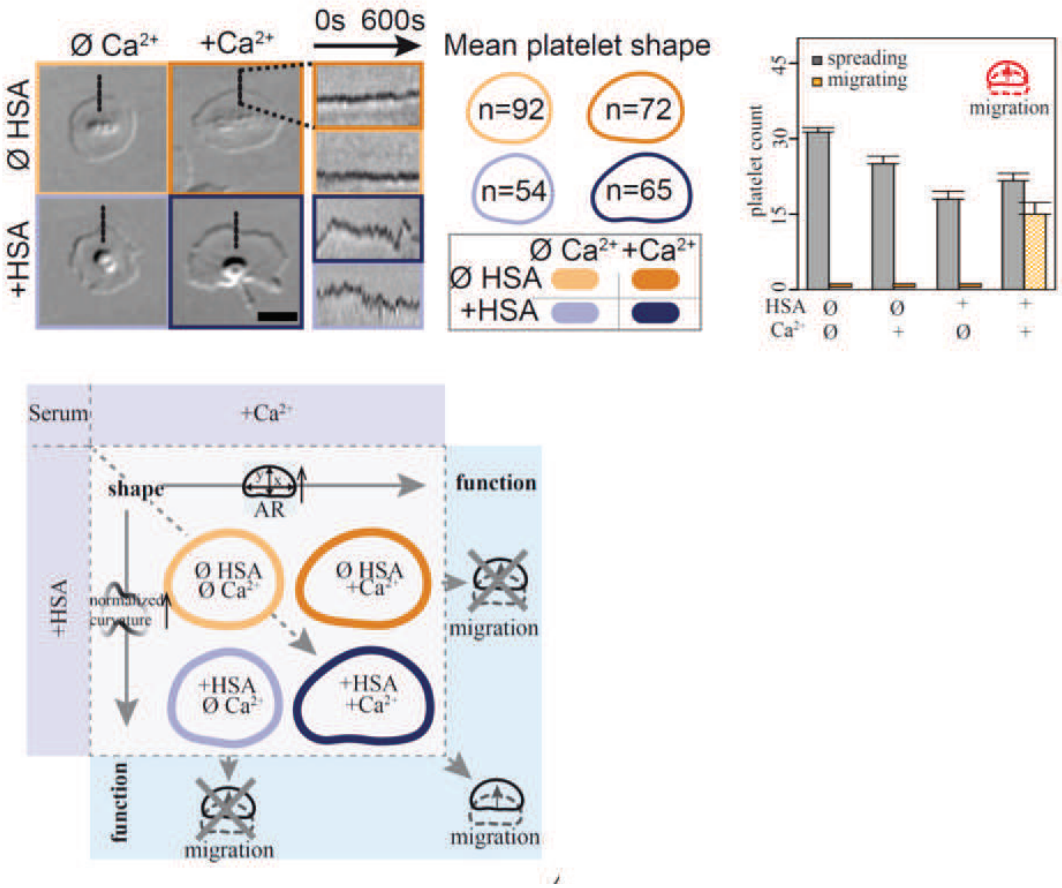

Figure 4.43 – Platelet migration depends on albumin and the presence of extracellular calcium. Upper panel: Representative DIC micrographs and related kymographs. Note the increased aspect ratio in the presence of calcium and the higher membrane fluctuations in the presence of albumin. Mean platelet shapes for the indicated number of measured platelets are shown on the left. Middle panel: Total number of spreading and migrating platelets per experiment is shown. Note, platelets only migrate in the presence of both albumin and calcium. Calcium=200μg/ml; Albumin=1500μg/ml. Lower panel: Graphical summary showing the relationship of platelet shape and functional outcome. Importantly, only platelets with both an elevated aspect ratio and normalized curvature (related to the presence of calcium and albumin, respectively) were migrating.

4.6 Extracellular calcium mediates the switch from spreading to migration by myosin IIa dependent trailing edge formation

Consistent with the prominent role of extracellular calcium in regulating platelet polarization and subsequent migration (see Fig. 4.41 and 4.42, both processes were immediately blocked when we removed extracellular calcium by adding citrate to migrating platelets (Fig. 4.44). This effect is specific to calcium, since other divalent cations did not promote, but rather inhibited platelet migration (Fig. 4.45), most likely by increasing integrin activation (Gailit and Ruoslahti, 1988). While exogenous calcium is dispensable for integrin-dependent platelet spreading, a threshold calcium concentration of $\geq 75\mu M$ is necessary to allow full-fledged migration (see Fig. 4.41). Together, this suggests that calcium-dependent processes other than integrin-affinity modulation are triggering the switch from platelet spreading to platelet polarization and migration. Modulation of intracellular calcium levels plays a fundamental role in the control of platelet function. In search of the mechanism underlying calcium-dependent control of migration, we therefore tested whether low extracellular calcium concentrations affect intracellular calcium oscillations. In calcium-free buffer, spreading platelets remained sessile while showing only minimal intracellular calcium oscillations. In contrast, amplitudes increased up to 8-fold in the presence of extracellular calcium (200 μM) and platelets became polarized and started to migrate (Fig. 4.46A,B). To test whether the observed intracellular calcium elevation is functionally relevant to platelet polarization and migration, we depleted intracellular calcium by pre-treating platelets with BAPTA-AM. At a concentration of 10 μM, BAPTA-AM signficantly reduced platelet polarization and migration without affecting platelet spreading (Fig. 4.46C,D,E). Higher concentrations of BAPTA-AM also abolished platelet spreading, indicating that the intracellular calcium levels required for spreading are lower than those required for polarization and migration (Fig. 4.46D). Elevation of intracellular calcium has previously been shown to control cellular polarization and migration through activation of myosin IIa, generating contractile forces necessary for rear retraction and adhesion release (Lee et al., 1999). We found activated myosin IIa mainly localized at the trailing-edge of migrating platelets (Fig. 4.47A). The activity of myosin IIa depends on myosin light chain phosphorylation (pMLC) and is regulated by the calcium-dependent myosin light chain kinase (MLCK) activation (Yang and Huang, 2005). Correspondingly, platelet pMLC was signficantly higher in the presence of cal-

cium compared to a calcium-free microenvironment or intracellular depletion (4.47B). To address whether myosin-mediated contraction functionally contributed to platelet polarization and migration we pharmacologically inhibited myosin IIa using blebbistatin. Myosin inhibition had no signficant impact on platelet spreading, but dose-dependently prevented absolute and fractional migration (Fig. 4.48). Population-based morphology analysis revealed a significantly increased aspect ratio of the blebbistatin-treated compared to vehicle-treated platelets, suggesting that platelets still polarize (Fig. 4.49). Correspondingly, single cell analysis shows that blebbistatin-treated platelets continue to polarize, however, they are unable to move their trailing-edge resulting in a reduced centroid velocity and an abnormal platelet elongation (Fig. 4.48 and Fig. 4.49). Platelets from MYH9-dficient mice revealed a similar migration defect (Fig. 4.50). Together, calcium triggers a cascade ultimately culminating in platelet migration: Influx from the extracellular space activates MLC. Subsequent myosin IIa-dependent contractile forces then initiate polarization and adhesion release at the platelet rear, leading to platelet migration.

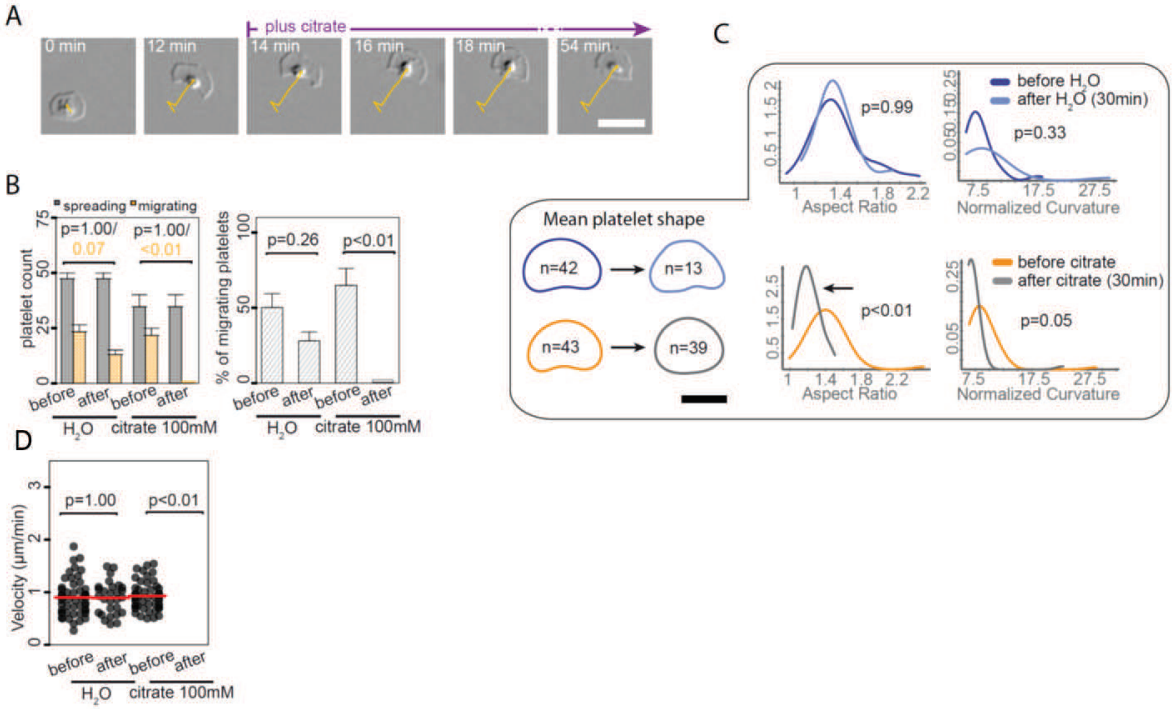

Figure 4.44 – A, Representative DIC time series of a migrating platelet before and after citrate treatment. Please note the immediate stop of migration and the subsequent loss of polarization. Scale bar = 10μm. B, Total number of spreading and migrating platelets per experiment and fraction of migrating platelets were quantified before and after treatment with citrate (100mM) or DMSO. Pooled from n=3 experiments; error bars=SEM; ANOVA/TukeyHSD. C, Shape analysis of migrating platelets before and after treatment with citrate (100mM) or DMSO. The mean shape and the analyzed platelet numbers are shown for each group. Scale bar=5μm. Smooth density histograms displaying area, aspect ratio and normalized curvature are depicted for each treatment; platelets were pooled from n=3 experiments; ANOVA/TukeyHSD. D, Single platelet velocities were quantified before and after treatment with Citrate (100mM) or DMSO. Pooled from n=3 experiments; red bars indicate mean velocity; ANOVA/TukeyHSD.

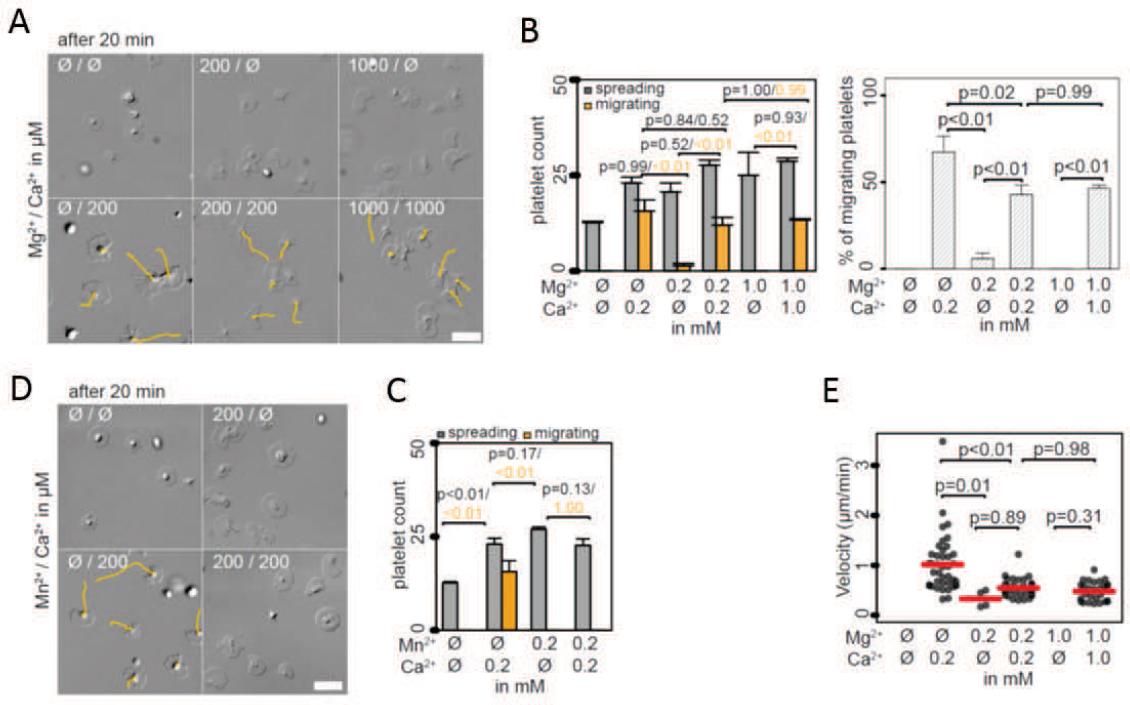

Figure 4.45 – Magnesium and manganese do not induce platelet migration. A, Representative DIC images of platelets migrating in the presence of the indicated magnesium and calcium concentrations. Yellow lines indicate the accumulated distance after 20min. Scale Bar = 10μm. B, and C, The total number of spreading and migrating platelets per experiment, fraction of migrating platelets and migration velocity are depicted for platelets migrating in the presence of the indicated magnesium and calcium concentrations. Platelets were pooled from n=3 experiments; red bars indicate the mean velocity; error bars=SEM; ANOVA/TukeyHSD. D, Representative DIC images of platelets migrating in the presence of the indicated manganese and calcium concentrations. Yellow lines indicate the accumulated distance after 20min. Scale Bar = 10μm. E, The total number of spreading and migrating platelets per experiment is depicted for platelets migrating in the presence of the indicated manganese and calcium concentrations. Platelets were pooled from n=3 experiments; error bars=SEM; ANOVA/TukeyHSD.

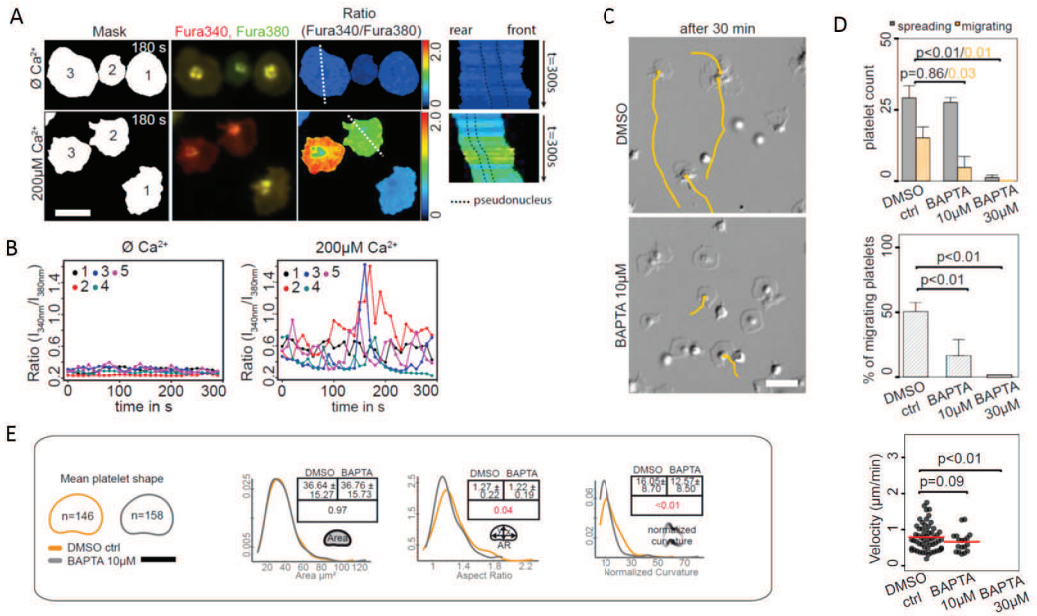

Figure 4.46 – Intracellular calcium oscillations trigger platelet migration. A, Binary masks of representative migrating platelets in the presence and absence of extracellular calcium (left). Platelets were loaded with Fura-2-AM (5μM) and images were recorded at 340nm (red) and 380nm (green). Ratio-images (340nm/380nm) are shown (right). Kymographs show the front-rear distribution of the Fura ratio along the white dotted line. Scale Bar = 5μm. B, Fura- ratios of representative platelets were recorded and plotted over time. C, Representative DIC images of DMSO (control) and BAPTA-AM (10μM) treated platelets. Yellow lines indicate the accumulated distance after 30min. Scale Bar = 10μm. D, Total number of spreading and migrating platelets , fraction of migrating platelets per experiment and migration velocity are depicted for BAPTA-AM (10μM, 30μM)- or DMSO-pre-treated platelets. Pooled from n=3 experiments; error bars=SEM; ANOVA/-TukeyHSD. E, Shape analysis of BAPTA (10μM) or DMSO (control) pre-treated platelets. The mean shape is shown for each group; Scale bar=5μm (left panels). Smooth density histograms displaying area, aspect ratio and normalized curvature for each group; the table shows mean±SD; p-values<0.05 (red) indicate significance; platelets were pooled from n=3 experiments; Wilcox test.

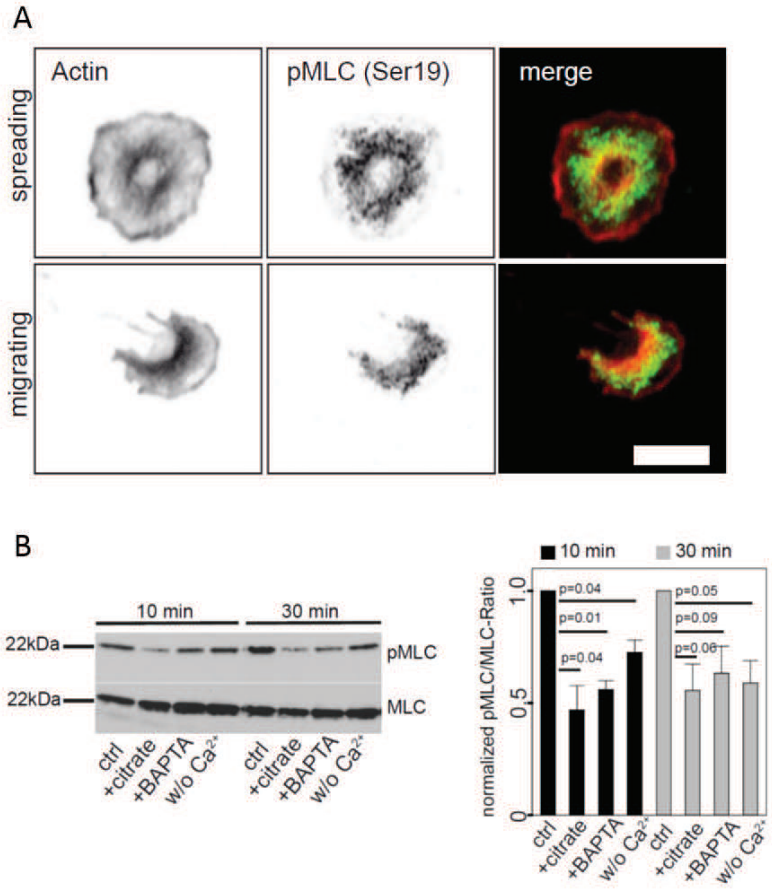

Figure 4.47 – Calcium oscillations trigger myosin light chain phosphorylation. A, Platelets were allowed to spread, immediately PFA-fixed before and after polarization/migration and stained with phalloidin-rhodamine (red) and anti-pMLC (green). Circularly spreading platelets have a concentric distribution of actin and pMLC. The overlay clearly shows a redistribution of myosin to the trailing edge of migrating platelets while an actin dense rim-like structure remains at the leading edge lamellipodium. Scale bar= 5μm. B, Myosin light chain phosphorylation (Ser16) is quantitatively reduced after depletion of intracellular calcium or removal from the extracellular space.

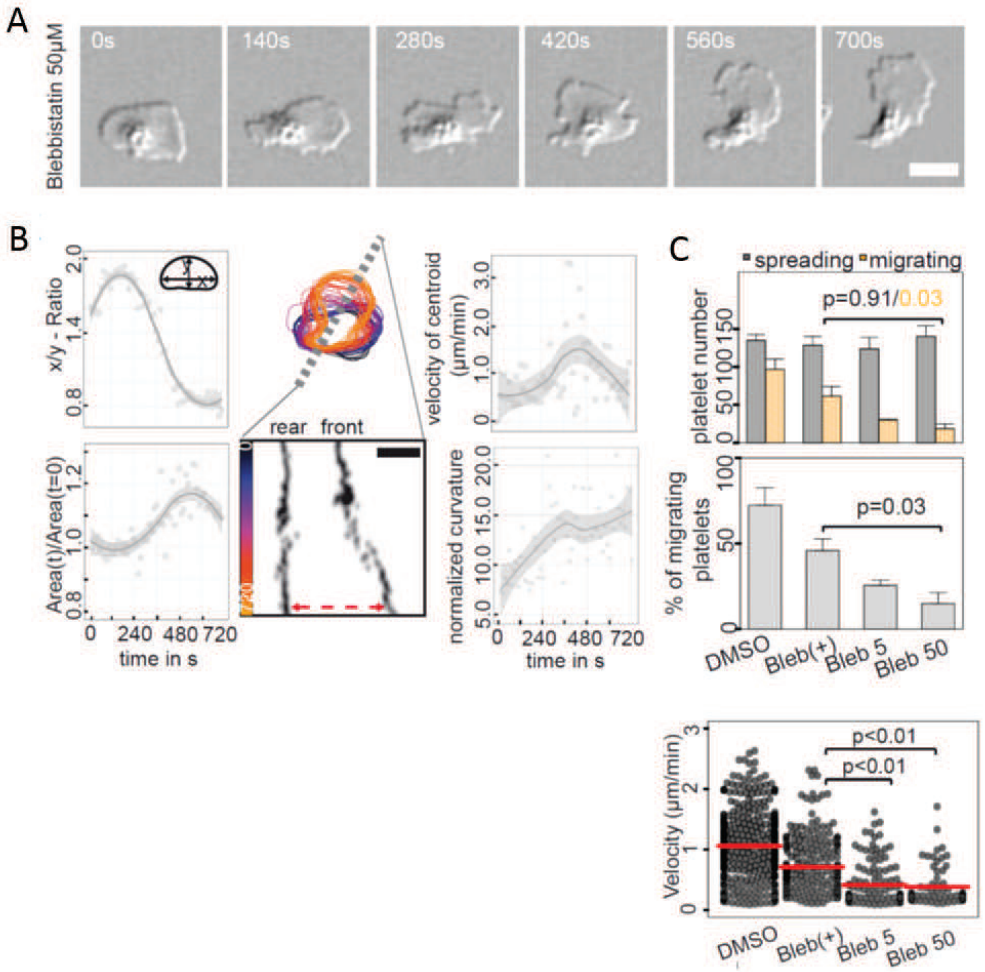

Figure 4.48 – Myosin IIa inhibition blocks platelet migration. A, DIC time series of a representative Blebbistatin (50μM) treated platelet during spreading and polarization. Scale bar= 5μm. B, The color-coded platelet outlines and the corresponding kymograph reveal the functional dissociation of front and back resulting in platelet elongation (red arrows) (right). Tracing of x/y-Ratio, Area, Centroid-velocity over time (left). C, Total number of spreading and migrating platelets per experiment and fraction of migrating platelets after Blebbistatin treatment. bleb(+)= 50μM Blebistatin (+) (inactive enantiomer); bleb 5/50= 5/50μM Blebbistatin(-). Platelets were pooled from n=5 experiments; error bars=SEM; ANOVA/TukeyHSD. Single platelet velocities of migrating platelets were quantified for Blebbistatin(-), Blebbistatin(+) or DMSO-treated platelets. Pooled from n=5 experiments; red bars = mean; Kruskal-Wallis/Wilcox.

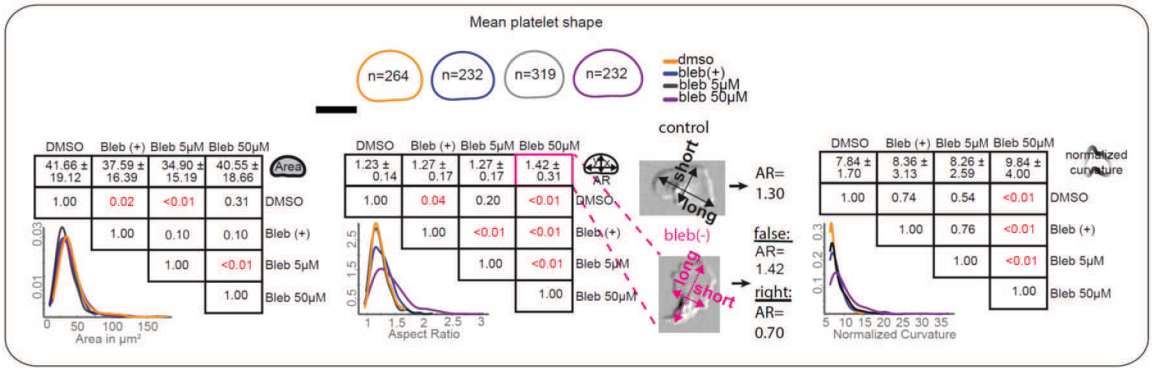

Figure 4.49 – Myosin IIa inhibition alters platelet polarization. Shape analysis of DMSO, 50μM Blebbistatin(+) (inactive enantiomer) and 5/50μM Blebbistatin(-) treated platelets. Please note that the aspect ratio is defined as long-axis (x)/short-axis (y) (see Material and Methods). Hyper-polarization of Blebbistatin-treated platelets leads to an inversion of the long axis and short axis axis and to a decreased aspect ratio. Since automatic shape analysis does not detect this inversion, the program retrieved a false increase in AR. Upper panels: Mean platelet shapes are shown for all groups and platelet numbers are indicated. Scale bar=5μm. Lower panel: Smooth density histograms displaying area and aspect ratio (x-axis) and normalize curvature as a density function (y-axis). Please note that the treatment with the inactive enantiomer Blebbistatin(+) (bleb(+)) also has an impact on platelet polarization measured by the aspect ratio. However, the comparison with the active Blebbistatin(-) reveals statistical significance. Platelets were pooled from 5 experiments; the tables show mean±SD; p-values<0.05 (red) indicate significance; Kruskal-Wallis/Wilcox.

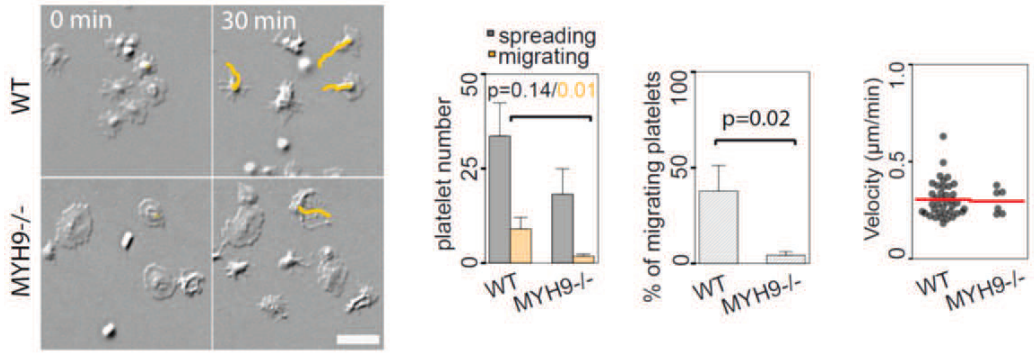

Figure 4.50 – MYH9-/- platelets do not migrate. DIC micrographs show WT (*PF4-Cre;MYH9$^{+/+}$*) and MYH9-/- (*PF4-Cre;MYH9$^{fl/fl}$*) platelets migrating for 30 min. Lower panels depict total numbersspreading and migrating platelets, fraction of migration and velocity of migration for n=5 independent experiments. p-values<0.05 indicate significance; Wilcox test. Scale bar= 10μm.

4.7 Platelet migration facilitates thrombus formation and reorganization in vitro and in vivo

Finally, we evaluated the biological relevance of platelet migration. *In vitro*, migrating platelets that come into contact with one another immediately start to form micro-aggregates (Fig. 4.51-4.55). These micro-aggregates continued to migrate collectively thereby recruiting additional platelets into a growing thrombus (Fig. 4.51 and 4.53). Inhibition of platelet migration by blocking $\alpha_{\mathrm{IIb}}\beta_3$ integrin, by depleting extra- and intracellular calcium or by inhibiting myosin-activation each abolished the formation of motile micro-aggregates (Fig. 4.53 and 4.54). This process was resistant to shearing flow at arterial rates and is therefore likely to contribute to platelet reorganization during thrombus formation *in vivo* (Fig. 4.53). To test this, we co-infused CFDA- or DDAO-tagged MYH9-deficient andcompensated control platelets into *PF4-Cre/R26R-Confetti* recipient mice undergoing vascular injury (for details see Materials and Methods). This allowed us to study the fate of individual platelets within the clot without altering the process of thrombus formation. Indeed, initial clot-retraction, a process that is known to partially depend on MYH9 (Leon et al., 2007; Calaminus et al., 2007), remained unaffected indicating that the low number of infused non-contractile platelets was compensated for by the myriad of untreated host platelets (Fig. 4.56 and 4.57). Correspondingly, the number of initially incorporated MYH9-/- platelets was comparable to control (Fig. 4.57). However, once recruited into the thrombus MYH9-/–platelets mainly remained sessile, while control platelets rearranged their position by migrating short distances (Fig. 4.56 and 4.57). Using this model we finally analyzed the relevance of platelet migration and evaluated its impact on thrombus architecture, specifically on the distribution of individual platelets within occlusive thrombi. Thrombi show a heterogeneous deposition of fibrinogen (Fig. 4.58). In vitro we found platelet migration to be most efficient at intermediate fibrinogen concentrations, while very high concentrations of fibrinogen suppress migration most likely due to an increase in substrate adhesiveness (Fig. 4.32). Hence, migration of platelets should lead to their preferential accumulation in areas of high fibrinogen over time. To test this, we measured the positioning of migrating (control) and non-migrating (MYH9-/-) platelets relative to the fibrinogen distribution (for details see Materials and Methods). As early as two hours after injury we observed significantly more control platelets accumulated at areas of high fibrinogen concentrations, indicating that this is a non-stochastic process favoring regions of

high adhesiveness. In contrast, significantly more non-migrating (MYH9-/-) platelets remained at sites of low fibrinogen deposition (Fig. 4.58 and 4.59), despite normal recruitment and incorporation into thrombi (Fig. 4.57 and 4.59). Interaction of platelets with high concentrations of fibrinogen increases their resistance towards shear (Bonnefoy et al., 2000), thus promoting thrombus consolidation and stabilization. During thrombus consolidation platelet accumulation at sites of high fibrinogen concentration occurs in two distinct waves (Fig. 4.59 and 4.60): A migration-independent wave triggered by the preferential adhesion of platelets to areas with high fibrinogen density and a second wave that depends on the myosin IIa-mediated migration of platelets within the thrombus and their autonomous relocation from fibrinogen-poor to fibrinogen-rich regions. More than one third of platelets are relocating to areas of high adhesiveness during the latter migration-dependent phase of thrombus consolidation (Fig. 4.59). The defect in thrombus stability and hemostasis observed in MYH9-deficient mice (Leon et al., 2007) as well as in patients with May-Hegglin-Anomaly (MHA), an autosomal dominant disorder associated with the MH9-gene (Godwin and Ginsburg, 1974), supports the critical contribution of platelet migration for thrombus consolidation.

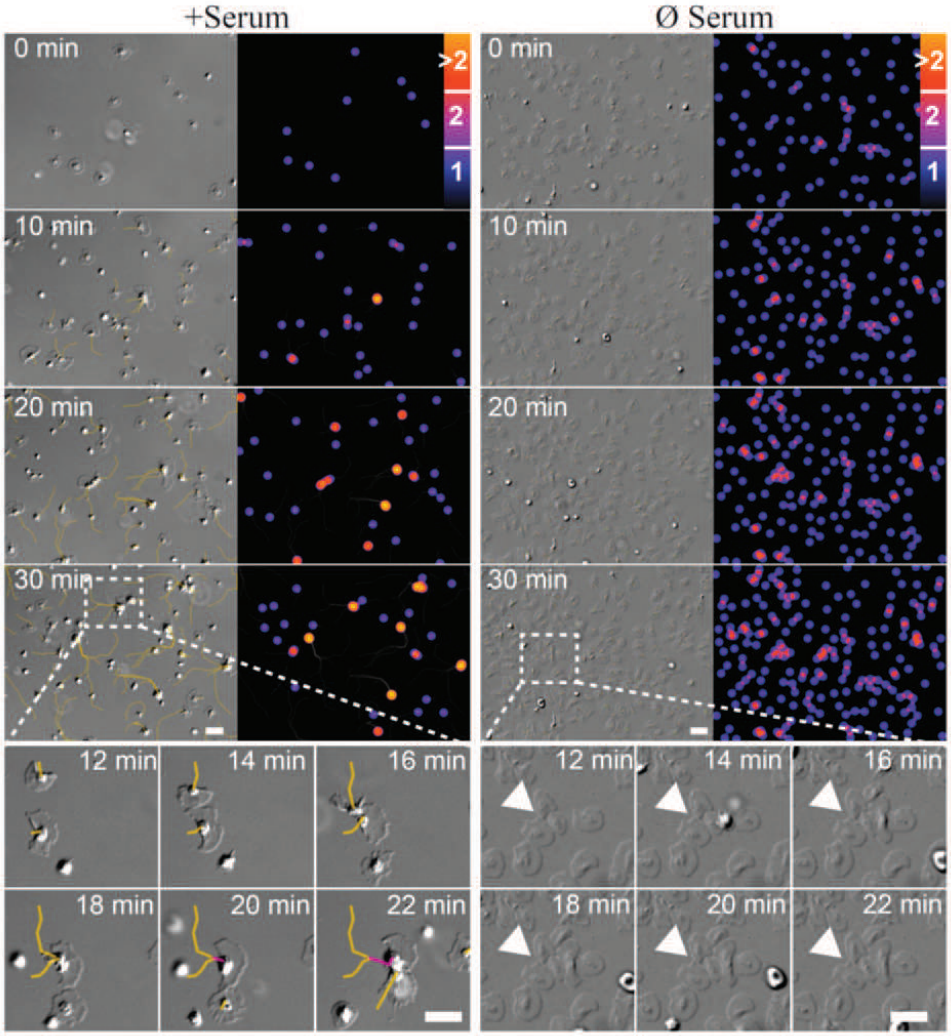

Figure 4.51 – Platelet migration promotes micro-thrombus formation. Upper panel: DIC time series of platelets migrating in the presence or absence of serum. Yellow lines indicate migration paths. Note the confluence of the paths at later time points. Left: When platelets get into physical contact micro-aggregates are formed (color-coded aggregate-size). Lower panel: Platelet-platelet interaction and agggregate-formation is depicted at higher magnification. Left: in the presence of serum, single migrating platelets (yellow line) that get into contact with each other, start forming aggregates and continue to migrate collectively (pink line). Right: In the absence of serum platelets, even though in close contact to each other remain sessile and do not form aggregates (white arrow head).

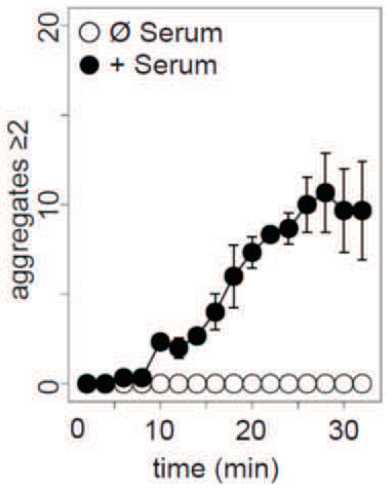

Figure 4.52 – Platelet migration promotes micro-thrombus formation (quantification from Fig. 4.51). Number of aggregates (≥2 platelets) was quantified over time. Note, the increasing number of aggregates in the presence of serum.

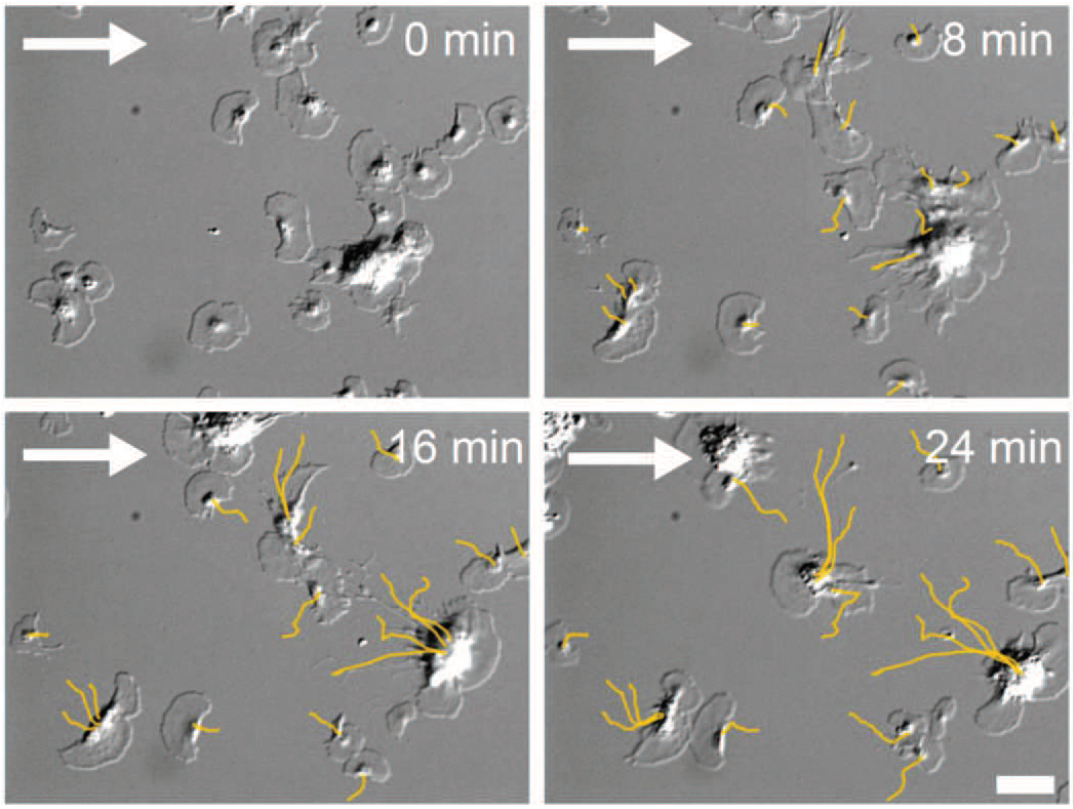

Figure 4.53 – Micro-thrombus formation is resistant of blood flow. Platelet migration and aggregate formation is resistant to aterial shear rates (1300/s). Flow direction is indicated by the white arrow.

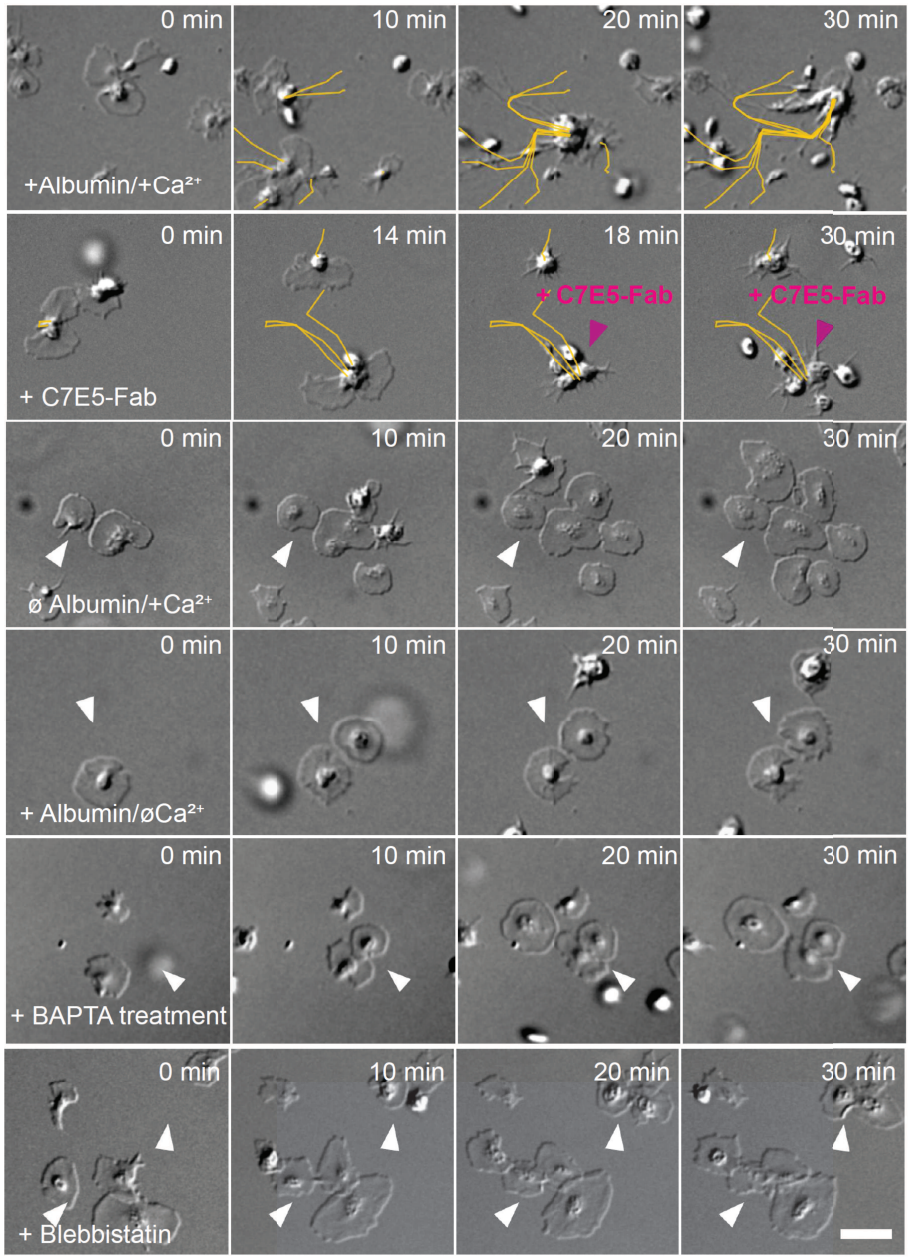

Figure 4.54 – Impaired micro-thrombus formation following inhibition of platelet migration. Platelet micro-aggregate formation depends on GPIIb ligation, extra-and intracellular calcium and myosin-activation, as well as a pro-migratory/anti-adhesive substratum (Albumin). Representative DIC time series are shown for the indicated experimental groups (1500μg/ml Albumin, 200μM Calcium, 10μM BAPTA-AM, 10μg/ml C7E5-Fab, 50μM Blebbistatin(-)). Yellow lines indicate platelet migration paths. White arrow heads highlight areas of close platelet-platelet contact. After treatment with C7E5-Fab microthrombi dis-aggregate (pink arrow head). Scale bar = 10μm.

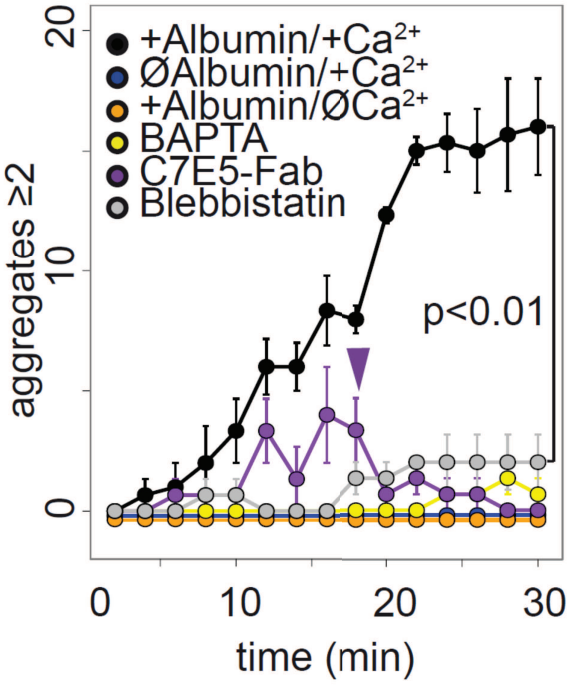

Figure 4.55 – Impaired micro-thrombus formation following inhibition of platelet migration (quantification from Fig. 4.54. Number of aggregates (≥2 platelets) was quantified over time for the indicated experimental groups. The purple arrow head indicates the timepoint of treatment with 10μg/ml C7E5-Fab. Statistical significance was tested for Albumin/Calcium and Blebbistatin(-) treatment after 30min; p-values<0.05 indicate significance; student's t-test; scale bar = 10μm.

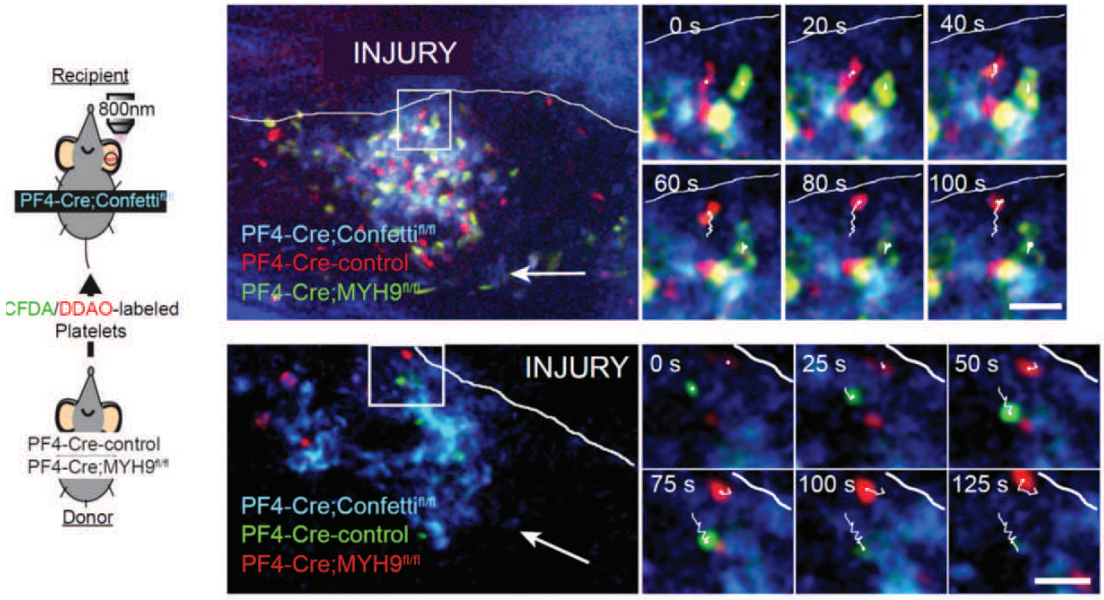

Figure 4.56 – MYH9-/- platelets show impaired migration *in vivo*. Washed platelets from *PF4-Cre*- and *PF4-Cre;MYH9fl/fl*-mice were stained with DDAO-SE or CFDA-SE and competitively transfused into *PF4-Cre;Confetti*-mice. White arrows indicate blood flow. White lines indicate migration paths. Note, that migratory behavior was independent of the staining procedure. Scale bar = 10μm.

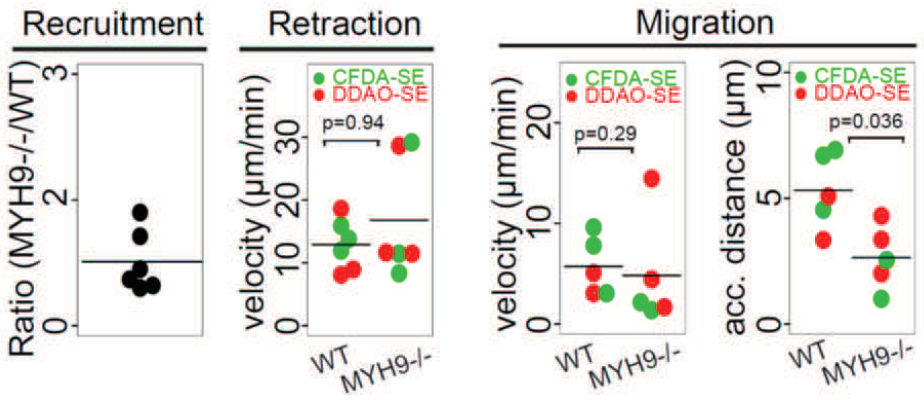

Figure 4.57 – MYH9-/- platelets show impaired migration *in vivo* (quantification from 4.56). Competitive recruitment of WT and MYH9-deficient platelets was measured as MYH9/WT-ratio. Single platelet velocities during clot retraction are shown. Single platelet velocities of migrating platelets and accumulated distances are shown. p-values<0.05 indicate significance; Wilcox test.

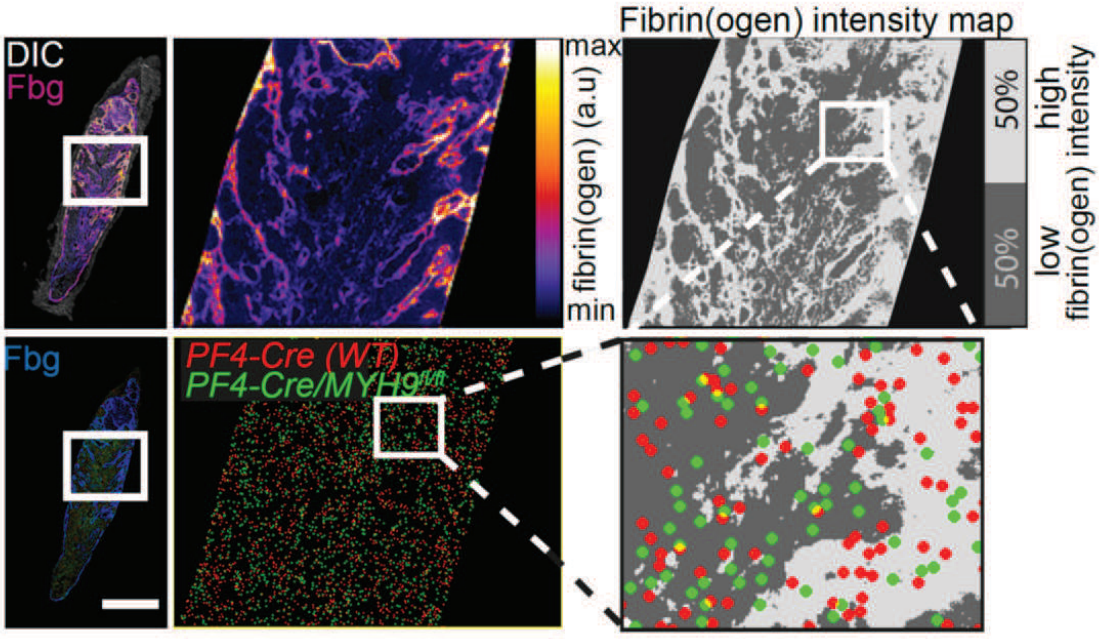

Figure 4.58 – Platelet migration reorganizes thrombus architecture. Left panel: cryosections of occlusive carotid artery thrombi after 2 h following FeCl-injury. Note, the heterogeneous distribution of fibrinogen (Alexa 546 labeled) within the thrombus. The distribution of *PF4-Cre* (green) - and *PF4-Cre;MYH9fl/fl* (red) platelets is depicted. right panel: fibrinogen intensity map: thrombi were segmented into 2 zones of equal area based on the indicated fibrinogen intensity-threshold (also see Fig. 3.2). The co-localization of fibrinogen intensity zones with platelets is shown at higher magnification below. Scale bar = 500μm.

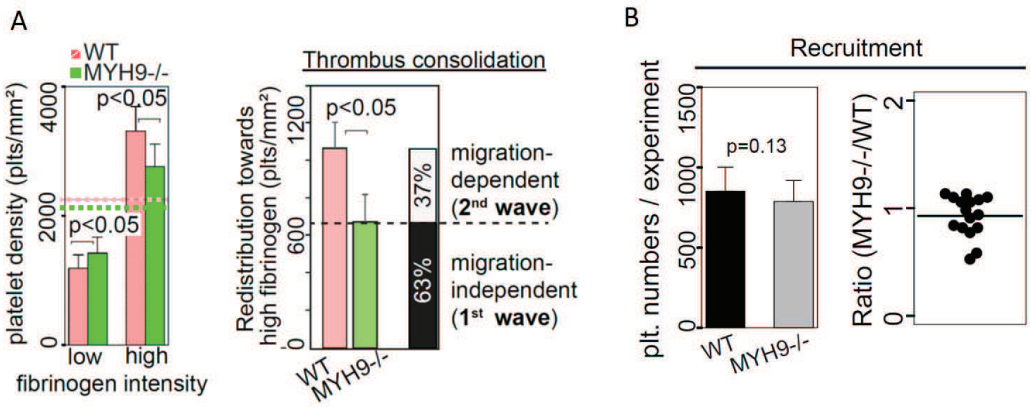

Figure 4.59 – Platelet migration reorganizes thrombus architecture (quantification from fig. 4.58). A, Left: Recruitment of platelets to fibrinogen intensity zones is shown as mean platelet densities (numbers/ mm^2). Dashed lines=stochastic platelet densities (fibrinogen-independent). Right: migration-dependent and -independent platelet redistribution. n=16 sections from 8 independent thrombi. P-values<0.05 indicate significance; paired t-test; scale bar=500 μm. B, Recruitment of *PF4-Cre-* and *PF4-Cre;MYH9fl/fl* platelets into occlusive carotid artery thrombi after 2h following FeCl-injury is measured by the mean total number of recruited platelets per experiment (right) and the ratio of *PF4-Cre;MYH9fl/fl* to *PF4-Cre* platelets (left). n=16; p-values<0.05 indicate significance; paired t-test.

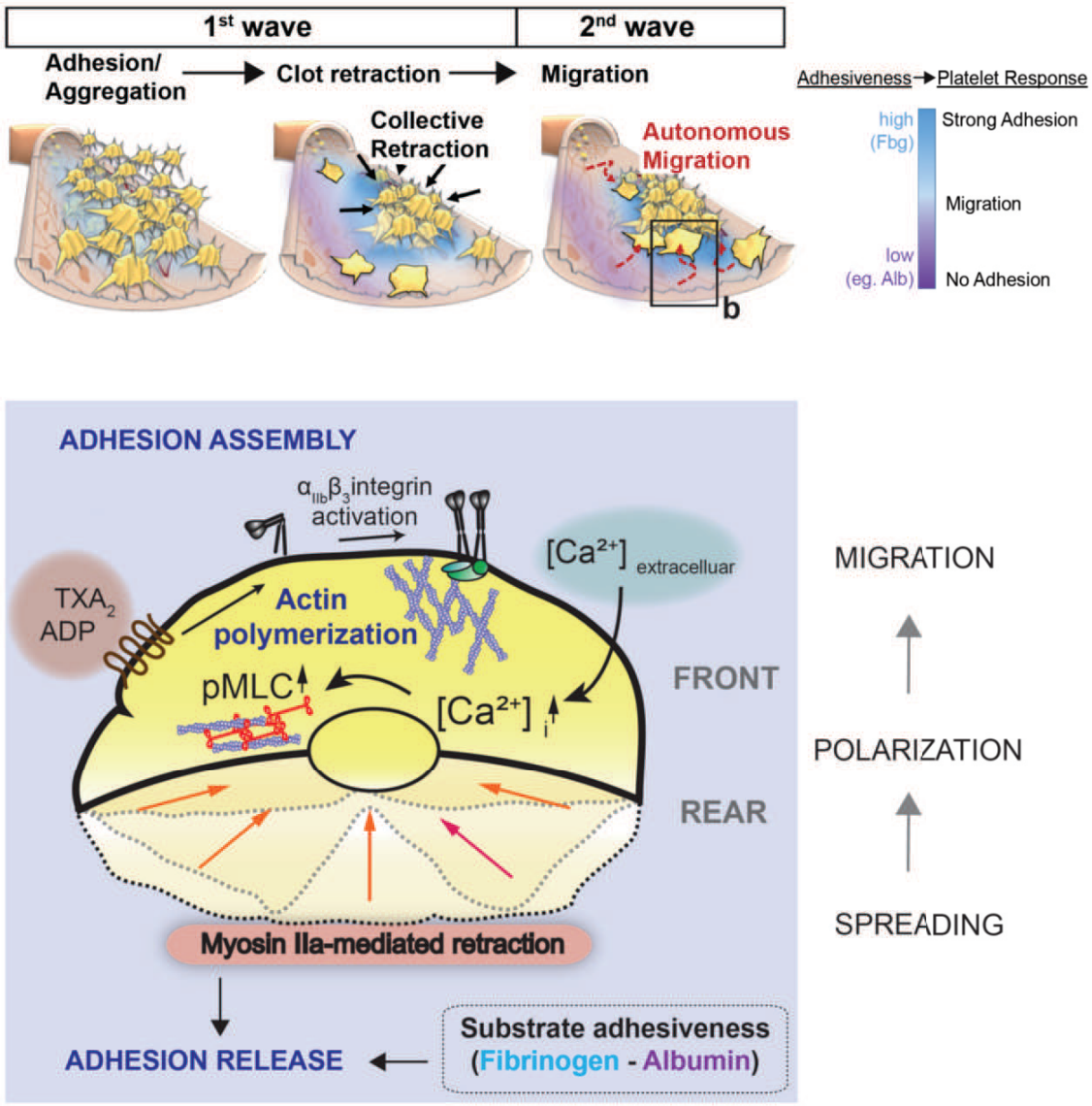

Figure 4.60 – Autonomous locomotion of anucleated platelets facilitates thrombus consolidation. Schematic presentation of migration- independent and- dependent waves of thrombus consolidation. Initial platelet recruitment to sites of vascular injury involves aggregation and collective clot-retraction (wave 1). Subsequent autonomous migration of platelets leads to redistribution within thrombi towards regions of higher adhesiveness (wave 2). Platelet migration requires a characteristic front-rear polarity. Actin-mediated protrusions and integrin-dependent adhesions are formed at the leading edge. A calcium-mediated increase in myosin IIa-dependent contractile forces then initiates retraction and adhesion release at the platelet rear resulting in forward locomotion.

5 Discussion

Platelet plug formation is considered to involve four distinct steps, platelet tethering, adhesion, followed by activation and aggregation. By intravital 2-photon microscopy of multicolor platelet reporter mice our study now identifies platelet migration as an additional and so far unrecognized event, which we show to control the spatio-temporal reorganization of individual platelets during thrombus formation in vivo. We demonstrate that migration of spread platelets is initiated by a morphologically distinct rearrangement of the platelet cytoskeleton, involving $\alpha_{\mathrm{IIb}}\beta_3$ ligation and actin polymerization at the leading edge, as well as albumin-facilitated and calcium-dependent myosin IIa-mediated adhesion release at the trailing edge (see Fig. 4.60). To overcome substrate adhesiveness and to maintain their characteristic polarized shape, migrating platelets have to generate contractile forces (see Fig. 4.60). Consequently, non-contractile, MYH9-deficient platelets show impaired platelet migration resulting in altered thrombus reorganization *in vivo*.

Non-mammalian vertebrates including birds have nucleated thrombocytes (Belamarich et al., 1966). However, this property has not been conserved during the evolution of specialized mammalian platelets, which are released as cytoplasmic fragments from megakaryocytes (Zhang et al., 2012) and no longer possess a nucleus. Consequently, the ability of mammalian platelets to migrate is linked to the fundamental question of whether cells can migrate despite the absence of a nucleus. The nucleus is important for de novo transcription, and its removal has originally been associated with impaired motility in amoebae (Clark, 1942; Mazia and Prescott, 1955). Meanwhile, however, experimentally derived enucleated cytoplasmic fragments of protozoan and metazoan cells have been shown to migrate without considerable impairment, indicating that the essential machinery driving locomotion is positioned within the cytoplasm and does not depend on a nucleus (Goldstein et al., 1960; Keller and Bessis, 1975; Euteneuer and Schliwa, 1984). Therefore, in theory the platelet as a terminally differentiated anucleate

cell fragment containing all contractile elements necessary for locomotion should also be able to migrate (Bettex-Galland1959). Indeed, we show here persistent migration of single platelets *in vitro* and *in vivo*, providing direct evidence for anucleate cell migration under physiological conditions in mammals, a phenomenon of potential relevance beyond platelet biology (Yount et al., 2007; Yipp et al., 2012).

The high density of individual platelets during thrombus formation has complicated imaging on a single cell level and the fate of individual platelets during this highly dynamic process remained unclear. Although previous studies raised the hypothesis that activated platelets might be able to migrate in the vicinity of vascular injuries (Lowenhaupt et al., 1973; Valone et al., 1974) or in the context of inflammation (Czapiga et al., 2004; Pitchford et al., 2008; Kraemer et al., 2010), direct *in vivo* evidence of platelet migration was lacking. Here, we generated multicolor platelet reporter textitPF4-Cre/R26R-Confetti-mice to trace individual platelets during thrombus formation *in vivo*. Due to the polyploidy of megakaryocytes, platelets from *PF4-Cre/R26R-Confetti*-mice show a wide range of individual colors enabling single platelet tracking *in vivo*. Using this novel mouse model we observed that platelets localizing within the tightly packed core region of the thrombus are immotile. However, a fraction of platelets within the thrombus periphery remains dynamic and rearranges their position in a process resembling migration. Migrating platelets show motility patterns distinct from tethering and retracting platelets, characterized by a lower velocity and a lower straightness of motility tracks. Platelet migration is resistant to blood flow, highlighting the active nature of this process and ruling out passive Brownian motion. We also excluded unspecific platelet motility caused by migrating leukocytes (von Brühl et al., 2012), since platelet migration was also present in leukocyte-depleted mice. Platelet migration follows a specific pattern of typical morphological changes. Prior to initiation of migration, platelets polarize changing their morphology from a symmetric pancake-like shape to a polarized half-moon-like shape. The resulting front-to-rear polarity is established by a protruding, fan-shaped lamellipodium at the leading edge and a contracting trailing edge, containing the cytoplasm-rich platelet "'pseudonucleus"'. Indeed, this robust polarization allows the morphological discrimination of migrating and non-migrating platelets by quantitative shape analysis, as previously observed in fish keratocytes (Keren et al., 2008). Symmetry breaking and initiation of cell motility relies on the spatial reorganization of cytoskeletal components. As such, the anisotropy of the actin-myosin IIa-system represents an established source of polarity, where actin poly-

merization is biased to the front end of a migrating cell, while myosin IIa retracts the rear (Yam et al., 2007). Correspondingly, we show here that polarization and migration of platelets requires actin-mediated protrusion at the leading edge and myosin IIa driven retraction of the trailing edge. But what are the molecular triggers initiating these critical rearrangements of the platelet cytoskeleton? Even though, migrating cells can polarize in the absence of extracellular asymmetric cues (Wedlich-Soldner and Li, 2003) many environmental guiding factors have been reported to reinforce cellular polarity and to maintain directional motility (Petrie et al., 2009). During thrombus formation, platelets also face a heterogeneous microenvironment constituted of diverse soluble as well as immobilized molecular cues, triggering the hierarchical architecture of a thrombus (Stalker et al., 2013). At the base of a penetrating vessel injury platelets strongly bind to the exposed subendothelial matrix. Correspondingly, we found that platelets do not migrate once in contact with collagen fibers. However, collagen-bound platelets release secondary mediators, including ADP and TXA2, and thus attract additional platelets to the site of injury (Packham et al., 1991). Here, we show that this ADP- and TXA2-enriched microenvironment surrounding the thrombus core, is also highly supportive for platelet migration. To spread and migrate on immobilized matrix-proteins platelets have to maintain their major adhesion receptor integrin $\alpha_{\mathrm{IIb}}\beta_3$ in an activated state, a process largely dependent on the converged signaling of various platelet G protein-coupled receptors (GPCRs). ADP-receptors (P2Y1, P2Y12) and TXA2-receptors (TPα, TPβ) are coupled to distinct G proteins, $G_{\alpha q}/G_{\alpha i}$ and $G_{\alpha q}/G_{\alpha 12/13}$, respectively (Offermanns, 2006). Correspondingly, in the absence of ADP-mediated $G_{\alpha i}$ signaling, $\alpha_{\mathrm{IIb}}\beta_3$ dependent spreading on plasma proteins is largely abolished (shown here and in Shigara et al. (2005)). On the other hand, TXA2 is mainly modulating the frequency and velocity of migration, possibly through enhanced contractile signaling mediated by $G_{\alpha 12/13}$ (Klages et al., 1999). In addition to these complementary effects, $G_{\alpha i}$ and $G_{\alpha 12/13}$ were shown to also synergize in $\alpha_{\mathrm{IIb}}\beta_3$ activation (Dorsam et al., 2002; Nieswandt et al., 2002). This is consistent with our observation that the highest efficiency of platelet spreading and migration are found in the presence of both mediators.

We also identified the substrate activated platelets are spreading and migrating on. Damaged blood vessels provide a scaffold for many adhesive plasma proteins, with fibrinogen, the major ligand of activated $\alpha_{\mathrm{IIb}}\beta_3$, being the most abundant among them (Denis and Wagner, 2007). Even though we detected high amounts of fibrinogen in the vicinity of vascular injuries and in areas of platelet migration *in vitro* and *in vivo*, fibrinogen alone

was not sufficient to promote platelet migration. Instead two additional serum factors, albumin and calcium, are necessary to restore platelet migration in the presence of fibrinogen. Albumin, the most abundant serum-protein is well known for its anti-adhesive properties and the presence of serum albumin reduces platelet spreading (Park et al., 1991). Accordingly, we observed a decreased number of spreading platelets at higher serum-to-fibrinogen ratios, while the fraction and speed of migrating platelets were increasing. This highlights the important role of modulation of substrate adhesiveness in the regulation of platelet migration, a general phenomenon previously demonstrated for other cell types (Gupton and Waterman-Storer, 2006; Barnhart et al., 2011). But how does albumin regulate fibrinogen-adhesiveness? Even though the presence of albumin quantitatively reduces the amount of immobilized fibrinogen, this does not explain its anti-adhesive action, since reduction of fibrinogen in the absence of albumin did not initiate migration (Appendix Fig. 5.1). In addition, at serum-to-fibrinogen ratios of approximately 10:1, spreading is not significantly reduced, while the number and fraction of migrating platelets dramatically increases, indicating that platelet migration and reduction of fibrinogen-dependent spreading do not correlate linearly. However, more detailed analysis of platelets spreading at these albumin concentrations shows an enhanced membrane ruffling, morphologically reflected by the increased curvature of their contour. Membrane ruffling is known to result from continuously retracting membrane protrusions due to inefficient anchorage to the substratum and therefore serves as an indicator of lower substratum adhesiveness (Borm et al., 2005; Gupton and Waterman-Storer, 2006). Our findings suggest that albumin alters fibrinogen-platelet and/or fibrinogen-surface interaction at concentrations that do not affect platelet spreading. In fact platelet interaction with surface-bound fibrinogen strongly depends on its conformational presentation, which is modulated by the co-absorption of albumin (Grinnell and Feld, 1981; Lindon et al., 1986; Park et al., 1991). Noteworthy this anti-adhesive action is not specific to albumin but can be replaced by other anti-adhesive proteins, including casein and ovalbumin (Appendix Fig. 5.2).

While the presence of albumin is required for establishing a low-adhesive, pro-migratory substratum, we found that threshold-levels of extracellular serum calcium constitute the molecular switch initiating the transition from spreading to migration. The important role of extracellular calcium transients in platelet activation and thrombus formation is well established and several calcium entry sites have been discovered, including the P2X1-receptor, the transient receptor potential ion channel 6 (TRPC6) and

store-operated calcium entry via Stim1-Orai1 (Vial et al., 1997; Hassock et al., 2002; Varga-Szabo et al., 2008; Braun et al., 2008). However, the role of calcium for platelet migration as a novel platelet function remains unaddressed. Here we show that transmembrane calcium fluxes are amplifying intracellular calcium oscillations, necessary for morphological polarization and subsequent platelet migration. Accordingly, removal of extracellular Ca^{2+} or buffering of $[Ca^{2+}]_i$ inhibits the migration of platelets. Calcium is well known as a key regulator of cell migration and spatio-temporally coordinated calcium fluxes mediate polarization, speed and directionality (Taylor et al., 1980; Brundage et al., 1991; Hahn et al., 1992; Eddy et al., 2000; Gomez et al., 2001; Evans and Falke, 2007; Wei et al., 2009; Tsai and Meyer, 2012; Tsai et al., 2014). While localized calcium fluxes at the leading edge of migrating cells are involved in directional steering and turning, an intracellular calcium gradient from the front to the back has been shown to correlate with myosin IIa mediated contractile forces necessary to release adhesion sites facilitating forward movement (Wei et al., 2009; Tsai et al., 2014; Lee et al., 1999; Martini and Valdeolmillos, 2010). Even though calcium-signals are not preferentially localized towards the rear of a migrating platelet, we found that global extracellular calcium-influx is required for MLC-phosphorylation (Ser19) and myosin IIa-activation. Consequently, platelet rear retraction is dramatically reduced in the absence of calcium oscillations. We thus defined calcium influx-mediated, myosin IIa-dependent adhesion release as a key regulatory step in initiating the transition from spreading to migration. Removal of extracellular calcium or inhibition of myosin IIa modulates platelet migration without affecting spreading.

But does platelet migration affect thrombus formation *in vivo*? *In vitro* expermients show that individual, initially dispersed platelets get into close contact as a result of migration. Once in direct contact platelets form micro-aggregates that continue migrating, while fusing with other aggregates, thereby accelerating thrombus growth. Consequently, platelets initially not precisely localized within a thrombus can intrinsically optimize their positioning and thereby facilitate thrombus consolidation. Importantly, platelet migration as an active cell-autonomous occurs independent of the collective, contractile movement associated with clot retraction (Ono et al., 2008). While clot retraction is important to quickly stop acute bleeding, platelet migration is a rather slow process unlikely to contribute to early steps of thrombus formation. Correspondingly, we show that platelet locomotion rather supports subsequent thrombus reorganization and consolidation by allowing platelets to reorientate towards regions of high fibrinogen

concentration. Autonomous migration therefore primarily enables recruited platelets to reposition to the areas of highest substrate adhesiveness within the heterogeneous meshwork of developing thrombi, increasing clot resistance to blood shear forces. In summary, we propose a new model of hemostatic and thrombotic plug formation, where platelet migration is governed by the local adhesiveness of the micro-environment to enhance the probability of platelet-platelet- and platelet-fibrinogen-interactions leading to thrombus consolidation at sites of injury. While our study identifies platelet migration as a dynamic regulator in the context of thrombosis, it may also provide the missing functional link to the poorly defined role of platelets in a wide range of (patho-)physiologies, including chronic inflammation, cell mediated host-pathogen defense and development (Boilard et al., 2010; Yeaman, 2014; Bertozzi et al., 2010).

Bibliography

Ananthakrishnan, R. and Ehrlicher, A. (2007): The forces behind cell movement, Int J Biol Sci **3**(5): 303–317.
URL: *http://www.ijbs.com/v03p0303.htm*

Atkinson, Ben T., Stafford, Margaret J., Pears, Catherine J. and Watson, Steve P. (2001): Signalling events underlying platelet aggregation induced by the glycoprotein vi agonist convulxin, Eur. J. Biochem. **268**(20): 5242–5248.
URL: *http://dx.doi.org/10.1046/j.0014-2956.2001.02448.x*

Barnhart, Erin L., Lee, Kun-Chun, Keren, Kinneret, Mogilner, Alex and Theriot, Julie A. (2011): An adhesion-dependent switch between mechanisms that determine motile cell shape, PLoS Biol **9**(5): e1001059.

Basani, Ramesh B., D'Andrea, Giovanna, Mitra, Neal, Vilaire, Gaston, Richberg, Mark, Kowalska, M. Anna, Bennett, Joel S. and Poncz, Mortimer (2001): Rgd-containing peptides inhibit fibrinogen binding to platelet aiib3 by inducing an allosteric change in the amino-terminal portion of aiib, J. Biol. Chem. **276**(17): 13975–13981.
URL: *http://www.jbc.org/content/276/17/13975.abstract*

Belamarich, Frank A., Fusari, Margaret H., Sherpo, David and Kien, Marja (1966): In vitro studies of aggregation of non-mammalian thrombocytes, Nature **212**(5070): 1579–1580.
URL: *http://dx.doi.org/10.1038/2121579a0*

Bennett, J.S., Berger, B.W. and Billings, P.C. (2009): The structure and function of platelet integrins, J. Thromb. Haemost. **7**: 200–205.

Bergmeier, W., Piffath, C.L., Goerge, T., Cifuni, S.M., Ruggeri, Z.M., Ware, J. and Wagner, D.D. (2006): The role of platelet adhesion receptor gpibalpha far exceeds

that of its main ligand, von willebrand factor, in arterial thrombosis, Proc Natl Acad Sci U S A. **103**(45): 16900–16905.

Bertozzi, Cara C., Schmaier, Alec A., Mericko, Patricia, Hess, Paul R., Zou, Zhiying, Chen, Mei, Chen, Chiu-Yu, Xu, Bin, Lu, Min-min, Zhou, Diane, Sebzda, Eric, Santore, Matthew T., Merianos, Demetri J., Stadtfeld, Matthias, Flake, Alan W., Graf, Thomas, Skoda, Radek, Maltzman, Jonathan S., Koretzky, Gary A. and Kahn, Mark L. (2010): Platelets regulate lymphatic vascular development through clec-2-slp-76 signaling, Blood **116**(4): 661–670.
URL: *http://www.bloodjournal.org/content/116/4/661.abstract*

Bettex-Galland, M. and Luscher, E. F. (1959): Extraction of an actomyosin-like protein from human thrombocytes, Nature **184**(4682): 276–277.
URL: *http://dx.doi.org/10.1038/184276b0*

Blair, P. and Flaumenhaft, R. (2009): Platelet alpha-granules: Basic biology and clinical correlates, Blood Rev **23**(4): 177–189.

Boilard, Eric, Nigrovic, Peter A., Larabee, Katherine, Watts, Gerald F. M., Coblyn, Jonathan S., Weinblatt, Michael E., Massarotti, Elena M., Remold-O'Donnell, Eileen, Farndale, Richard W., Ware, Jerry and Lee, David M. (2010): Platelets amplify inflammation in arthritis via collagen-dependent microparticle production, Science **327**(5965): 580–583.
URL: *http://www.sciencemag.org/content/327/5965/580.abstract*

Bonnefoy, Arnaud, Liu, Qingde, Legrand, Chantal and Frojmovic, Mony M. (2000): Efficiency of platelet adhesion to fibrinogen depends on both cell activation and flow, Biophysical Journal **78**(6): 2834–2843.
URL: *http://www.cell.com/biophysj/abstract/S0006-3495(00)76826-3*

Borm, Bodo, Requardt, Robert P., Herzog, Volker and Kirfel, Gregor (2005): Membrane ruffles in cell migration: indicators of inefficient lamellipodia adhesion and compartments of actin filament reorganization, Exp. Cell Res. **302**(1): 83–95.
URL: *http://www.sciencedirect.com/science/article/pii/S0014482704005142*

Boyden, Stephen (1962): The chemotactic effect of mixtures of antibody and antigen on polymorphonuclear leucocytes, The Journal of Experimental Medicine **115**(3): 453–466.
URL: *http://jem.rupress.org/content/115/3/453.abstract*

Braun, Attila, Varga-Szabo, David, Kleinschnitz, Christoph, Pleines, Irina, Bender, Markus, Austinat, Madeleine, Bösl, Michael, Stoll, Guido and Nieswandt, Bernhard (2008): Orai1 (cracm1) is the platelet soc channel and essential for pathological thrombus formation, Blood **113**(9): 2056–2063.
URL: *http://www.bloodjournal.org/content/113/9/2056.abstract*

Brundage, RA, Fogarty, KE, Tuft, RA and Fay, FS (1991): Calcium gradients underlying polarization and chemotaxis of eosinophils, Science **254**(5032): 703–706.
URL: *http://www.sciencemag.org/content/254/5032/703.abstract*

Burton, Kevin, Park, Jung H. and Taylor, D. Lansing (1999): Keratocytes generate traction forces in two phases, Molecular Biology of the Cell **10**(11): 3745–3769.
URL: *http://www.molbiolcell.org/content/10/11/3745.abstract*

Calaminus, SD, Auger, JM, McCarty, OJ, Wakelam, MJ, Machesky, LM and Watson, SP (2007): Myosiniia contractility is required for maintenance of platelet structure during spreading on collagen and contributes to thrombus stability., J Thromb Haemost **5**(10): 2136–2145–.
URL: *http://europepmc.org/abstract/MED/17645784*

Casella, James F., Flanagan, Michael D. and Lin, Shin (1981): Cytochalasin d inhibits actin polymerization and induces depolymerization of actin filaments formed during platelet shape change, Nature **293**(5830): 302–305.
URL: *http://dx.doi.org/10.1038/293302a0*

Chou, J., Mackman, N., Merrill-Skoloff, G., Pedersen, B., Furie, B.C. and Furie, B. (2004): Hematopoietic cell-derived microparticle tissue factor contributes to fibrin formation during thrombus propagation, Blood **104**(10): 3190–3197.

Clark, AM (1942): Some effects of removing the nucleus from amoeba, Aust J Exp Biol Med **20**(4): 241–247.
URL: *http://dx.doi.org/10.1038/icb.1942.40*

Coller, B S (1985): A new murine monoclonal antibody reports an activation-dependent change in the conformation and/or microenvironment of the platelet glycoprotein iib/iiia complex., J Clin Invest **76**(1): 101–108.
URL: *http://www.jci.org/articles/view/111931*

Corash, L, Chen, HY, Levin, J, Baker, G, Lu, H and Mok, Y (1987): Regulation of thrombopoiesis: effects of the degree of thrombocytopenia on megakaryocyte ploidy and platelet volume, Blood **70**(1): 177–185.
URL: *http://bloodjournal.hematologylibrary.org/content/70/1/177.abstract*

Cornelissen, I., Palmer, D., David, T., Wilsbacher, L., Concengco, C., Conley, P., Pandey, A. and Coughlin, S.R. (2010): Roles and interactions among protease-activated receptors and p2ry12 in hemostasis and thrombosis, Proc Natl Acad Sci U S A. **107**(43): 18605–18610.

Coughlin, S.R. (2005): Protease-activated receptors in hemostasis, thrombosis and vascular biology, J. Thromb. Haemost. **3**(8): 1800–1814.

Czapiga, Meggan, Gao, Ji-Liang, Kirk, Allan and Lekstrom-Himes, Julie (2004): Human platelets exhibit chemotaxis using functional n-formyl peptide receptors, Exp. Hematol. **33**(1): 73–84.
URL: *http://www.exphem.org/article/S0301-472X(04)00351-0/abstract*

Daley, Jean M., Thomay, Alan A., Connolly, Michael D., Reichner, Jonathan S. and Albina, Jorge E. (2008): Use of ly6g-specific monoclonal antibody to deplete neutrophils in mice, J. Leukoc. Biol. **83**(1): 64–70.
URL: *http://www.jleukbio.org/content/83/1/64.abstract*

Davydovskaya, Polina, Janko, Marek, Gaertner, Florian, Ahmad, Zerkah, Simsek, Özlem, Massberg, Steffen and Stark, Robert W. (2012): Blood platelet adhesion to printed von willebrand factor, J. Biomed. Mater. Res. **100A**(2): 335–341.
URL: *http://dx.doi.org/10.1002/jbm.a.33275*

Denis, Cecile V. and Wagner, Denisa D. (2007): Platelet adhesion receptors and their ligands in mouse models of thrombosis, Arterioscler. Thromb. Vasc. Biol. **27**(4): 728–739.
URL: *http://atvb.ahajournals.org/content/27/4/728.abstract*

Doering, Yvonne, Pawig, Lukas, Weber, Christian and Noels, Heidi (2014): The cxcl12/cxcr4 chemokine ligand/receptor axis in cardiovascular disease, Frontiers in Physiology **5**: –.
URL: *http://www.frontiersin.org/Journal/Abstract*

Dorsam, Robert T., Kim, Soochong, Jin, Jianguo and Kunapuli, Satya P. (2002): Coordinated signaling through both g12/13 and gi pathways is sufficient to activate gpiib/iiia in human platelets, J. Biol. Chem. **277**(49): 47588–47595.
URL: *http://www.jbc.org/content/277/49/47588.abstract*

Dubois, C., Panicot-Dubois, L., Merrill-Skoloff, G., Furie, B. and Furie, B. C. (2006): Glycoprotein vi-dependent and -independent pathways of thrombus formation in vivo, Blood **107**(10): 3902–3906.

Duquesnoy, RJ, Lorentsen, DF and Aster, RH (1975): Platelet migration inhibition: a new method for detection of platelet antibodies, Blood **45**(6): 741–747.
URL: *http://www.bloodjournal.org/content/45/6/741.abstract*

Eddy, R.J., Pierini, L.M., Matsumura, F. and Maxfield, F.R. (2000): Ca2+-dependent myosin ii activation is required for uropod retraction during neutrophil migration, J. Cell Sci. **113**(7): 1287–1298.
URL: *http://jcs.biologists.org/content/113/7/1287.abstract*

Emambokus, Nikla R and Frampton, Jonathan (2003): The glycoprotein iib molecule is expressed on early murine hematopoietic progenitors and regulates their numbers in sites of hematopoiesis, Immunity **19**(1): 33–45.
URL: *http://www.cell.com/immunity/abstract/S1074-7613(03)00173-0*

Engelmann, Bernd and Massberg, Steffen (2013): Thrombosis as an intravascular effector of innate immunity, Nat Rev Immunol **13**(1): 34–45.
URL: *http://dx.doi.org/10.1038/nri3345*

Euteneuer, Ursula and Schliwa, Manfred (1984): Persistent, directional motility of cells and cytoplasmic fragments in the absence of microtubules, Nature **310**(5972): 58–61.
URL: *http://dx.doi.org/10.1038/310058a0*

Evans, John H. and Falke, Joseph J. (2007): Ca2+ influx is an essential component of the positive-feedback loop that maintains leading-edge structure and activity in macrophages, Proc Natl Acad Sci U S A. **104**(41): 16176–16181.
URL: *http://www.pnas.org/content/104/41/16176.abstract*

Feng, D., Nagy, J.A., Pyne, K., Dvorak, H.F. and Dvorak, A.M. (1998): Platelets exit venules by a transcellular pathway at sites of f-met peptide-induced acute inflammation in guinea pigs, Int Arch Allergy Immunol **116**(3): 188–195.
URL: *http://www.karger.com/DOI/10.1159/000023944*

Fox, Joan E. B. and Phillips, David R. (1981): Inhibition of actin polymerization in blood platelets by cytochalasins, Nature **292**(5824): 650–652.
URL: *http://dx.doi.org/10.1038/292650a0*

Fukata, Masaki, Nakagawa, Masato and Kaibuchi, Kozo (2003): Roles of rho-family gtpases in cell polarisation and directional migration, Curr. Opin. Cell Biol. **15**(5): 590–597.
URL: *http://www.sciencedirect.com/science/article/pii/S0955067403000978*

Furie, Bruce and Furie, Barbara C. (2008): Mechanisms of thrombus formation, N Engl J Med **359**(9): 938–949.
URL: *http://dx.doi.org/10.1056/NEJMra0801082*

Gachet, C. (2008): P2 receptors, platelet function and pharmacological implications, Thrombosis and Haemostasis **99/3**: 466–472.

Gailit, J and Ruoslahti, E (1988): Regulation of the fibronectin receptor affinity by divalent cations., J. Biol. Chem. **263**(26): 12927–12932.
URL: *http://www.jbc.org/content/263/26/12927.abstract*

George, Mariam and Vaughan, John H. (1962): In vitro cell migration as a model for delayed hypersensitivity., Experimental Biology and Medicine **111**(2): 514–521.
URL: *http://ebm.sagepub.com/content/111/2/514.abstract*

Giannone, Grégory, Dubin-Thaler, Benjamin J., Döbereiner, Hans-Günther, Kieffer, Nelly, Bresnick, Anne R. and Sheetz, Michael P. (2004): Periodic lamellipodial contractions correlate with rearward actin waves., Cell **116**(3): 431–443.

Gleissner, C.A., von Hundelshausen, P. and Ley, K. (2008): Platelet chemokines in vascular disease, Arteriosclerosis, Thrombosis, and Vascular Biology **28**(11): 1920–1927.

Godwin, Herman A. and Ginsburg, A. David (1974): May-hegglin anomaly: A defect in megakaryocyte fragmentation?, British Journal of Haematology **26**(1): 117–127.
URL: *http://dx.doi.org/10.1111/j.1365-2141.1974.tb00455.x*

Goldstein, L., Cailleau, R. and Crocker, T.T. (1960): Nuclear-cytoplasmic relationships in human cells in tissue culture: Ii. the microscopic behavior of enucleate human cell fragments, Exp. Cell Res. **19**(2): 332–342.
URL: *http://www.sciencedirect.com/science/article/pii/0014482760900124*

Gomez, Timothy M., Robles, Estuardo, Poo, Mu-ming and Spitzer, Nicholas C. (2001): Filopodial calcium transients promote substrate-dependent growth cone turning, Science **291**(5510): 1983–1987.
URL: *http://www.sciencemag.org/content/291/5510/1983.abstract*

Grinnell, Frederick and Feld, Marian K. (1981): Adsorption characteristics of plasma fibronectin in relationship to biological activity, J. Biomed. Mater. Res. **15**(3): 363–381.
URL: *http://dx.doi.org/10.1002/jbm.820150308*

Gupton, Stephanie L. and Waterman-Storer, Clare M. (2006): Spatiotemporal feedback between actomyosin and focal-adhesion systems optimizes rapid cell migration, Cell **125**(7): 1361–1374.
URL: *http://linkinghub.elsevier.com/retrieve/pii/S0092867406007197*

Hahn, Klaus, DeBiasio, Robbin and Taylor, D. Lansing (1992): Patterns of elevated free calcium and calmodulin activation in living cells, Nature **359**(6397): 736–738.
URL: *http://dx.doi.org/10.1038/359736a0*

Hassock, Sheila R., Zhu, Michael X., Trost, Claudia, Flockerzi, Veit and Authi, Kalwant S. (2002): Expression and role of trpc proteins in human platelets: evidence that trpc6 forms the store-independent calcium entry channel, Blood **100**(8): 2801–2811.
URL: *http://www.bloodjournal.org/content/100/8/2801.abstract*

Inoue, Osamu, Suzuki-Inoue, Katsue, Dean, William L., Frampton, Jon and Watson, Steve P. (2003): Integrin a2b1 mediates outside-in regulation of platelet spreading on collagen through activation of src kinases and plcy2, J. Cell Biol. **160**(5): 769–780.
URL: *http://jcb.rupress.org/content/160/5/769.abstract*

Isenberg, W M, McEver, R P, Phillips, D R, Shuman, M A and Bainton, D F (1987): The platelet fibrinogen receptor: an immunogold-surface replica study of agonist-induced ligand binding and receptor clustering., J. Cell Biol. **104**(6): 1655–1663.
URL: *http://jcb.rupress.org/content/104/6/1655.abstract*

Jackson, Shaun P. (2007): The growing complexity of platelet aggregation, Blood **109**(12): 5087–5095.
URL: *http://www.bloodjournal.org/content/109/12/5087.abstract*

Jedlitschky, G., Greinacher, A. and Kroemer, H.K. (2012): Transporters in human platelets: physiologic function and impact for pharmacotherapy, Blood **119**(15): 3394–3402.

Jin, Jianguo, Quinton, Todd M., Zhang, Jin, Rittenhouse, Susan E. and Kunapuli, Satya P. (2002): Adenosine diphosphate (adp)-induced thromboxane a2 generation in human platelets requires coordinated signaling through integrin aiibbiia and adp receptors, Blood **99**(1): 193–198.
URL: *http://bloodjournal.hematologylibrary.org/content/99/1/193.abstract*

Jones, S.W., Johnson, K., Potter, D. and Griffin, J. (1999): Process Technology for the Twenty-first Century, Semiconductor Consulting Services.
URL: *http://books.google.de/books?id=gyL4GgAACAAJ*

Kakoma, I, Carson, C A, Ristic, M, Stephenson, E M, Hildebrandt, P K and Huxsoll, D L (1978): Platelet migration inhibtion as an indicator of immunologically mediated target cell injury in canine ehrlichiosis., Infection and Immunity **20**(1): 242–247.
URL: *http://iai.asm.org/content/20/1/242.abstract*

Kamps, Angela R. and Coffman, Clark R. (2005): G protein-coupled receptor roles in cell migration and cell death decisions, Annals of the New York Academy of Sciences **1049**(1): 17–23.
URL: *http://dx.doi.org/10.1196/annals.1334.003*

Kanaji, Taisuke, Russell, Susan and Ware, Jerry (2002): Amelioration of the macrothrombocytopenia associated with the murine bernard-soulier syndrome, Blood **100**(6): 2102–2107.
URL: *http://www.bloodjournal.org/content/100/6/2102.abstract*

Kansas, GS (1996): Selectins and their ligands: current concepts and controversies, Blood **88**(9): 3259–3287.
URL: *http://www.bloodjournal.org/content/88/9/3259.abstract*

Kardash, Elena, Bandemer, Jan and Raz, Erez (2011): Imaging protein activity in live embryos using fluorescence resonance energy transfer biosensors, Nat. Protocols **6**(12): 1835–1846.
URL: *http://dx.doi.org/10.1038/nprot.2011.395*

Keller, H. U. and Bessis, M. (1975): Migration and chemotaxis of anucleate cytoplasmic leukocyte fragments, Nature **258**(5537): 723–724.
URL: *http://dx.doi.org/10.1038/258723a0*

Keren, Kinneret, Pincus, Zachary, Allen, Greg M., Barnhart, Erin L., Marriott, Gerard, Mogilner, Alex and Theriot, Julie A. (2008): Mechanism of shape determination in motile cells, Nature **453**(7194): 475–480.
URL: *http://dx.doi.org/10.1038/nature06952*

Klages, Birgit, Brandt, Ursula, Simon, Melvin I., Schultz, Günter and Offermanns, Stefan (1999): Activation of g12/g13 results in shape change and rho/rho-kinase-mediated myosin light chain phosphorylation in mouse platelets, J. Cell Biol. **144**(4): 745–754.
URL: *http://jcb.rupress.org/content/144/4/745.abstract*

Koike, Yuhki, Tanaka, Koji, Okugawa, Yoshinaga, Morimoto, Yuhki, Toiyama, Yuji, Uchida, Keiichi, Miki, Chikao, Mizoguchi, Akira and Kusunoki, Masato (2011): In vivo real-time two-photon microscopic imaging of platelet aggregation induced by selective laser irradiation to the endothelium created in the beta-actin-green fluorescent protein transgenic mice, J Thromb Thrombolysis. **32**(2): 138–145–.
URL: *http://dx.doi.org/10.1007/s11239-011-0600-y*

Kraemer, Bjoern., Borst, Oliver, Gehring, Eva-Maria, Schoenberger, Tanja, Urban, Benjamin, Ninci, Elena, Seizer, Peter, Schmidt, Christine, Bigalke, Boris, Koch, Miriam, Martinovic, Ivo, Daub, Karin, Merz, Tobias, Schwanitz, Laura, Stellos, Konstantinos, Fiesel, Fabienne, Schaller, Martin, Lang, Florian, Gawaz, Meinrad and Lindemann, Stephan (2010): Pi3 kinase-dependent stimulation of platelet migration by stromal cell-derived factor 1 (sdf-1), J. Mol. Med. **88**(12): 1277–1288.
URL: *http://dx.doi.org/10.1007/s00109-010-0680-8*

Kraemer, Bjoern F., Schmidt, Christine, Urban, Benjamin, Bigalke, Boris, Schwanitz, Laura, Koch, Miriam, Seizer, Peter, Schaller, Martin, Gawaz, Meinrad and Lindemann, Stephan (2011): High shear flow induces migration of adherent human platelets, Platelets **22**(6): 415–421.
URL: *http://dx.doi.org/10.3109/09537104.2011.556277*

Ladoux, Benoit and Nicolas, Alice (2012): Physically based principles of cell adhesion

mechanosensitivity in tissues, Rep. Prog. Phys. **75**(11): 116601–.
URL: *http://stacks.iop.org/0034-4885/75/i=11/a=116601*

Lam, Wilbur A., Chaudhuri, Ovijit, Crow, Ailey, Webster, Kevin D., Li, Tai-De, Kita, Ashley, Huang, James and Fletcher, Daniel A. (2011): Mechanics and contraction dynamics of single platelets and implications for clot stiffening, Nat Mater **10**(1): 61–66.
URL: *http://dx.doi.org/10.1038/nmat2903*

Lammermann, Tim, Bader, Bernhard L., Monkley, Susan J., Worbs, Tim, Wedlich-Soldner, Roland, Hirsch, Karin, Keller, Markus, Forster, Reinhold, Critchley, David R., Fassler, Reinhard and Sixt, Michael (2008): Rapid leukocyte migration by integrin-independent flowing and squeezing, Nature **453**(7191): 51–55.
URL: *http://dx.doi.org/10.1038/nature06887*

Lauffenburger, Douglas A and Horwitz, Alan F (1996): Cell migration: A physically integrated molecular process, Cell **84**(3): 359–369.
URL: *http://www.cell.com/cell/abstract/S0092-8674(00)81280-5*

Lee, Juliet, Ishihara, Akira, Oxford, Gerry, Johnson, Barry and Jacobson, Ken (1999): Regulation of cell movement is mediated by stretch-activated calcium channels, Nature **400**(6742): 382–386.
URL: *http://dx.doi.org/10.1038/22578*

Legate, Kyle R. and Fässler, Reinhard (2009): Mechanisms that regulate adaptor binding to beta-integrin cytoplasmic tails, Journal of Cell Science **122**(2): 187–198.
URL: *http://jcs.biologists.org/content/122/2/187.abstract*

Lellouch-Tubiana, A, Lefort, J, Pirotzky, E, Vargaftig, B B and Pfister, A (1985): Ultrastructural evidence for extravascular platelet recruitment in the lung upon intravenous injection of platelet-activating factor (paf-acether) to guinea-pigs., British journal of experimental pathology **66**(3): 345–355.
URL: *http://www.ncbi.nlm.nih.gov/pmc/articles/PMC2041063/*

Leon, Catherine, Eckly, Anita, Hechler, Beatrice, Aleil, Boris, Freund, Monique, Ravanat, Catherine, Jourdain, Marie, Nonne, Christelle, Weber, Josiane, Tiedt, Ralph, Gratacap, Marie-Pierre, Severin, Sonia, Cazenave, Jean-Pierre, Lanza, Francois,

Skoda, Radek and Gachet, Christian (2007): Megakaryocyte-restricted myh9 inactivation dramatically affects hemostasis while preserving platelet aggregation and secretion, Blood **110**(9): 3183–3191.
URL: *http://bloodjournal.hematologylibrary.org/content/110/9/3183.abstract*

Li, Z., Delaney, M.K., O'Brien, K.A. and Du, X. (2010): Signaling during platelet adhesion and activation, Arterioscler. Thromb. Vasc. Biol. **30**(12): 2341–2349.

Lindon, JN, McManama, G, Kushner, L, Merrill, EW and Salzman, EW (1986): Does the conformation of adsorbed fibrinogen dictate platelet interactions with artificial surfaces?, Blood **68**(2): 355–362.

Livet, Jean, Weissman, Tamily A., Kang, Hyuno, Draft, Ryan W., Lu, Ju, Bennis, Robyn A., Sanes, Joshua R. and Lichtman, Jeff W. (2007): Transgenic strategies for combinatorial expression of fluorescent proteins in the nervous system, Nature **450**(7166): 56–62.
URL: *http://dx.doi.org/10.1038/nature06293*

Lombardi, Maria L., Knecht, David A., Dembo, Micah and Lee, Juliet (2007): Traction force microscopy in dictyostelium reveals distinct roles for myosin ii motor and actin-crosslinking activity in polarized cell movement, Journal of Cell Science **120**(9): 1624–1634.
URL: *http://jcs.biologists.org/content/120/9/1624.abstract*

Lowenhaupt, Rosalin Wu, Miller, Mary Ann and Glueck, Helen I. (1973): Platelet migration and chemotaxis demonstrated in vitro, Thromb. Res. **3**(5): 477–487.
URL: *http://www.sciencedirect.com/science/article/pii/0049384873901102*

Lowenhaupt, RW, Glueck, HI, Miller, MA and Kline, DL (1977): Factors which influence blood platelet migration, The Journal of laboratory and clinical medicine **90**(1): 37–45.
URL: *http://europepmc.org/abstract/MED/17642*

Lowenhaupt, RW, Silberstein, EB, Sperling, MI and Mayfield, G (1982): A quantitative method to measure human platelet chemotaxis using indium- 111-oxine-labeled gel-filtered platelets, Blood **60**(6): 1345–1352.
URL: *http://www.bloodjournal.org/content/60/6/1345.abstract*

Mangin, P., Yap, C.L., Nonne, C., Sturgeon, S.A., Goncalves, I., Yuan, Y., Schoenwaelder, S.M., Wright, C.E., Lanza, F. and Jackson, S.P. (2006): Thrombin overcomes the thrombosis defect associated with platelet gpvi/fcrgamma-deficiency, Blood **107**(11): 4346–4353.

Martini, Francisco J. and Valdeolmillos, Miguel (2010): Actomyosin contraction at the cell rear drives nuclear translocation in migrating cortical interneurons, J. Neurosci. **30**(25): 8660–8670.
URL: *http://www.jneurosci.org/content/30/25/8660.abstract*

Massberg, Steffen, Brand, Korbinian, Grüner, Sabine, Page, Sharon, Müller, Elke, Müller, Iris, Bergmeier, Wolfgang, Richter, Thomas, Lorenz, Michael, Konrad, Ildiko, Nieswandt, Bernhard and Gawaz, Meinrad (2002): A critical role of platelet adhesion in the initiation of atherosclerotic lesion formation, J. Exp. Med. **196**(7): 887–896.
URL: *http://jem.rupress.org/content/196/7/887.abstract*

Massberg, Steffen, Gawaz, Meinrad, Grüner, Sabine, Schulte, Valerie, Konrad, Ildiko, Zohlnhöfer, Dietlind, Heinzmann, Ulrich and Nieswandt, Bernhard (2003): A crucial role of glycoprotein vi for platelet recruitment to the injured arterial wall in vivo, J. Exp. Med. **197**(1): 41–49.
URL: *http://jem.rupress.org/content/197/1/41.abstract*

Maxwell, Mhairi J., Westein, Erik, Nesbitt, Warwick S., Giuliano, Simon, Dopheide, Sacha M. and Jackson, Shaun P. (2006): Identification of a 2-stage platelet aggregation process mediating shear-dependent thrombus formation, Blood **109**(2): 566–576.
URL: *http://bloodjournal.hematologylibrary.org/content/109/2/566.abstract*

Mazharian, Alexandra, Ghevaert, Cedric, Zhang, Lin, Massberg, Steffen and Watson, Steve P. (2011): Dasatinib enhances megakaryocyte differentiation but inhibits platelet formation, Blood **117**(19): 5198–5206.
URL: *http://www.bloodjournal.org/content/117/19/5198.abstract*

Mazia, Daniel and Prescott, David M. (1955): The role of the nucleus in protein synthesis in amoeba, Biochim. Biophys. Acta **17**(0): 23–34.
URL: *http://www.sciencedirect.com/science/article/pii/0006300255903164*

Mccarty, O. J. T., Zhao, Y., Andrew, N., Machesky, L. M., Staunton, D., Frampton, J. and Watson, S. P. (2004): Evaluation of the role of platelet integrins in fibronectin-

dependent spreading and adhesion, J. Thromb. Haemost. **2**(10): 1823–1833.
URL: *http://dx.doi.org/10.1111/j.1538-7836.2004.00925.x*

Meijering, E., Dzyubachyk, O. and Smal, I. (2012): Imaging and Spectroscopic Analysis of Living Cells (Methods in Enzymology), Bd. 504, Elsevier.

Mendoza, Michelle C., Besson, Sebastien and Danuser, Gaudenz (2012): Quantitative fluorescent speckle microscopy (qfsm) to measure actin dynamics, Current Protocols in Cytometry S. 62:2.18.12.18.26.
URL: *http://dx.doi.org/10.1002/0471142956.cy0218s62*

Nakamura, Masanori, Shibazaki, Masahiko, Nitta, Yasutaka and Endo, Yasuo (1998): Translocation of platelets into disse spaces and their entry into hepatocytes in response to lipopolysaccharides, interleukin-1 and tumour necrosis factor: the role of kupffer cells, Journal of Hepatology **28**(6): 991–999.
URL: *http://www.journal-of-hepatology.eu/article/S0168-8278(98)80348-6/abstract*

Nathan, P (1973): The migration of human platelets in vitro, Thrombosis et diathesis haemorrhagica **30**(1): 173–177.
URL: *http://europepmc.org/abstract/MED/4788745*

Nieswandt, Bernhard, Bergmeier, Wolfgang, Eckly, Anita, Schulte, Valerie, Ohlmann, Philippe, Cazenave, Jean-Pierre, Zirngibl, Hubert, Offermanns, Stefan and Gachet, Christian (2001): Evidence for cross-talk between glycoprotein vi and gi-coupled receptors during collagen-induced platelet aggregation, Blood **97**(12): 3829–3835.
URL: *http://bloodjournal.hematologylibrary.org/content/97/12/3829.abstract*

Nieswandt, Bernhard, Schulte, Valerie, Zywietz, Alexandra, Gratacap, Marie-Pierre and Offermanns, Stefan (2002): Costimulation of gi- and g12/g13-mediated signaling pathways induces integrin aiibbiiia-mediated activation in platelets, J. Biol. Chem. **277**(42): 39493–39498.
URL: *http://www.jbc.org/content/277/42/39493.abstract*

Nurden, A. T. (2005): Qualitative disorders of platelets and megakaryocytes, Journal of Thrombosis and Haemostasis **3**(8): 1773–1782.

Offermanns, Stefan (2006): Activation of platelet function through g protein-coupled receptors, Circ. Res. **99**(12): 1293–1304.
URL: *http://circres.ahajournals.org/content/99/12/1293.abstract*

Olorundare, OE, Simmons, SR and Albrecht, RM (1992): Cytochalasin d and e: effects on fibrinogen receptor movement and cytoskeletal reorganization in fully spread, surface-activated platelets: a correlative light and electron microscopic investigation, Blood **79**(1): 99–109.
URL: *http://bloodjournal.hematologylibrary.org/content/79/1/99.abstract*

Ono, Akiko, Westein, Erik, Hsiao, Sarah, Nesbitt, Warwick S., Hamilton, Justin R., Schoenwaelder, Simone M. and Jackson, Shaun P. (2008): Identification of a fibrin-independent platelet contractile mechanism regulating primary hemostasis and thrombus growth, Blood **112**(1): 90–99.
URL: *http://www.bloodjournal.org/content/112/1/90.abstract*

Packham, MA, Bryant, NL, Guccione, MA, Kinlough-Rathbone, RL and Mustard, JF (1989): Effect of the concentration of ca2+ in the suspending medium on the responses of human and rabbit platelets to aggregating agents., Thromb Haemost **62**(3): 968–976–.
URL: *http://europepmc.org/abstract/MED/2512683*

Packham, M.A, Rand, M.L, RÃ$\frac{1}{4}$ben, D.H and Kinlough-Rathbone, R.L (1991): Effect of calcium concentration and inhibitors on the responses of platelets stimulated with collagen: Contrast between human and rabbit platelets, Comparative Biochemistry and Physiology Part A: Physiology **99**(4): 551 – 557.
URL: *http://www.sciencedirect.com/science/article/pii/0300962991901305*

Palecek, Sean P., Loftus, Joseph C., Ginsberg, Mark H., Lauffenburger, Douglas A. and Horwitz, Alan F. (1997): Integrin-ligand binding properties govern cell migration speed through cell-substratum adhesiveness, Nature **385**(6616): 537–540.
URL: *http://dx.doi.org/10.1038/385537a0*

Park, K., Mao, F. W. and Park, H. (1991): The minimum surface fibrinogen concentration necessary for platelet activation on dimethyldichlorosilane-coated glass, J. Biomed. Mater. Res. **25**(3): 407–420.
URL: *http://dx.doi.org/10.1002/jbm.820250311*

Paul, Benjamin Z. S., Jin, Jianguo and Kunapuli, Satya P. (1999): Molecular mechanism of thromboxane a2-induced platelet aggregation: Essential role for p2t, J. Biol. Chem. **274**(41): 29108–29114.
URL: *http://www.jbc.org/content/274/41/29108.abstract*

Petrie, Ryan J., Doyle, Andrew D. and Yamada, Kenneth M. (2009): Random versus directionally persistent cell migration, Nat Rev Mol Cell Biol **10**(8): 538–549.
URL: *http://dx.doi.org/10.1038/nrm2729*

Pincus, Z., Z. and Theriot, J. A. (2007): Comparison of quantitative methods for cell-shape analysis, J. Microsc. **227**(2): 140–156.
URL: *http://dx.doi.org/10.1111/j.1365-2818.2007.01799.x*

Pitchford, Simon C., Momi, Stefania, Baglioni, Stefano, Casali, Lucio, Giannini, Silvia, Rossi, Roberta, Page, Clive P. and Gresele, Paolo (2008): Allergen induces the migration of platelets to lung tissue in allergic asthma, Am J Respir Crit Care Med **177**(6): 604–612.
URL: *http://dx.doi.org/10.1164/rccm.200702-214OC*

Pollard, Thomas D. and Cooper, John A. (2009): Actin, a central player in cell shape and movement, Science **326**(5957): 1208–1212.
URL: *http://www.sciencemag.org/content/326/5957/1208.abstract*

Rafelski, Susanne M. and Theriot, Julie A. (2004): Crawling toward a unified model of cell motility: Spatial and temporal regulation of actin dynamics, Annu. Rev. Biochem. **73**(1): 209–239: PMID: 15189141.
URL: *http://www.annualreviews.org/doi/abs/10.1146/annurev.biochem.73.011303.073844*

Reid, G., Wielinga, P., Zelcer, N., van der Heijden, I., Kuil, A., de Haas, M., Wijnholds, J. and Borst, P. (2003): The human multidrug resistance protein mrp4 functions as a prostaglandin efflux transporter and is inhibited by nonsteroidal antiinflammatory drugs, Proceedings of the National Academy of Sciences **100**(16): 9244–9249.

Ridley, Anne J., Schwartz, Martin A., Burridge, Keith, Firtel, Richard A., Ginsberg, Mark H., Borisy, Gary, Parsons, J. Thomas and Horwitz, Alan Rick (2003): Cell migration: Integrating signals from front to back, Science **302**(5651): 1704–1709.
URL: *http://www.sciencemag.org/content/302/5651/1704.abstract*

Ryningen, Anita, Jensen, Baard Olav and Holmsen, Holm (1999): Role of autocrine stimulation on the effects of cyclic amp on protein and lipid phosphorylation in collagen-activated and thrombin-activated platelets, Eur. J. Biochem. **260**(1): 87–96.
URL: *http://dx.doi.org/10.1046/j.1432-1327.1999.00135.x*

Savage, B., Almus-Jacobs, F. and Ruggeri, Z.M. (1998): Specific synergy of multiple substrate-receptor interactions in platelet thrombus formation under flow., Cell **94(5)**: 657–66.

Schindelin, Johannes, Arganda-Carreras, Ignacio, Frise, Erwin, Kaynig, Verena, Longair, Mark, Pietzsch, Tobias, Preibisch, Stephan, Rueden, Curtis, Saalfeld, Stephan, Schmid, Benjamin, Tinevez, Jean-Yves, White, Daniel James, Hartenstein, Volker, Eliceiri, Kevin, Tomancak, Pavel and Cardona, Albert (2012): Fiji: an open-source platform for biological-image analysis, Nat Meth **9**(7): 676–682.
URL: *http://dx.doi.org/10.1038/nmeth.2019*

Schmidt, E.-M., Kraemer, B.F., Borst, O., Münzer, P., Schönberger, T., Schmidt, C., Leibrock, C., Towhid, S.T., Seizer, P., Kuhl, D., Stournaras, C., Lindemann, S., Gawaz, M. and Lang, F. (2012): Sgk1 sensitivity of platelet migration, Cell Physiol Biochem **30**(1): 259–268.
URL: *http://www.karger.com/DOI/10.1159/000339062*

Schmidt, Eva-Maria, Münzer, Patrick, Borst, Oliver, Kraemer, Bjoern F., Schmid, Evi, Urban, Benjamin, Lindemann, Stephan, Ruth, Peter, Gawaz, Meinrad and Lang, Florian (2011): Ion channels in the regulation of platelet migration, Biochemical and Biophysical Research Communications **415**(1): 54–60.
URL: *http://www.sciencedirect.com/science/article/pii/S0006291X1101792X*

Schumann, Kathrin, Lämmermann, Tim, Bruckner, Markus, Legler, Daniel F., Polleux, Julien, Spatz, Joachim P., Schuler, Gerold, Förster, Reinhold, Lutz, Manfred B., Sorokin, Lydia and Sixt, Michael (2010): Immobilized chemokine fields and soluble chemokine gradients cooperatively shape migration patterns of dendritic cells, Immunity **32**(5): 703–713.
URL: *http://www.cell.com/immunity/abstract/S1074-7613(10)00166-4*

Schwarz Henriques, Sarah, Sandmann, Rabea, Strate, Alexander and Köster, Sarah (2012): Force field evolution during human blood platelet activation, Journal of Cell Science **125**(16): 3914–3920.
URL: *http://jcs.biologists.org/content/125/16/3914.abstract*

Shigara, M., Miyata, S., Kato, H., Kashiwagi, H., Honda, S., Kurata, Y., Tomiyama, Y. and Kanakura, Y. (2005): Impaired platelet function in a patient with p2y12 deficiency caused by a mutation in the translation initiation codon, J. Thromb. Haemost.

3(10): 2315–2323.
URL: *http://dx.doi.org/10.1111/j.1538-7836.2005.01554.x*

Snippert, Hugo J., van der Flier, Laurens G., Sato, Toshiro, van Es, Johan H., van den Born, Maaike, Kroon-Veenboer, Carla, Barker, Nick, Klein, Allon M., van Rheenen, Jacco, Simons, Benjamin D. and Clevers, Hans (2010): Intestinal crypt homeostasis results from neutral competition between symmetrically dividing lgr5 stem cells, Cell **143**(1): 134–144.
URL: *http://www.cell.com/cell/abstract/S0092-8674(10)01064-0*

Stalker, Timothy J., Traxler, Elizabeth A., Wu, Jie, Wannemacher, Kenneth M., Cermignano, Samantha L., Voronov, Roman, Diamond, Scott L. and Brass, Lawrence F. (2013): Hierarchical organization in the hemostatic response and its relationship to the platelet-signaling network, Blood **121**(10): 1875–1885.
URL: *http://bloodjournal.hematologylibrary.org/content/121/10/1875.abstract*

Stark, Konstantin, Eckart, Annekathrin, Haidari, Selgai, Tirniceriu, Anca, Lorenz, Michael, von Bruhl, Marie-Luise, Gartner, Florian, Khandoga, Alexander Georg, Legate, Kyle R, Pless, Robert, Hepper, Ingrid, Lauber, Kirsten, Walzog, Barbara and Massberg, Steffen (2013): Capillary and arteriolar pericytes attract innate leukocytes exiting through venules and 'instruct' them with pattern-recognition and motility programs, Nat Immunol **14**(1): 41–51.
URL: *http://dx.doi.org/10.1038/ni.2477*

Takeda, Kunio, Wada, Akira, Yamamoto, Kazuo, Moriyama, Yoshiko and Aoki, Koichiro (1989): Conformational change of bovine serum albumin by heat treatment, J. Protein Chem. **8**(5): 653–659–.
URL: *http://dx.doi.org/10.1007/BF01025605*

Taylor, D L, Blinks, J R and Reynolds, G (1980): Contractile basis of ameboid movement. vii. aequorin luminescence during ameboid movement, endocytosis, and capping., J. Cell Biol. **86**(2): 599–607.
URL: *http://jcb.rupress.org/content/86/2/599.abstract*

Thomas, D.W., Mannon, R.B., Mannon, P.J., Latour, A., Oliver, J.A., Hoffman, M., Smithies, O., Koller, B.H. and Coffman, T.M. (1998): Coagulation defects and altered hemodynamic responses in mice lacking receptors for thromboxane a2., The Journal of Clinical Investigation **102**(11): 1994–2001.

Tiedt, Ralph, Schomber, Tibor, Hao-Shen, Hui and Skoda, Radek C. (2006): Pf4-cre transgenic mice allow the generation of lineage-restricted gene knockouts for studying megakaryocyte and platelet function in vivo, Blood **109**(4): 1503–1506.
URL: *http://bloodjournal.hematologylibrary.org/content/109/4/1503.abstract*

Tsai, Feng-Chiao and Meyer, Tobias (2012): Ca2+ pulses control local cycles of lamellipodia retraction and adhesion along the front of migrating cells, Current Biology **22**(9): 837–842.
URL: *http://www.sciencedirect.com/science/article/pii/S0960982212003247*

Tsai, Feng-Chiao, Seki, Akiko, Yang, Hee Won, Hayer, Arnold, Carrasco, Silvia, Malmersjö, Seth and Meyer, Tobias (2014): A polarized ca2+, diacylglycerol and stim1 signalling system regulates directed cell migration, Nat Cell Biol **16**(2): 133–144.
URL: *http://dx.doi.org/10.1038/ncb2906*

Turbill, P., Beugeling, T. and Poot, A.A. (1996): Proteins involved in the vroman effect during exposure of human blood plasma to glass and polyethylene, Biomaterials **17**(13): 1279–1287.
URL: *http://www.sciencedirect.com/science/article/pii/S0142961296800044*

Valone, Frank H., Austen, K. Frank and Goetzl, Edward J. (1974): Modulation of the random migration of human platelets, J Clin Invest **54**(5): 1100–1106.
URL: *http://www.jci.org/articles/view/107854*

Varga-Szabo, David, Braun, Attila, Kleinschnitz, Christoph, Bender, Markus, Pleines, Irina, Pham, Mirko, Renne, Thomas, Stoll, Guido and Nieswandt, Bernhard (2008): The calcium sensor stim1 is an essential mediator of arterial thrombosis and ischemic brain infarction, J. Exp. Med. **205**(7): 1583–1591.
URL: *http://jem.rupress.org/content/205/7/1583.abstract*

Vial, C., Hechler, B., Léon, C., Cazenave, JP. and Gachet, C. (1997): Presence of p2x1 purinoceptors in human platelets and megakaryoblastic cell lines., Thromb Haemost. **78**(6): 1500–4.

von Brühl, Marie-Luise, Stark, Konstantin, Steinhart, Alexander, Chandraratne, Sue, Konrad, Ildiko, Lorenz, Michael, Khandoga, Alexander, Tirniceriu, Anca, Coletti, Raffaele, Köllnberger, Maria, Byrne, Robert A., Laitinen, Iina, Walch, Axel, Brill, Alexander, Pfeiler, Susanne, Manukyan, Davit, Braun, Siegmund, Lange, Philipp,

Riegger, Julia, Ware, Jerry, Eckart, Annekathrin, Haidari, Selgai, Rudelius, Martina, Schulz, Christian, Echtler, Katrin, Brinkmann, Volker, Schwaiger, Markus, Preissner, Klaus T., Wagner, Denisa D., Mackman, Nigel, Engelmann, Bernd and Massberg, Steffen (2012): Monocytes, neutrophils, and platelets cooperate to initiate and propagate venous thrombosis in mice in vivo, J. Exp. Med. **209**(4): 819–835.
URL: *http://jem.rupress.org/content/209/4/819.abstract*

Weber, Michele, Hauschild, Robert, Schwarz, Jan, Moussion, Christine, de Vries, Ingrid, Legler, Daniel F., Luther, Sanjiv A., Bollenbach, Tobias and Sixt, Michael (2013): Interstitial dendritic cell guidance by haptotactic chemokine gradients, Science **339**(6117): 328–332.
URL: *http://www.sciencemag.org/content/339/6117/328.abstract*

Wedlich-Soldner, Roland and Li, Rong (2003): Spontaneous cell polarization: undermining determinism, Nat Cell Biol **5**(4): 267–270.
URL: *http://dx.doi.org/10.1038/ncb0403-267*

Wei, Chaoliang, Wang, Xianhua, Chen, Min, Ouyang, Kunfu, Song, Long-Sheng and Cheng, Heping (2009): Calcium flickers steer cell migration, Nature **457**(7231): 901–905.
URL: *http://dx.doi.org/10.1038/nature07577*

Weiss, E.J., Hamilton, J.R., Lease, K.E. and Coughlin, S.R. (2002): Protection against thrombosis in mice lacking par3, Blood **100**(9): 3240–3244.

Wulf, Gerald G., Luo, Kang-Li, Goodell, Margaret A. and Brenner, Malcolm K. (2002): Anti-cd45 mediated cytoreduction to facilitate allogeneic stem cell transplantation, Blood **101**(6): 2434–2439.
URL: *http://bloodjournal.hematologylibrary.org/content/101/6/2434.abstract*

Yam, Patricia T., Wilson, Cyrus A., Ji, Lin, Hebert, Benedict, Barnhart, Erin L., Dye, Natalie A., Wiseman, Paul W., Danuser, Gaudenz and Theriot, Julie A. (2007): Actin-myosin network reorganization breaks symmetry at the cell rear to spontaneously initiate polarized cell motility, J. Cell Biol. **178**(7): 1207–1221.
URL: *http://jcb.rupress.org/content/178/7/1207.abstract*

Yang, Shengyu and Huang, Xin-Yun (2005): Ca2+ influx through l-type ca2+ channels controls the trailing tail contraction in growth factor-induced fibroblast cell migration,

J. Biol. Chem. **280**(29): 27130–27137.
URL: *http://www.jbc.org/content/280/29/27130.abstract*

Yeaman, Michael R. (2014): Platelets: at the nexus of antimicrobial defence, Nat Rev Micro **12**(6): 426–437.
URL: *http://dx.doi.org/10.1038/nrmicro3269*

Yipp, Bryan G, Petri, Bjorn, Salina, Davide, Jenne, Craig N, Scott, Brittney N V, Zbytnuik, Lori D, Pittman, Keir, Asaduzzaman, Muhammad, Wu, Kaiyu, Meijndert, H Christopher, Malawista, Stephen E, de Boisfleury Chevance, Anne, Zhang, Kunyan, Conly, John and Kubes, Paul (2012): Infection-induced netosis is a dynamic process involving neutrophil multitasking in vivo, Nat Med **18**(9): 1386–1393.
URL: *http://dx.doi.org/10.1038/nm.2847*

Yount, Garret, Taft, RyanJ., Luu, Tri, Rachlin, Kenneth, Moore, Dan and Zhang, Wei (2007): Independent motile microplast formation correlates with glioma cell invasiveness, J Neurooncol **81**(2): 113–121–.
URL: *http://dx.doi.org/10.1007/s11060-006-9211-4*

Zhang, Lin, Orban, Martin, Lorenz, Michael, Barocke, Verena, Braun, Daniel, Urtz, Nicole, Schulz, Christian, von Brühl, Marie-Luise, Tirniceriu, Anca, Gaertner, Florian, Proia, Richard L., Graf, Thomas, Bolz, Steffen-Sebastian, Montanez, Eloi, Prinz, Marco, Müller, Alexandra, von Baumgarten, Louisa, Billich, Andreas, Sixt, Michael, Fässler, Reinhard, von Andrian, Ulrich H., Junt, Tobias and Massberg, Steffen (2012): A novel role of sphingosine 1-phosphate receptor s1pr1 in mouse thrombopoiesis, J. Exp. Med. **209**(12): 2165–2181.
URL: *http://jem.rupress.org/content/209/12/2165.abstract*

A manuscript was prepared from the results of this thesis is currently under revison:

Florian Gaertner, Zerkah Ahmad, Gökce Yavuz, Michael Lorenz, Sue Chandraratne, Irene Schubert, Marek Janko, Roman Hennel, Leo Nicolai, Konstantin Stark, Ralph T. Böttcher, Catherine Leon, Christian Gachet, Thomas Gudermann, Michael Mederos y Schnitzler, Zachary Pincus, Kirsten Lauber, Michael Sixt, Steffen Massberg. *Autonomous locomotion of anucleated platelets facilitates thrombus consolidation* (under revision).

Appendix

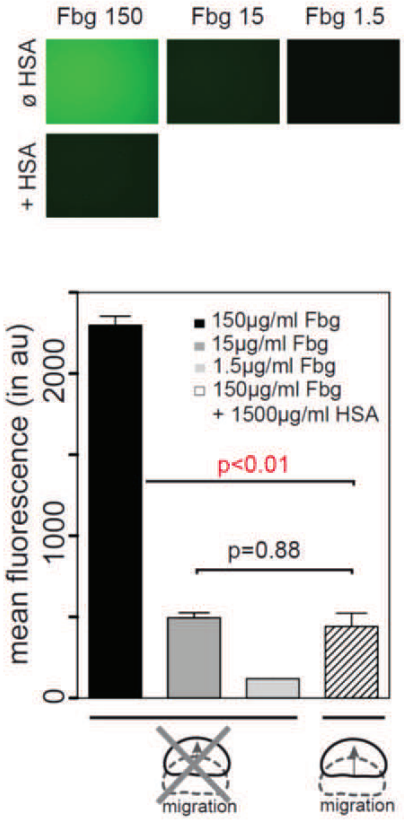

Figure 5.1 – Quantitative reduction of immobilized fibrinogen is not sufficent to induce platelet migration. Immobilized fibrinogen was quantified by measuring the fluorescence intensity of Alexa 488 labeled fibrinogen. mean±SD is shown; p-values<0.05 (red) indicate significance; n=3 experiments; ANOVA/TukeyHSD

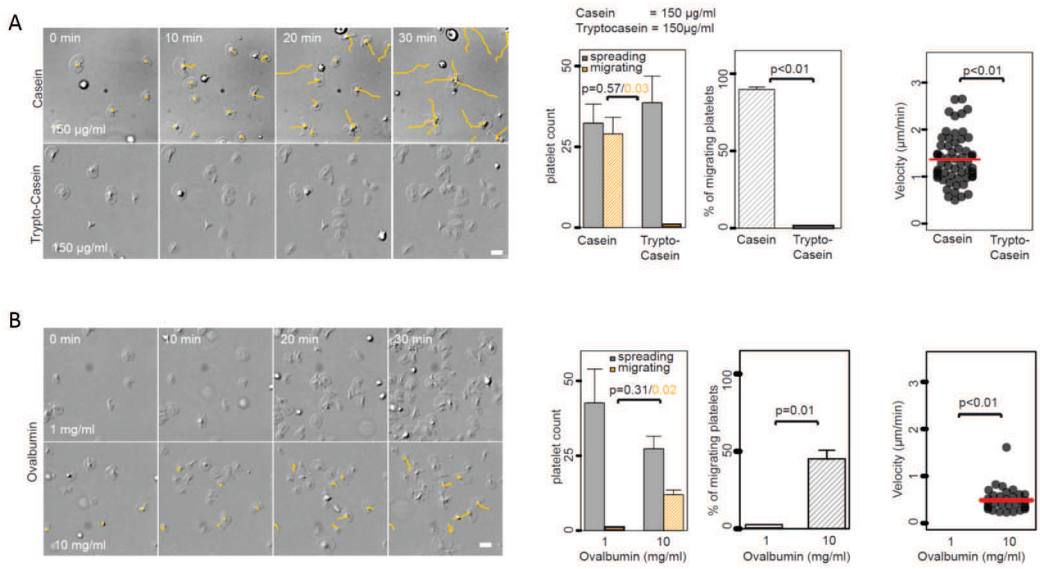

Figure 5.2 – Anti-adhesive proteins can induce platelet migration in the absence of albumin. A, Platelet migration was observed at the indicated concentrations of casein. Trypsin-digested (tryptocasein) was used as negative control. The total number of spreading and migrating platelets per experiment, fraction of migrating platelets and migration velocity are depicted. Platelets were pooled from n=3 experiments; p-values<0.05 indicate significance; student's t-test; scale bar = 10μm.